VOLUMETRIC TISSUE REDUCTION IN UPPER AIRWAYS BY RF THERAPY IN PATIENTS WITH SLEEP DISORDERS

Master Thesis

Submitted to the Research Group

Biomedical Sensing

Institute of Electrodynamics, Microwave and Circuit Engineering

Vienna University of Technology

by

Babak Dabiri Razlighi

Registration number: 01228565

Advisor:

Proj.-Ass. DI Stefan Kampusch

Ao.Univ.Prof. Dipl.Ing. Dr.techn. Eugenijus Kaniusas

Acknowledgments

I would first like to appreciate my thesis advisor Ao.Univ.Prof. Dipl.Ing. Dr.techn. Eugenijus Kaniusas of the Biomedical Sensing group of the Institute of Electrodynamics, Microwave and Circuit Engineering, Vienna University of Technology. He conducted me over this thesis, which I proposed, and whenever I confronted a problem or questions warmly accepted my invitation to follow and verify my experiments and results.

I would also like to thank Proj.-Ass. DI Stefan Kampusch. Without his passionate participation and input, the validation survey could not have been successfully conducted. He supported me with all the requirements and reviewed the results patiently. I am gratefully indebted to him for his very valuable comments on this thesis.

This thesis needed many components and measurement devices which were provided on behalf of the Biomedical Sensing group at the Institute of Electrodynamics, Microwave and Circuit Engineering.

Finally, I must express my very profound gratitude to my mother and to my friend Hadi Samadi for providing me with unfailing support and continuous encouragement throughout my years of study and through the process of researching and writing this thesis. This accomplishment would not have been possible without them. Thank you all.

Babak Dabiri Razlighi

Abstract

Recently, medical interest has focused on snoring sounds as an important symptom of the sleep apnea syndrome, i.e., a temporal and repetitive cessation of effective respiration during sleep at night in patients with sleep disorder. Therefore, many efforts have been made to treat such patients with different methods. Although minimally invasive tissue ablation by high frequency current has shown satisfactory results with minimum risk factors, low cost and repeatable procedure in comparison with other methods. Perforation on mucus layer, overtreatment and less painful recovery still are major drawbacks. Nowadays, Tissue ablation with impedance or temperature control plays an important role to reduce those risks. Nevertheless, all these efforts have been made in the lower range of high frequency current (300-400 kHz) in which tissue has higher impedance and current passes mostly through the extracellular and not the intracellular space in the tissue.

This thesis considered to provide an ablation and coagulation system in the radiofrequency range (4 MHz), in which biological tissue shows lower impedance and homogeneous current passage through the tissue. Tissue coagulation at this range of frequency needs lower energy application to the target tissue and reduces risk of overtreatment and unwanted scars and provides better healing recovery process with direct feedback over the process from the tissue.

Hence, a 4 MHz RF ablation system was designed, which is able to be used in a closed loop control system. With sampling of the root mean square of the voltage over a calibrated variable impedance and monitoring of the control parameters in a feedback loop, the transfer function of the system was elicited. Therefore, by this approach the coagulation process benefits not only from the advantages of the higher frequency current, but also from the real-time impedance control as a feedback from the tissue. Moreover, one parameter sampling reduces the measurement fault and system hardware complexity.

Result showed that the closed loop control system, controls the system by quantitative data based on boundary conditions like temperature, impedance and given energy over the coagulation process and follows the biological changes at the output stage. All results were verified with an applied calibrated variable impedance and tested in the laboratory with real biological tissue.

The outlook for this approach is, utilizing a clinical based study to optimize the treatment and provide an interface between physician and system in order to prevent the risk of overtreatment and unwanted ablation on one side and characterize the best appropriate therapy for the patients based on individual specifications like body mass index, age, gender and other screening factors on the other side. Furthermore, by generalizing to other tissues, like glandular tissues, the method could be used to reduce the hypertrophic glands like tonsil instead of resecting.

Kurzfassung

In jüngster Zeit konzentrierte sich das medizinische Interesse auf Schnarchgeräusche als ein wichtiges Symptom des Schlafapnoe-Syndroms, d.h. eine zeitliche und wiederholte Beendigung einer wirksamen Atmung während des Schlafes bei Nacht bei Patienten mit Schlafstörungen. Daher wurden viele Anstrengungen unternommen, um solche Patienten mit verschiedenen Methoden zu behandeln. Obwohl die minimal-invasive Gewebeablation durch den Hochfrequenzstrom mit minimalen Risikofaktoren zufriedenstellende Ergebnisse gezeigt hat, mit niedrigen Kosten und als robust wiederholbare Verfahren, sind die Perforation der Schleimhaut, eine Überbehandlung und Schmerzen während der Regeneration nach wie vor große Nachteile. Heutzutage spielt die Gewebeablation mit der Impedanz- oder Temperaturregelung eine wichtige Rolle, um diese Risiken zu reduzieren. Trotzdem wurden all diese Anstrengungen im unteren Bereich des Hochfrequenzstroms (300-400 kHz) durchgeführt, bei dem Gewebe eine höhere Impedanz und Stromflüsse überwiegend im extrazellulären und nicht im intrazellulären Raum des Gewebes konzentriert sind.

Diese Diplomarbeit erarbeitet ein Ablations- und Koagulationssystem im Hochfrequenzbereich (4 MHz), in dem biologisches Gewebe eine niedrigere Impedanz und einen homogenen Stromdurchgang durch das Gewebe zeigt. Die Gewebekoagulation in diesem Frequenzbereich erfordert einen geringeren Energieanwendung im Zielgewebe und verringert das Risiko von Überbeanspruchung und unerwünschten Narben und sorgt für einen besseren Heilungsverlauf mit direkter Rückmeldung über den Prozess aus dem Gewebe.

Daher wurde ein 4 MHz HF-Ablationssystem entwickelt, das in einem geschlossenen Regelungssystem eingesetzt werden kann. Über die Abtastung der Spannung über eine kalibrierte variable Impedanz und überwachen der Steuerparameter in der Rückkopplungsschleife, wurde die Übertragungsfunktion des Systems bestimmt. Daher kommen durch diesen Ansatz des Koagulationsprozesses nicht nur die Vorteile des höher frequenten Stroms zum Tragen, sondern auch die Echtzeit-Impedanzkontrolle als Rückkopplung aus dem Gewebe. Darüber hinaus reduziert eine Parameterabtastung den Messfehler und die Systemhardwarekomplexität.

Das Ergebnis zeigt, dass das Regelkreissystem das Systemverhalten auf der Grundlage von quantitative Daten wie Temperatur, Impedanz und gegebener Energie über den Koagulationsprozess reguliert und den biologischen Veränderungen an der Endstufe folgt. Alle Ergebnisse wurden mit einer angewandten kalibrierten variablen Impedanz verifiziert und im Labor mit realem biologischen Gewebe getestet.

Als Ausblick kann der entwickelte Ansatz in einer klinischen Studie zur Optimierung der Behandlung eingesetzt werden. Weiters muss eine Schnittstelle zwischen Arzt und System geschaffen werden, um das Risiko einer Überbehandlung und unerwünschte Ablation auf der einen Seite zu verhindern und auf der anderen Seite die am besten geeignete Therapie für die Patienten auf der Grundlage von individuelle Spezifikationen wie Body Mass Index, Alter, Geschlecht und andere Screening-Faktoren zu charakterisieren. Darüber hinaus könnte durch Verallgemeinerung auf andere Gewebe wie Drüsengewebe, die Methode verwendet werden um hypertrophische Drüsen wie Mandeln zu reduzieren, anstatt zu resezieren.

Hiermit erkläre ich, dass die vorliegende Arbeit gemäß dem Code of Conduct Regeln zur Sicherung guter wissenschaftlicher Praxis, insbesondere ohne unzulässige Hilfe Dritter und ohne Benutzung anderer als der angegebenen Hilfsmittel, angefertigt wurde. Die aus anderen Quellen direkt oder indirekt übernommenen Daten und Konzepte sind unter Angabe der Quelle gekennzeichnet. Die Arbeit wurde bisher weder im In noch im Ausland in gleicher oder in ähnlicher Form in anderen Prüfungsverfahren vorgelegt.

Wien, 02.09.2017

Table of content

List of abbreviation

PSSV	Power Supply Setting Voltage
AHI	Apnea–Hypopnea Index
PCG	Phonocardiogram
mVoltage	measured voltage across the tissue
BMI	Body Mass Index
BIS	Bio Impedance Spectroscopy
SNS	Sympathetic Nervous System).
f_C	heart rate
f_R	respiratory rate
f_{RI}	fundamental harmonic frequency
S_{PCG}	Acoustic biosignal phonocardiogram
OHA	Obstructive Sleep Hypopnea
ICSD	International Classification of Sleep Disorders
CPAP	Continuous Positive Airway Pressure
UPPP	uvulopalatopharyngoplasty
RF	Radiofrequency
RFITT	Radiofrequency-induced thermotherapy
VAS	Visual Analog Scale
OSAHS	Obstructive Sleep Spnea-Hypopnea Syndrome
R_e	extracellular resistance
R_i	intracellular resistance
C_m	membrane capacitance
Z	Impedance
φ	phase angle
X_c	reactance
ε_r	relative dielectric permittivity constant
ε_0	permittivity constant of vacuum
V_b	body volume
L	length
A	surface area

TBW	Total Body Water.
ECF	Extracellular Fluid
m	mass
c	thermal capacitance coefficient
Q	energy
K	coagulation depth
P_{HF}	high frequency power
P_{min}	minimum power
P_{opt}	optimum power
LLETZ	large loop excision of transformation zone of the cervix of the uterus
DC	Direct Current
PWM	Pulse Width Modulator
MOSFET	Metal Oxid Field Effect Transistor
FET	Field Effect Transistor
AVR	Advanced Virtual Risc
IEC	International Electrotechnical Commission
AC	Alternative current
HVDC	High Voltage Direct Current
P	power
W	watt
RMS	Root Mean Square
V_{pp}	Peak-to-Peak Voltage
LCD	Liquid Crystal Display
JTAG	Joint Test Action Group
CPLD	Complex Programmable Logic Devices
DAC	Digital to Analogue Convertor
T	Temperature
Z_{coag}	coagulation impedance
Z_{min}	minimum impedance

Table of Figures

Tables

1. Introduction

Sleep disorders due to the structural changes in upper airways lead to snoring or apnea. The noise of snoring is created by vibration and flapping of the skin tissues lining the throat; and the uvula hanging from the soft palate at the back of the mouth, towards the throat. As you breathe, the rush of air over these uneven or narrowing surfaces creates vibration, which generates a whistling or thundering noise. This turbulent air flow through the breathing passage can be caused by narrowness of the nasal passage, which can contribute to the fluttering of the soft palate. Tongues that fall back into the passageway may also attribute to snoring noise, as the airway might sometimes become blocked. Consequently, in most patients, snoring can be due to multiple factors playing a part in the snoring process. Lifestyle factors contributing to congestion of the soft tissues of the airways include smoking, alcohol and being overweight.

People who snore generally have an increased risk of high blood pressure and stroke. Snoring can also contribute to fatigue and morning tiredness, which can be a risk if the sufferer drives, or is employed in an occupation where alertness is essential to safety. Snoring can also be a sign of sleep apnea, which brings additional health risks[1].

Nowadays, volumetric tissue reduction by RF current is known as a successful approach by physicians and represents a repeatable treatment with minimal invasion. Low cost and long-lasting effect on upper airways and enhance the stiffness in vibrating structure muscles, has introduced this method as a very common treatment.

Although many efforts have been made to represent RF therapy as a superior approach, main concerns on risk factors still are left. In accordance with the recent researches, the frequency range of RF current and secure control on ablation process have a great influence on desired results.

A survey showed a superior effect of 4MHz RF therapy and less side effect beside convenient recovery time for the patients [2]. In this research, 4 different RF generators were used to reduce the tissue volume in upper airways region. Although 3 of them had impedance control, the one with 4MHz without impedance control (Elman generator) showed better clinical result and more comfortable treatment and recovery, 3 other systems with lower frequency had no risk of perforation but patients complained sever pain and post inflammatory trauma. Therefore, this idea came up to author mind to implement real-time impedance monitoring in a real-time manner to benefit the patients with both convenient and secure treatment procedure in 4MHz.

As the tissue ablation is a consequence of temperature rise to a certain level that protein structure denature and degrade by the immune system, some approaches represented a direct thermocouple in direct contact with the target tissue, whilst other proposed impedance monitoring as secondary factor related to the temperature. Thermocouple insertion in tip of the applicator needs a very precise and high manufacturing technology which increases the disposable components cost. Therefore, it would be more cost effective to sense the tissue changes via the voltage drop and current passing through the target tissue.

Hence, most approaches proposed a very common basic method to monitor the tissue changes in which current and voltage across the tissue are sensed and calculated impedance corresponds directly to the coagulation process.

In this thesis, RF current in the range of 4MHz proposed to improve the recovery time with less trauma and pain, and only voltage drop across the tissue was sensed. This novel method

decreases the sampling fault just to one parameter (no need current sampling) and a closed loop control system regulates the functionality of the coagulation process.

Although, 4MHz frequency has privileges in biological aspects, switching in high voltage and sampling is a struggling issue. Technical challenges in order to sample and calibrate the system need a sustainable method to assure the coagulation process. Therefore, a standard calibration method is necessary in order to follow the tissue changes based on a calibrated system.

Moreover, real time impedance monitoring shows an exponential behavior with very steep changes over coagulation process. Therefore, the time response of the system should be considered to be enough sensitive to the impedance changes to control the coagulation rate. Hence, signal processing and sampling should be very fast to be enough precis and fast.

In addition, a closed loop control system can control a whole coagulation process automatically and terminate the RF energy application to the tissue at the right time. Therefore, the more control parameters could collaborate in control process the risk of unwanted results will decrease. This control loop is the most important process besides the impedance calculation to set the control parameters like the coagulation rate, temperature, given energy and treatment duration. In fact, control loop provides the physician as much as possibilities to define the treatment features for different cases, since these parameters increase the specificity for treatments corresponds to the severity of the patient problem, physical situation like BMI (Body Mass Index), gender, age and even the treatment localization in upper airways like nasal, tongue base and soft palate.

In this thesis has been tried to have a contemporary overview of all possible treatments for this kind of disorder not only the non-surgical also surgical methods. A complete overview on different types of apnea and classification based on the location of the sound source, diagnostically relevant type of snoring, and the waveform of snoring sounds in the time domain was done to screen the patients for the best treatment method. Calibration process and results in real biological tissue verify the effectivity and precision of control system.

2. Clinical problem, therapeutic methods and case screening

2.1 Anatomical overview on respiratory tract

In humans, the respiratory tract is the part of the anatomy of the respiratory system involved with the process of respiration. Air is breathed in through the nose or the mouth Figure 2-1. In the nasal cavity, a layer of mucous membrane acts as a filter and traps pollutants and other harmful substances found in the air. Next, air moves into the pharynx, a passage that contains the intersection between the esophagus and the larynx. The opening of the larynx has a special flap of cartilage, the epiglottis, that opens to allow air to pass through but closes to prevent food from moving into the passageway[3].

From the larynx, air moves into the trachea and down to the intersection that branches to form the right and left primary (main) bronchi. Each of these bronchi branch into secondary (lobar) bronchi that branch into tertiary (segmental) bronchi that branch into smaller structures called bronchioles that eventually connect with tiny specialized structures called alveoli that function in gas exchange.
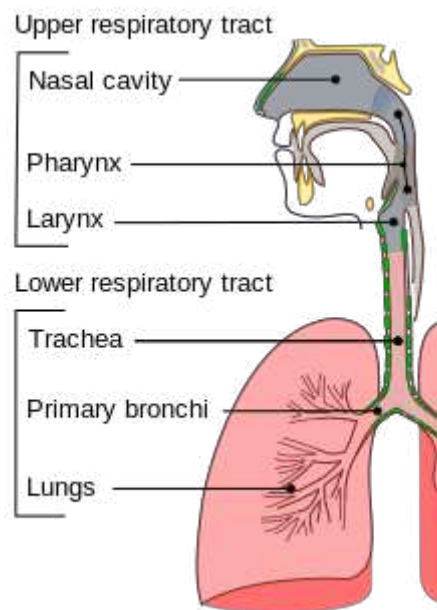
Figure 2- 1 Respiratory tract [13].

The lungs which are located in the thoracic cavity, are protected from physical damage by the rib cage. At the bottom of the lungs is a sheet of skeletal muscle called the diaphragm. The diaphragm separates the lungs from the stomach and intestines. It is also necessary for the process of breathing and is controlled by the SNS (sympathetic nervous system).

The lungs are encased in a serous membrane that enfolds on itself to form a two-layer protective barrier that we call the pleura. The inner membrane is called the visceral pleura while the outer membrane is called the parietal pleura. Between these two membranes is a cavity called the pleural cavity that contains a fluid. This fluid is used to decrease the amount of friction that lungs experience during breathing.

The respiratory tract is divided into the upper airways and lower airways. The upper airways or upper respiratory tract includes the nose and nasal passages, paranasal sinuses, the pharynx, and the portion of the larynx above the vocal folds (cords). The lower airways or lower respiratory tract includes the portion of the larynx below the vocal folds, trachea, bronchi and bronchioles. The lungs can be included in the lower respiratory tract or as separate entity and include the respiratory bronchioles, alveolar ducts, alveolar sacs, and alveoli.

Upper respiratory tract

The upper respiratory tract, can refer to the parts of the respiratory system lying above the sternal angle (outside of the thorax), above the vocal folds, or above the cricoid cartilage. The larynx is sometimes included in both the upper and lower airways Figure 2-2. The larynx is also called the voice box and has the associated cartilage that produces sound. The tract consists of the nasal cavity and paranasal sinuses, the pharynx (nasopharynx, oropharynx and laryngopharynx) and sometimes includes the larynx [3].
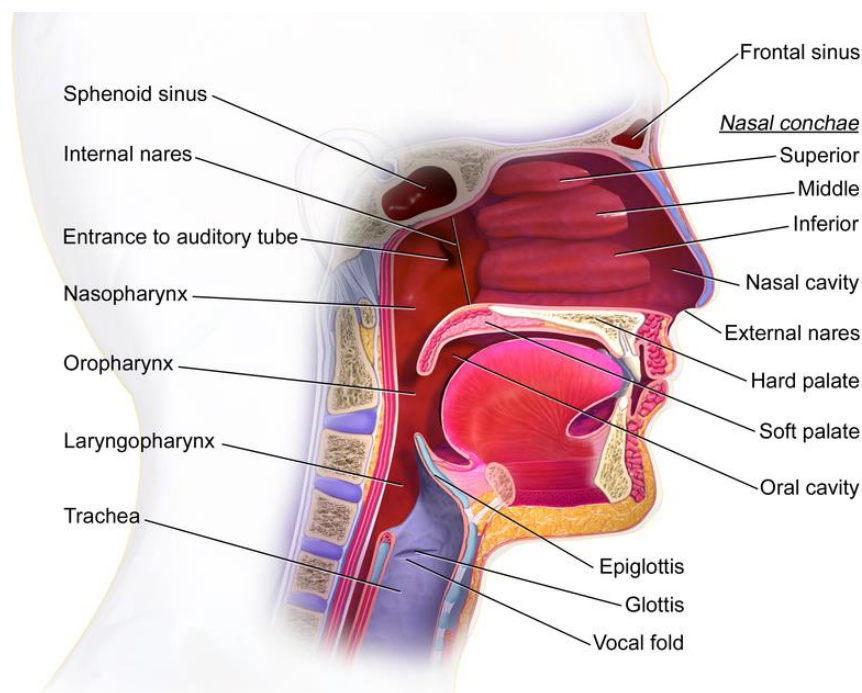
Figure 2- 2 Details of upper respiratory tract [14].

Mouth cavity

The mouth, consists of 2 regions, the vestibule and the oral cavity proper. The vestibule is the area between the teeth, lips and cheeks [4]. The oral cavity is bounded at the sides and in front by the alveolar process (containing the teeth) and at the back by the isthmus of the fauces (Figure 2- 1). Its roof is formed by hard palate and soft palate and the floor is formed by the mylohyoid muscles and is occupied mainly by the tongue. A mucous membrane – the oral mucosa, lines the sides and under surface of the tongue to the gums, lining the inner aspect of the jawbone (mandible). It receives the secretions from the submaxillary and sublingual salivary glands.
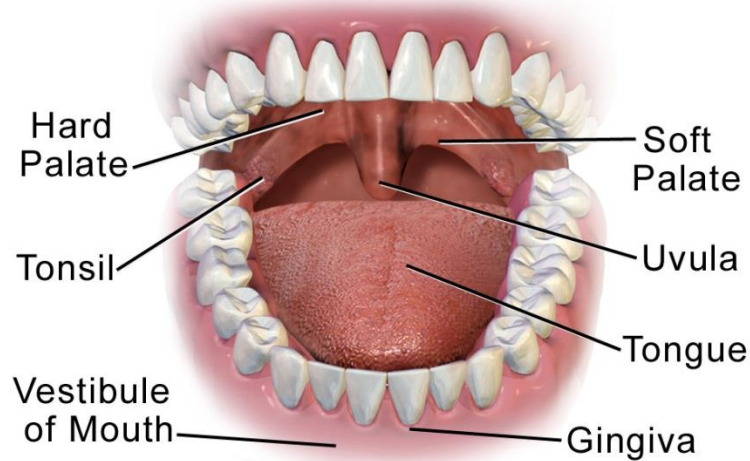
Figure 2- 3 Anatomy of the mouth [14].

Body sounds

A large variety of acoustic biosignals, i e., permanent biosignals according to their classification , originates in the inner human body, including heart sounds, lung sounds, and snoring sounds. Auscultation of lung sounds and snoring sounds is applied to detect respiratory disturbances. Recently, medical interest has also focused on snoring sounds as an important symptom of the sleep apnea syndrome, i.e., a temporal and repetitive cessation of effective respiration during sleep at night. Vibrating structures in the body yield acoustic sounds. This oscillation creates acoustic pressure waves travelling [5].

2.2 Sleep disorders due to the upper airways

2.2.1 Snoring Sounds and anatomical causes

While heart and lung sounds clinical investigations for in the focus of centuries, only recently medical interest has focused on snoring sounds while sleeping. In general, these sounds are related to vibrations of instable structures in the upper airways (such as the soft palate or uvula), radial oscillation of (pharyngea) flexible airway walls and oscillatory narrowing of airways (up to their complete occlusion), and turbulences of the air (Figure 2-2). Snoring sounds are favored by various physiologic and social factors whereas these sounds yield direct information on the dynamics and ventilation of the upper airways, e.g. for the diagnosis of apneas. Snoring could be related to sleep deprivation and thus to other severe pathologies. In particular, the snoring is proceeded by a temporal decrease in the diameter of the oropharynx (Figure 2-4), which can be even reduced to a slit. Figure 2-4a, b demonstrates the narrowing of the pharynx by video images. Likewise, the (supraglottic) resistance of the airway to the air flow increases by a factor of about 3, which in the case and obstructive snoring (i.e., spontaneous snoring during sleep) leads of heavy to initial flow limitation before onset of the snoring. In particular, the flow first increases as the driving pressure increases but then it saturates, i.e., the air flow becomes limited.

As the snoring begins and continues mainly during inspiration fluttering of loose structures in the upper airways occur, especially vibrations of the soft palate and pharyngeal walls. Likewise, the appearance of repetitive and steady sound structures in the time domain during snoring coincides with the time course of airway wall motions and the time course of the air flow oscillation [5].
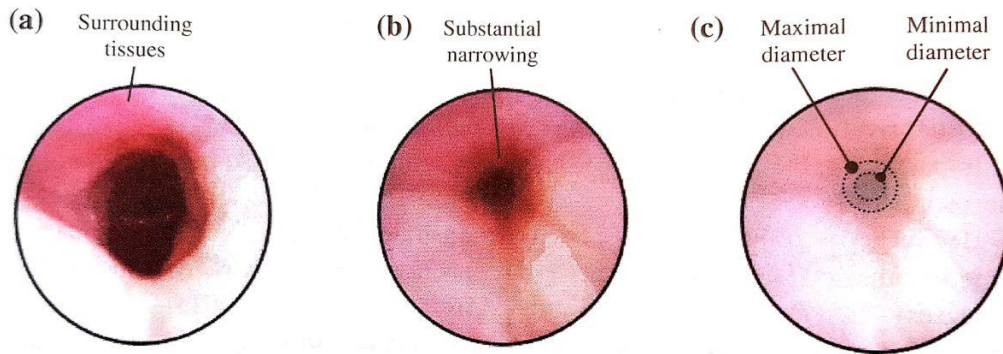
Figure 2- 4 Video images of the pharynx as recorded from the mouth cavity. (a) Before inspiration. (b) During inspiration. (c) During inspiration [10].

Figures 2-4c and 2-4a illustrate such elastic oscillations of airway walls provided that a local narrowing (tow-limiting segment) is present within the depicted highly compliant airway. Aeroelastic interactions occur between the air flow and the airway wall. At the constriction, the air flow is confined to a smaller cross sectional area A (Figure 2-5a). Consequently, the velocity u of the air flow increases at the constriction site ($u2 > u1$) because the net flow

$$q^A = <u>.A \qquad (2\text{-}1)$$

does not change along the airway (i.e., q^A is assumed to be constant). The lateral pressure p of the air flow must correspondingly decrease (p2< p1). Favoring the narrowing of the constriction even more. Likewise, radial forces keeping the airway open are reduced and thus there is an inward swing of airway walls ; the constricted site becomes more pronounced and unstable at $q^A \neq 0$.

However, elastic forces appear progressively in airway walls, which are directed outwards and cause the deflected walls to swing back to their neutral position; an oscillatory vibration of airway walls results the latter mechanism dominates also the generation of wheezes in obstructed sites. On the other hand, a collapsible airway experiencing a local pressure decrease (Figure 2-5 a) can even collapse and completely occlude the lumen for a brief period of time (Figure 2-5 b) In particular, large amplitude oscillations of airway walls can yield partial or complete occlusion of the airway, with the point of maximum constriction moving upstream along the airway. Repetitive openings of occluded airway generate abrupt pressure equalizations (popping openings) and tissue vibrations, which emit series of explosive and discontinuous sound structures- reoccurring with the frequency of the openings - in the time domain. Further narrowing of the oropharynx during snoring may lead to even louder snoring and labored breathing. In extreme cases, progressive narrowing can yield a sustained and complete occlusion of the upper airway, which then manifests as obstructive sleep apnea[5].
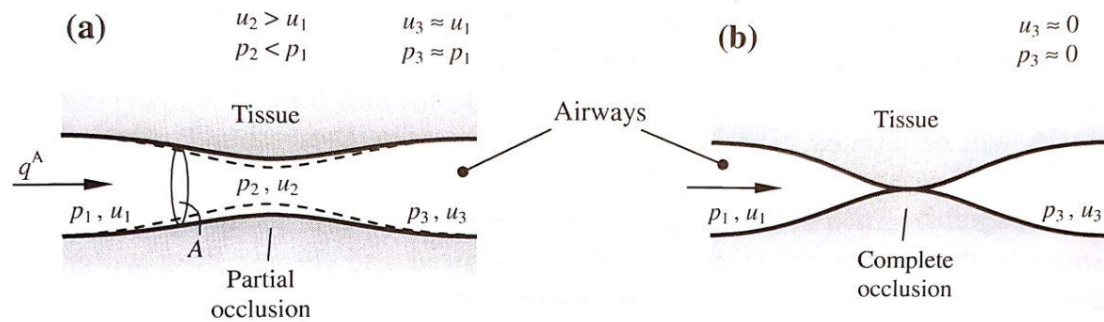
Figure 2- 5 (a) Narrowing airways generates continuous snoring sound. The relations of the pressure p and velocity u of the air flow q^A along the depicted airway are indicated. (b) Collapsed airways generates obstructive snoring sounds due to repetitive and temporal occlusion of large upper airways[5].

In addition, local turbulences of the air in the upper airways seem to contribute to the emission of snoring sounds. That is, the (increased) level of u in the (narrowed) (Figure 2-5 a) determines if noise-like broadband sounds will be emitted, whereas the frequency range of these sounds depends on this level of u.

2.2.1.1 Classification of the snoring sounds

classifications are based on

- the location of the sound source,
- the diagnostically relevant type of snoring,
- and the waveform of snoring sounds in the time domain.

Snoring accordance with the location of the sound source

Nasal snoring

Resulting mainly inspiratory sounds originate in the course uvula vibrations while the soft palate and the back of the tongue remain in close contact. On the other hand, spontaneous nasal snoring is also due to the palate or pharyngeal wall vibrations. nasal snoring shows discrete sharp peaks below 500Hz [5].

Oral snoring

This snoring through the open mouth (breathing exclusively through the mouth) is characterized by vibrations of the whole soft palate and a dramatic decrease in the cross-sectional area of the oropharynx yielding a lower oscillation frequency of about 30 Hz in comparison with the nasal snoring.

Oronasal snoring

These snoring sounds (breathing through the nose and mouth) exhibit a mixture of sounds similar to nasal snoring and fricative noisy sounds characteristic of a source in the turbulent flow. Likewise, in the frequency domain a mixture of discrete sharp peaks and broad-band (white) noise dominate in the range of up to about 1,300 Hz[5].

Considering the diagnostically relevant types of the snoring:

Normal snoring

Spontaneous snoring is always preceded by the limitation of the air flow and the narrowing of the pharyngeal airway. Normal snoring sounds show a regular rattling character with dominant frequency components in the range of 100-600 Hz and minor components up to 1 kHz[5].

obstructive snoring

This pathological type of snoring (dominating in humans with the obstructive sleep apnea) is associated with repetitive temporal occlusion and opening of a strongly narrowed and collapsible airway. Obstructive snoring sounds are louder than normal snoring sounds and have fricative high-pitched quality. Typically, regular discrete peaks, i.e., spectral harmonics, can be observed in the frequency domain with the frequency components extending up to 2 kHz[5].

Simulated snoring

This kind of an intentionally provoked snoring is not preceded by flow limitation, even though preceded by an increase in the supraglottic resistance of the airway, at variance with the spontaneous snoring during sleep. The narrowing of the pharyngeal airway is probably produced by voluntary contraction of the pharyngeal constrictor muscles. The presence of the hysteresis loop has also been reported) Simulated snoring sounds resemble complex-waveform snoring (as described below) with multiple equally-spaced peaks of power in the frequency domain ranging up to 800 Hz[5].

waveform of snoring sounds in the time domain

Simple waveform snoring

This type of snoring shows a nearly sinusoidal waveform or a periodic waveform with a secondary deflection) over time with minor secondary oscillations. Consequently, only one up to three equally-spaced peaks (i.e., only a few harmonics) dominate in the frequency domain in the range of about 100-240 Hz while the first peak (at the lowest frequency) is usually the most prominent. The simple-waveform snoring probably results from the vibration of airway walls around their neutral position without the actual closure of the lumen (compare Figure 2-5a).

Complex waveform snoring

It is characterized by repetitive, equally-spaced segments in the time domain, whereas each segment starts with a large deflection and ends with a decaying wave. The repetitive segments arise with the frequencies in the range of about 6 Hz, thus the frequencies are lower than in the simple-waveform snoring. More rapid, secondary oscillations within each segment occur in the range of up to about 1,000 Hz. Therefore, a comb-like structure with multiple peaks of different amplitudes can be observed in the frequency domain.

Figure 2-6 illustrates normal snoring sounds in more detail, which were auscultated at the chest during sleep.
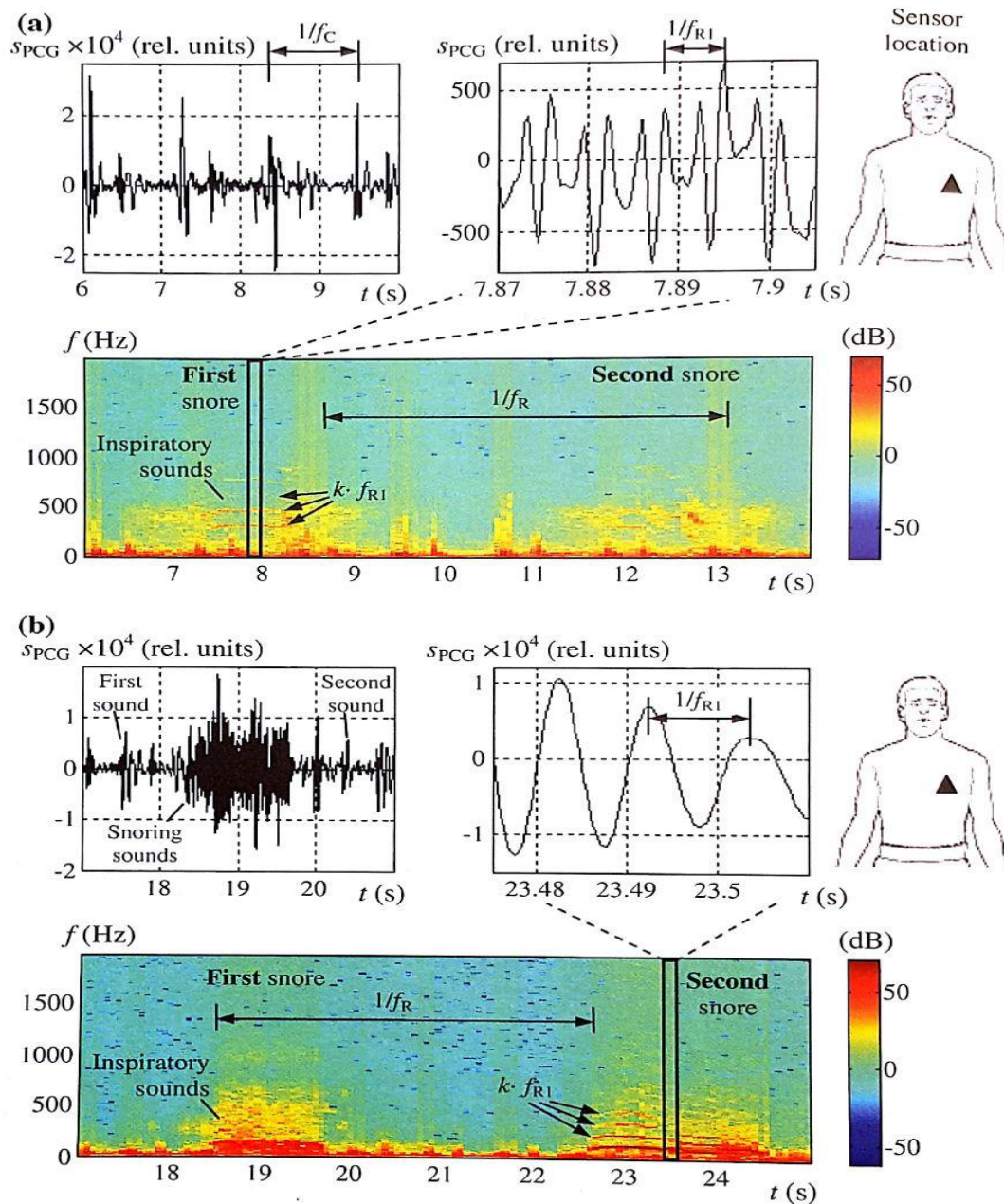
Figure 2- 6 Normal snoring sounds during sleep. (a) Relatively silent snoring from a male subject, as illustrated by an acoustic biosignal phonocardiogram SPCG from the chest region. (b) Relatively loud snoring from another male subject. A zoomed region of S_{PCG} with the duration of 35ms is given in each case at the time of a snoring event (right upper subfigure). The heart rate f_C and respiratory rate f_R are indicated. The corresponding spectrograms (lower figures) with shown fundamental harmonic frequency f_{RI} are given for comparison. For parameters of the spectrograms[5].

2.2.2 Apneic sound

There is strong evidence that obstructive snoring during sleep may be an intermediate symptom in the history of the sleep apnea syndrome. In particular, the obstructive sleep apnea is characterized by a complete occlusion of the upper airways and ceased breathing. The intermittent respiratory arrest is marked by intermittent absence of breathing sounds. i.e.. lung and snoring sounds, which yields a unique acoustical fingerprint of apneas among body sounds.

9

When an obstructive apnea terminates, a gasp for the air follows and very loud high frequency, explosive apneic sounds are usually induced by reopening of the collapsed airways at the tongue base. These inspiratory sounds appear to be highly different from regular, rattling snoring sounds in nonapneic subjects[5].

In the frequency domain, this snore shows a broad spectral peak at around 450 Hz and another one at around 1 kHz; both peaks probably raised by filtering and modification of the noise in the airway.

The acoustical fingerprint of obstructive sleep hypopnea characterized by a more reduction of the respiratory airflow is demonstrated in Figure 2-7.
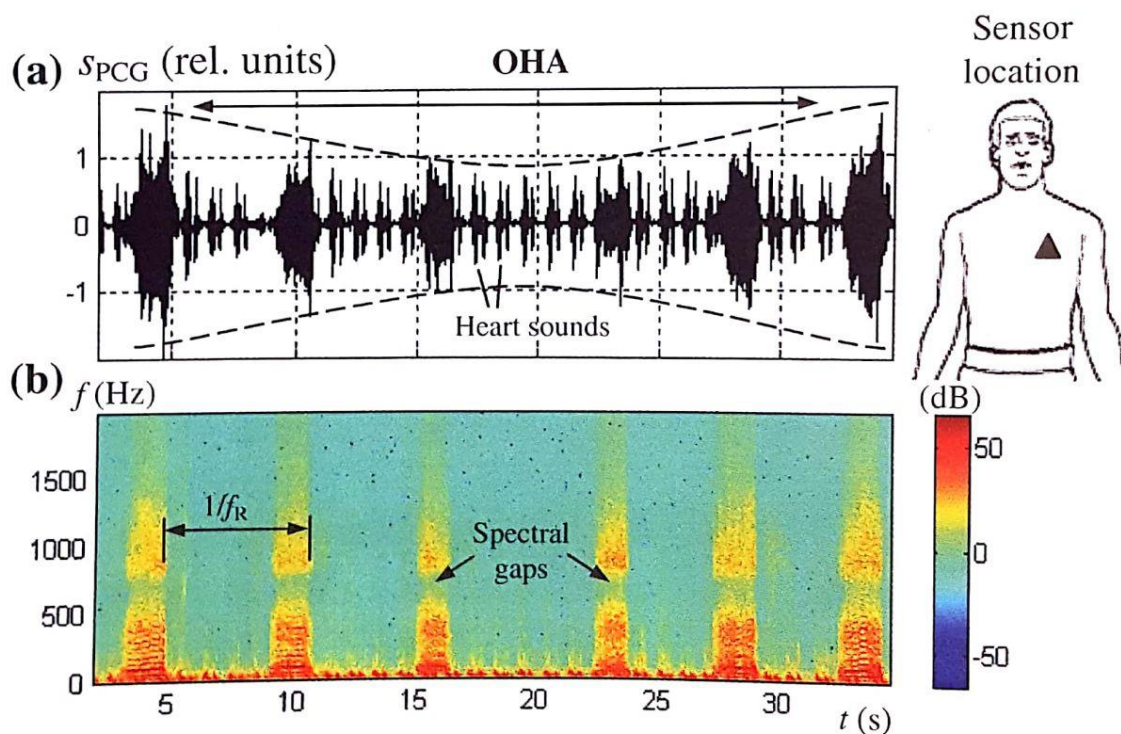
Figure 2- 7 Apneic sounds during obstructive sleep hypopnea (OHA). (a) Acoustic biosignal phonocardiogram SPCG from the chest region. (b) The corresponding spectrogram with indicated respiratory rate f_R[5].

2.3 Diagnosis and treatment of snoring

Guidelines for diagnosis and treatment of snoring as an isolated symptom are hard to find in the international literature. This may be explained by the difficulties in defining snoring, in objectively assessing snoring and treatment outcome, and in the lack of well-controlled clinical trials concerning the treatment of this phenomenon. In 2010, the German Society of Otorhinolaryngology, Head and Neck Surgery published the S1 guideline: Diagnosis and Treatment of Snoring in Adults .This guideline has been revised and updated in the present S2k guideline.

In accordance with the International Classification of Sleep Disorders ICSD-2, snoring can be diagnosed under the following circumstances:

- The subject or the bed partner complains about respiration-dependent acoustic phenomena, usually related to inspiration. Objective parameters defining these sounds as "snoring" are lacking.
- The subject does not complain about insomnia or hypersomnia that can be attributed to the snoring.
- Sleep testing shows no signs of sleep-disordered breathing.

2.3.1 Clinical presentation

The snorers (or the bed partners) complain about socially disruptive snoring. The degree of annoyance is essential in the evaluation of snoring and is highly dependent on the bed partner. Furthermore, those affected by snoring often complain about a sore throat and nocturnal awakenings due to his or her own snoring. Due to the high prevalence of snoring, it often occurs simultaneously but independent of a sleep disorder (e.g., snoring and insomnia).

2.3.2 Diagnostic measures

From a diagnostic point of view, snoring is often accompanied by obstructions of the upper airway, and therefore, a strict differentiation between snoring and snoring as a symptom of OSA is not easy to make. Often pathological structures along the upper airway may be the reason for snoring with or without obstructions of the upper airway. Standardized diagnostic measures are listed below. Additional measures may be performed individually, for example, prior to a certain treatment. All diagnostic measures are comprised in an algorithm[6], which can be found in Figure 2-8.
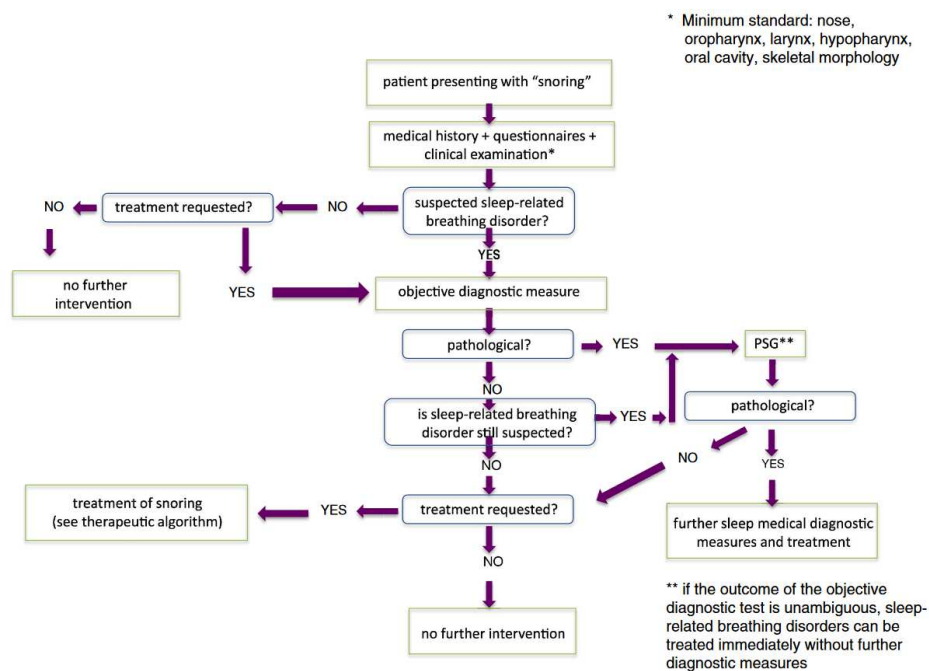
Figure 2- 8 Algorithm of diagnostic measures [11].

Medical history

I. Specific evaluation of snoring (selection):

- Timeline of complaints (e.g., every night, intermittently)
- Occurrence during night (permanently/intermittently, related to body position)
- Causative situations or risk factors (e.g., alcohol or nicotine consumption, presence of allergic or nonallergic rhinitis, nasal obstruction)
- Manner of snoring (e.g., regular or irregular frequency, loudness, character of sound)

II. Sleep medical history (selection):

- Insomnia
- Nocturnal awakenings (e.g., associated with shortness of breath)
- Lack of concentration during the daytime
- Daytime sleepiness
- Reduction in overall performance
- Complaints of dry mouth or headaches in the morning

III. Relevant comorbidities (selection)

- Cardiac and vascular diseases (e.g., hypertension, arrhythmia, myocardial infarction, stroke)
- Overweight or obesity
- Diabetes

2.3.3 Clinical examination

The aim of clinical examination is to identify changes in the upper airway that may cause snoring or obstructions of the upper airway. As with a medical history, the results of the clinical examination may be very similar in snorers and those with obstructions of the upper airway. Anatomical findings of the upper airway may cause snoring with or without obstruction of the upper airway.

1. Nose/nasopharynx
   The following structures should be examined:
   - Bony and cartilaginous nasal skeleton
   - Nostrils
   - Nasal septum
   - Nasal turbinate
   - Meatus of the nose
   - Nasopharynx
2. Oropharynx
   - Size and position of the base of the tongue
   - Size of the tonsils
   - Size and position of the soft palate
   - Size and position of the uvula
3. Larynx/hypopharynx/neck
4. Oral cavity/dentition
5. Facial skeleton

6. Technical diagnostic measures
7. Drug-induced sleep endoscopy
8. Pressure sensors
9. Sleep testing
10. Acoustic analysis

2.3.4 Acoustic analysis

The snoring addressed in this guideline usually consists of low frequencies (<500Hz), whereas obstructive events associated with OSA usually comprise frequencies above 500Hz. Current knowledge finds that lower frequencies originate from vibrations of the soft palate and the uvula. Higher frequencies occur if there is partial or complete airway collapse. Highly collapsible oropharyngeal structures (e.g., tonsils, base of the tongue, lateral pharyngeal walls) are considered to be the origin of snoring sounds [3,33–38]. If an acoustic analysis of snoring sounds is considered, it should be performed via air conduction to record frequencies over 1,000Hz correctly [39]. Microphones with body contact or snoring analysis with the help of pressure transducers lead to a reduction of intensities above 1,000Hz. To date, acoustic analysis of snoring is not a standardized diagnostic measure. Due to improved polygraphic or polysomnographic recording and analysis, acoustic analysis may provide valuable information in the future to differentiate snoring. The commonly used snoring indices as assessed with outpatient recordings or polysomnography (PSG) currently are not validated or comparable, so they cannot be used for qualitative or quantitative snoring assessment.

2.4 Therapeutic principles

The snoring addressed in this guideline is not a disease associated with medical hazard, and generally, there is no medical indication for treatment. However, given the recent data that shows snoring as a potential risk factor for developing OSA, cardiovascular diseases, and increased mortality, this estimation may change in the future. Currently, there is no evidence that early treatment for snoring in adults can prevent progression to OSA or lower cardiovascular risk. Consequently, snoring is not treated unless the snorer requests treatment. Therapeutic principles are summarized in an algorithm that is presented in Figure 2-9.
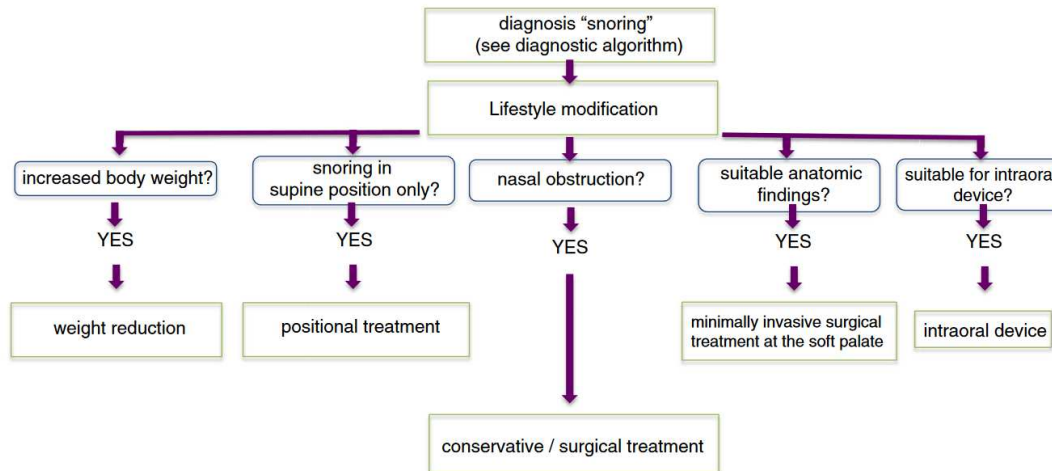
Figure 2- 9 Algorithm of therapeutic principles [11].

2.4.1 Intraoral devices

The Mandibular advancement splint is a custom-made 2-piece device (Somnomed Ltd, Australia) with vertical extensions on the lower component and ramps on the upper component which induced a forward mandibular posture Figure 2- 10 [7].

Figure 2- 10 Upper and lower plates of the mandibular advancement splint [12].

mandibular protrusion mobility side effects documented in OSA, such as hypersalivation and discomfort or pain in the masticatory muscles or the temporo-mandibular joint , potential dental side effects, Evaluations of thermoplastic (boil-and-bite) devices have been controversial, especially regarding efficiency and stability [8].

2.4.2 Pillar procedure

The Pillar Procedure is a minimally invasive treatment for snoring and obstructive sleep apnea. In the United States, this procedure was FDA indicated in 2004[9]. During this procedure, three to six Dacron (the material used in permanent sutures) strips are inserted into the soft palate

Figure 2-11, using a modified syringe and local anaesthetic. While the procedure was initially approved for the insertion of three "pillars" into the soft palate, it was found that there was a significant dosage response to more pillars, with appropriate candidates. As a result of this outpatient operation, which typically lasts no more than 30 minutes, the soft palate is more rigid, possibly reducing instances of sleep apnea and snoring. This procedure addresses one of the most common causes of snoring and sleep apnea vibration or collapse of the soft palate (the soft part of the roof of the mouth). If there are other factors contributing to snoring or sleep apnea, such as conditions of the nasal airway or an enlarged tongue, it will likely need to be combined with other treatments to be more effective[9].
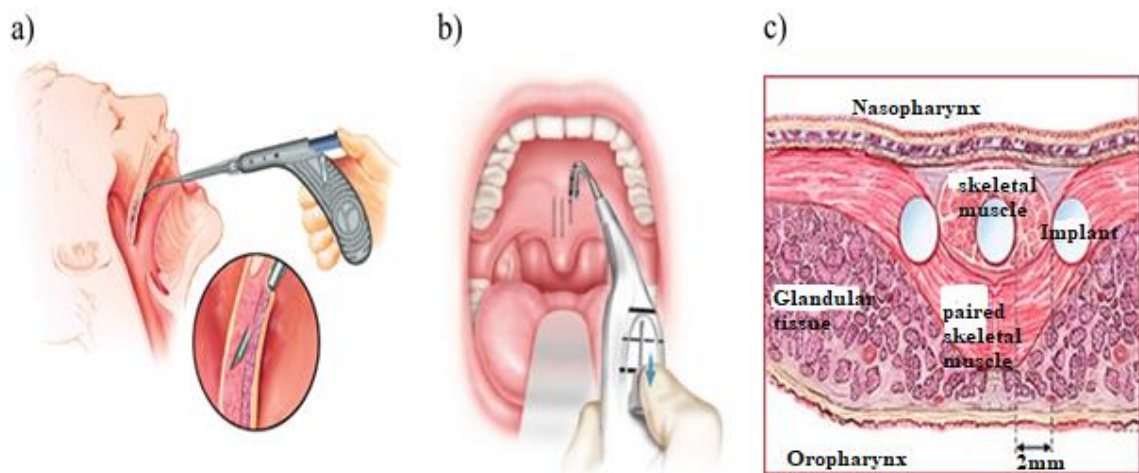
Figure 2- 11 Pillar procedure to increase stiffness of soft palate a) lateral section of pillar insertion b) frontal view positioning of pillar Dacron's c) soft palate section and positioning of pillar Dacron's [14].

2.4.3 Orthopedic pillows

Orthopedic pillows are the least intrusive option for reducing snoring. These pillows are designed to support the head and neck in a way that ensures the jaw stays open and slightly forward Figure 2-12. This helps keep the airways unrestricted as possible and in turn leads to a small reduction in snoring.

A reduction of snoring, both with and without OSA, has been demonstrated with this change in position. However, techniques for avoiding the supine position are accompanied by low long-term compliance due to the discomfort and disturbed sleep quality when turning from one side to the other [10].
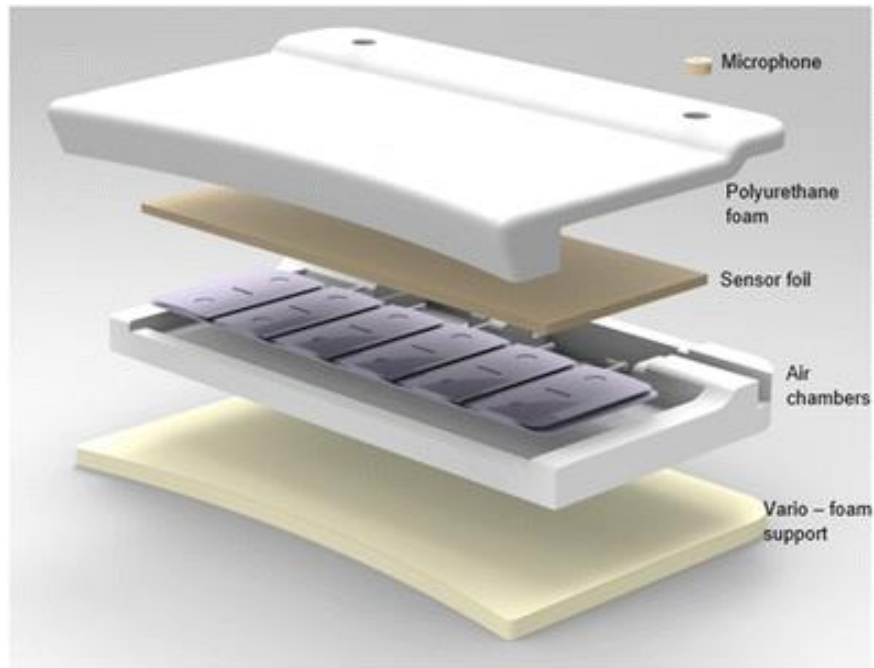
Figure 2- 12 Structure of the Basic Sissel pillow model, The pillow Sissel ® (Sissel Novacare, Bad Dürkheim, Germany) is made of polyurethane foam, has two integrated microphones, a sensor foil for detecting the head position on the pillow, and 2 × 6 air chambers, w which can be individually targeted by a pneumatic system [10].

2.4.4 Positive airway pressure

A continuous positive airway pressure (CPAP) machine is often used to control sleep apnea and the snoring associated with it. It is a relatively safe medical treatment. To keep the airway open, a device pumps a controlled stream of air through a flexible hose to a mask worn over the nose, mouth, or both. A CPAP is usually applied through a CPAP mask which is placed over the nose and/or mouth. The air pressure required to keep the airway open is delivered through this and it is attached to a CPAP machine which is like an air compressor. The effective treatment of obstructive sleep apnea can decrease Sympatico onia and, consequently, blood pressure. Furthermore, it can improve inflammatory and metabolic parameters resulting in a decreased cardiovascular risk[11]. As OSA reflects counteracting forces of the upper airway dilating muscles and an imbalance of the intra-pharyngeal pressure present in inspiration, CPAP neutralizes this by applying a continuous positive pressure through a nose mask (Figure 2-13) [12].
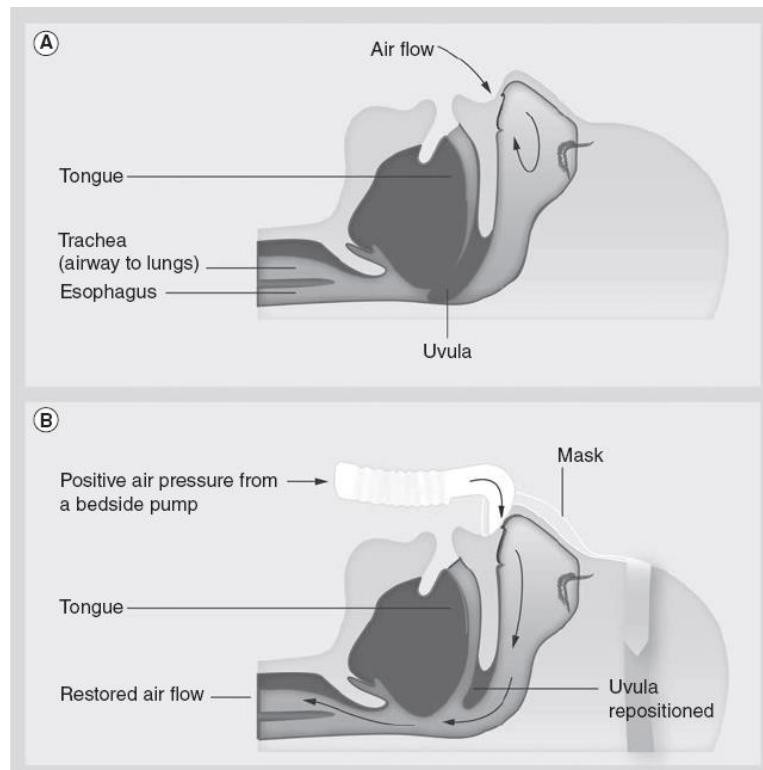
Figure 2- 13 Continuous positive airway pressure. (A) Obstructive sleep apnea. (B) Continuous positive airway pressure opens airway [17].

The air that CPAP delivers is generally "normal air" – not concentrated oxygen. The machine utilizes the air pressure as an "air splint" to keep the airway open. In obstructive sleep apnea, the airway at the rear of the throat is prone to closure.

2.4.5 Palatal implant surgery

This therapy is a novel palatal surgery combined with uvulopalatopharyngoplasty (UPPP) and radiofrequency ablation of the inferior turbinate for the treatment of moderate to severe obstructive sleep apnea [13] .The graft materials for the soft palate support are titanium mesh and titanium screws. The titanium mesh is cut and ground into an inverted ''U''-shaped soft palate support part with one end that could be fixed to the hard palate (Figure 2-14). Its dimensions are length 40 mm; width 25 mm; thickness 0.5 mm. The diameter of the titanium screw is 2 mm and its length 4 mm. Graft materials are routinely disinfected before later use.

Figure 2- 14 The soft palate implant graft [24].

A curved transverse incision is made at the center 10 mm above the junction of the soft and hard palate. The soft palate support part is implanted in the soft palate with the middle part of the inverted ''U'' facing upward and adhering closely to the hard palate (Figure 2-15).
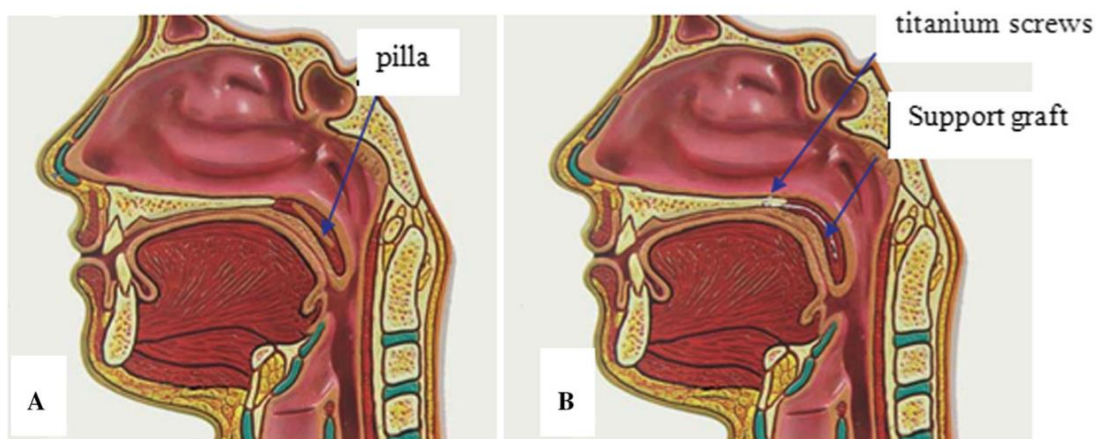
Figure 2- 15 Comparison of the Pillar implant and the soft palate implant support surgery [18].

Two titanium screws were placed through the holes for fixation, and the incision was then sutured. The procedures of surgery and graft placement are summarized in Figure 3-16 as follows: Figure 2-16a (top left): the mimic used for superimposition of graft surgery procedure Figure 2-16b (top right): position of the initial incision; Figure 2-16c (bottom left): incision and graft insertion positions, and Figure 2-16d (bottom right):

Figure 2- 16 Surgery and graft placement. a Top left the mimic used for superimposition of graft surgery procedure. b Top right position of the initial incision. c Bottom left incision and graft insertion positions. d Bottom right after closure [24].

2.4.6 Radiofrequency techniques in treatment of sleep-disordered breathing

Radiofrequency (RF) tissue volumetric reduction was developed to reduce tongue-based obstruction by way of an outpatient, minimally invasive procedure using local anesthesia and causing minimal discomfort with a low complication rate. The research to bring this technique to fruition demonstrated the usefulness of temperature-controlled RF for other areas of the upper airway. Radiofrequency may be used to treat nasal obstruction by reducing the size of the inferior turbinate. Soft palatal reduction is an alternative treatment for primary snoring, upper airway resistance syndrome, and mild obstructive sleep apnea syndrome.

The RF energy ablation of soft tissues has been applied successfully, in the past, to humans by specialists in the fields of cardiology, neurology, oncology, and urology [14-17]. Temperature-controlled RF delivers RF at 460kHz by a high-frequency alternating current flow into the tissue, creating ionic agitation. This ionic agitation heats the tissue and as the temperature rises higher than 47°C, protein coagulation and tissue necrosis ensue. In the first study evaluating RF for sleep-disordered breathing, a porcine study [18] evaluated the relationship of lesion size to total RF energy delivery and subsequent tissue volume reduction. Heat is transported by way of conduction to tissue farther away from the electrode and extends the size of the lesion. The computer algorithm controls the power to maximize the lesion size, resulting in tissue coagulation with no charring. The healing process was analyzed through a serial histologic analysis in the porcine model and demonstrated favorable wound healing with a well-defined lesion after 24 hours, with an acute inflammatory response and edematous response. Collagen deposition begins approximately 12 days after injury, and at 3 weeks, chronic inflammation, fibrosis, and tissue volume reduction from scar contracture occur [18].

The first human clinical study evaluating the use of RF was in the soft palate for snoring and sleep-disordered breathing, and the investigators concluded that the technique was safe with minimal complications, and bleeding, infection, speech disturbances, and swallowing problems were not observed. Results of RF for snoring reduction revealed that the pretreatment snoring level was reduced by an overall mean of 77%[19]. The safety and efficacy reported in the previous animal study were confirmed in the human palate.

2.4.6.1 Radiofrequency devices

The medical RF device (Gyrus ENT LLC, Memphis, TN) is delivering at 460 kHz signals using an RF generator with custom-fabricated needle electrodes. The essential RF energy parameters of power (watts), temperature limits (Celsius), resistance (Ohm), treatment time (seconds), and total energy delivery in joules (watt x seconds) are controlled by a computer algorithm. The necessary feedback for temperature adjustment is provided by multiple micro thermocouples embedded along the electrode. The 22-gauge RF electrodes have a 10-mm active tip. A protective thermal sheath is used on the proximal portion of the electrode to eliminate surface damage. The maximum temperature gradient is regulated to less than 90°C, with a target temperature between 80°C to 85°C. The computer algorithm maximizes the RF lesion size.

2.4.7 Classification of disease severity before therapy

The understanding of the classification of sleep-disordered breathing is shown in Table 2-1.

Table 2- 1 Classification of disease severity before therapy [20].

	Primary snoring	Upper airway resistance syndrome	Obstructive sleep apnea syndrome
AHI* events per hour	< 5	<5	>5
SaO2 during sleep	<90%	>=90%	<90%
peak negative end-inspiratory esophageal pressure or inspiratory nadir (Pes)	Less negative than -10 cm H_2O	more negative than -10 cm H_2O	-
excessive daytime sleepiness	-	2/3 of patients	Most of patients

*AHI = Apnea–Hypopnea Index

Locational classification of upper airway in RF treatment

In order to cover upper airways treatment, three main regions are considered:

- nasal obstruction
- soft palatal obstruction
- hypopharyngeal obstruction
- Tongue-base

In the following each region and related disorder and treatment methods will be discussed.

3.4.7.1 nasal obstruction

The pathophysiology of nasal obstruction causing upper airway collapse is an increased nasal resistance, an increased velocity of air flow, an increased negative intraluminal pressure, and resultant partial obstruction and vibration of tissues of the upper airway predisposed to collapse, including the soft palate, tongue, and lateral pharyngeal walls.
Nasal obstruction may be caused by nasal rim or nasal valve collapse, septal deviation, adenoid hypertrophy, nasal polyps or tumors, and inferior turbinate hypertrophy. If inferior turbinate hypertrophy is the cause of the nasal obstruction, RF is an excellent treatment modality. The

technique can be performed on an outpatient basis with local anesthesia, with a minimal risk of post-treatment complications and minimal discomfort.

The rationale for nasal surgery is to improve nasal patency, which establishes physiologic breathing and minimizes oral breathing during sleep. Oral breathing during sleep causes the tongue to be positioned posteriorly, increasing the risk of upper airway obstruction. Also, resolving nasal obstruction reduces nasal resistance and improves the negative intraluminal pressure, which generates upper airway collapse.

2.4.7.2 Inferior turbinate radiofrequency indications

Nasal obstruction is caused by inferior turbinate enlargement. Radiofrequency can be used along the entire length of the inferior turbinate, depending on the location and magnitude of the turbinate hypertrophy. This technique has been attempted by the author for the middle turbinate, but because the thickness of the submucosa is much thinner than the inferior turbinate, direct surgical excision is the preferred technique for a concha bollosum or middle turbinate hypertrophy [18].
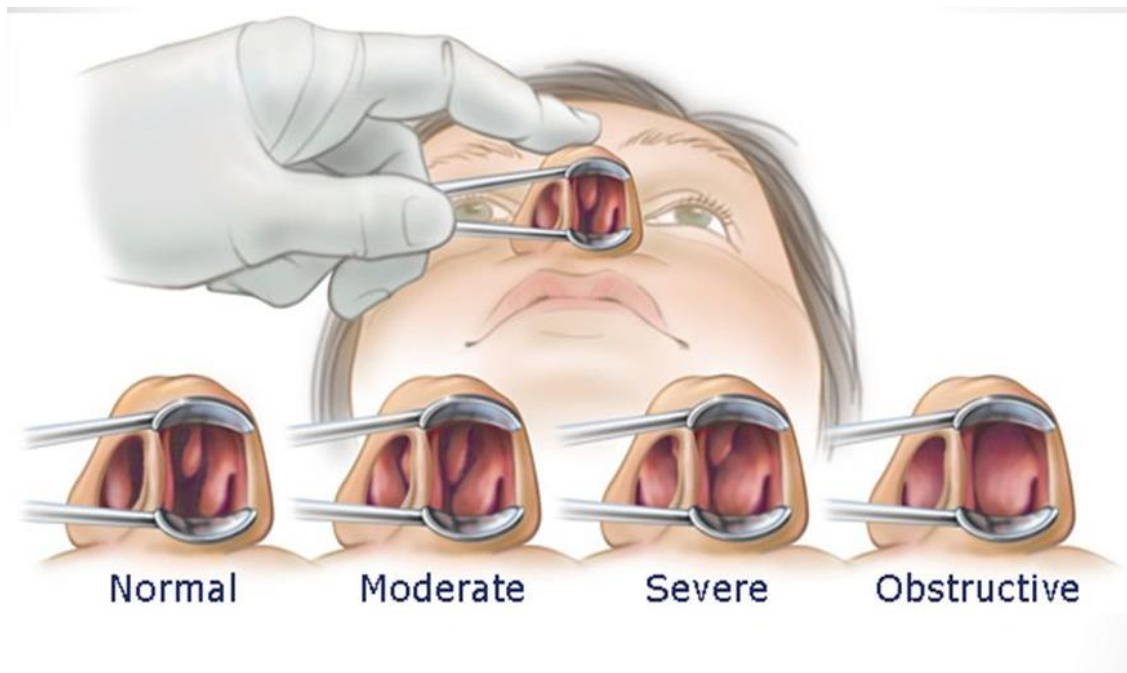
Figure 2- 17 Turbinate hypertrophy [31].

Submucosal coagulation through radiofrequency-induced thermotherapy of the inferior turbinate (RFITT) (Figure 2-17) can improve nasal passage by means of a minimally invasive procedure causing shrinkage of turbinate volume. Several studies have shown that mucus ciliary function also remains intact with RFITT [20]. Radiofrequency of the inferior turbinate can be performed on an outpatient basis.
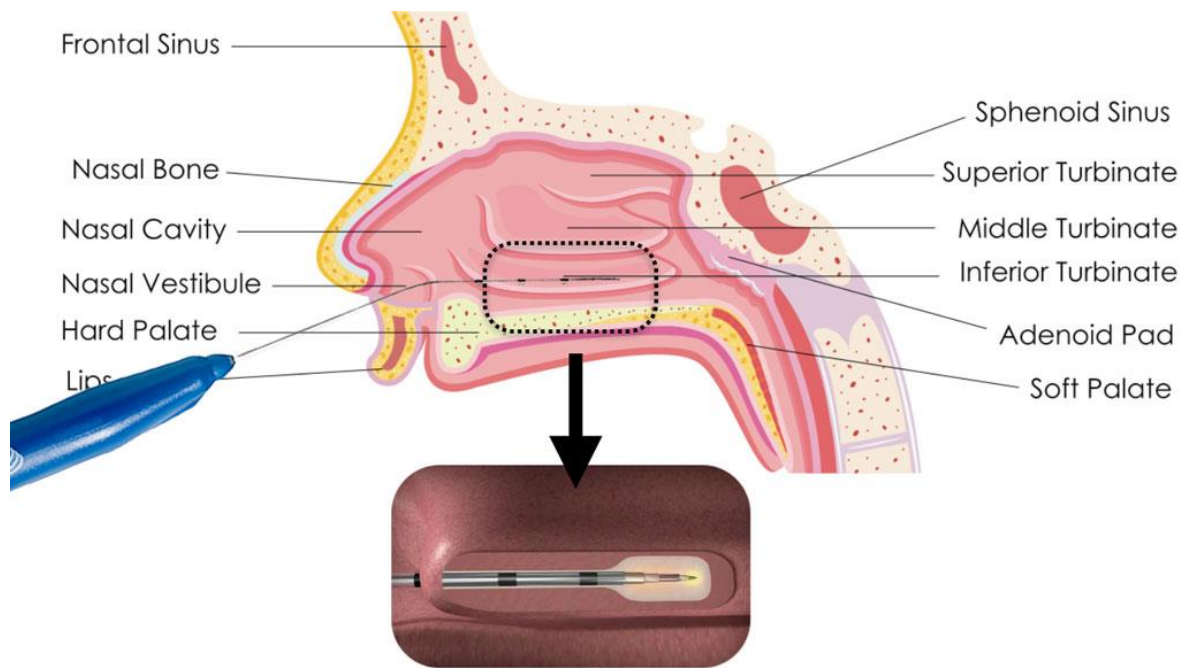
Figure 2- 18 Inferior turbinoplasty with RF ablation [32].

Powell et al. did the RF ablation by a mean of 413 J of RF energy was delivered to each inferior turbinate. The investigators discovered an overall reduction in size of the inferior turbinate by 27% on a four-point scale (n =17) compared with the VAS subjective patient improvement of nasal patency [18].

Therefore, Inferior turbinate RF is a technically simple, minimally invasive procedure that can be performed as an outpatient procedure under local anesthesia with improved nasal obstruction, minimal side effects, and unchanged ciliary and mucous properties.

2.4.7.3 soft palatal obstruction

Patients with primary snoring seek treatment because of the social annoyance and disruption of sleep of a bed partner. The etiology of primary snoring in approximately 85% of patients is partial airway obstruction from soft palatal redundancy causing tissue vibration, with resultant sound production[21].
The initial procedure devised to address primary snoring was the Uvulopalatopharyngoplast. The recommended maximum amount of energy delivered to the superior midline soft palate is 750 J; the recommended maximum amount to the uvular base and the paramedian areas is 350 J. In patients with a long uvula, sharp amputation of the uvular tissue up to the muscle reflection may improve the success rate without any additional post-treatment discomfort.
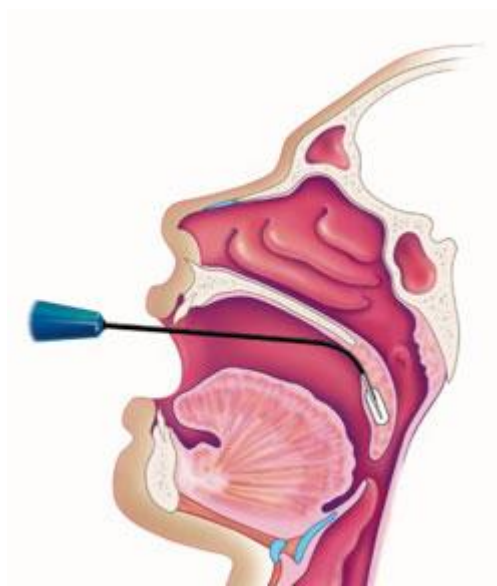
Figure 2- 19 Lateral section of RF ablation insertion inside the soft palate [33].

The soft palate from the uvular base to the posterior nasal spine and the paramedian area extending approximately 2cm laterally from the midline is selected for treatment. The RF energy delivery maximizes the size of the lesion. A 22-gauge RF needle electrode in a custom-fabricated device allows placement of the electrode under the palatal mucosa in the area selected for treatment. This electrode is bent with a crimping tool on an individual patient basis to contour to the curvature of the soft palate Figure 2- 19.
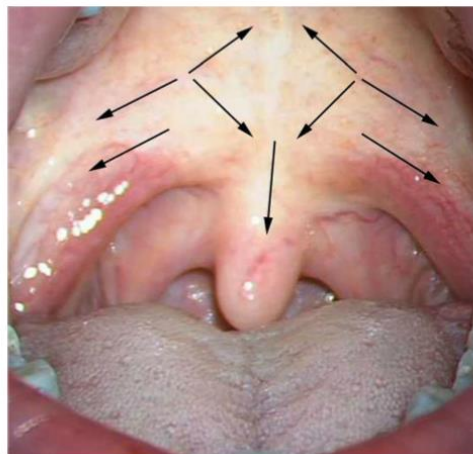
Figure 2- 20 Position of palatal punctures for the RFT: one median, six paramedian and two lateral punctures [33].

Two sessions of RFT (Radiofrequency treatment) with nine lesions to the soft palate significantly improved OSAHS patients ' AHI and HRQoL. RFT protocol with nine lesions

Figure 2-20 to the soft palate seems to be an effective and safe treatment modality associated with low morbidity in selected mild to moderate OSAHS patients [22].

2.4.7.4 hypopharyngeal obstruction

The pathophysiology of sleep-disordered breathing is collapse or obstruction of the upper airway during sleep. This obstruction may be partly or entirely due to the hypopharynx, and there are preoperative factors that may suggest the hypopharyngeal area as a site of collapse. Once the hypopharynx is suggested to be a site of collapse of the upper airway in sleep-disordered breathing, determining reconstructive procedure is the next step. Tongue-base RF is an alternative treatment to decrease the volume of the tongue and to improve the posterior airway space.

2.4.7.5 Tongue-base radiofrequency treatment

Patients diagnosed with obstructive sleep apnea for whom the preoperative evaluation suggests tongue-base collapse as the cause of the hypopharyngeal obstruction are candidates for RF. A single or dual-channel tongue probe may be selected to deliver the RF energy. If the dual-channel probe is selected, the author prefers to bend the probe proximal to the retractable sheath to separate the two RF lesions farther apart. Potential sites of treatment include the midline, paramedian, and ventral tongue areas Figure 2-21.
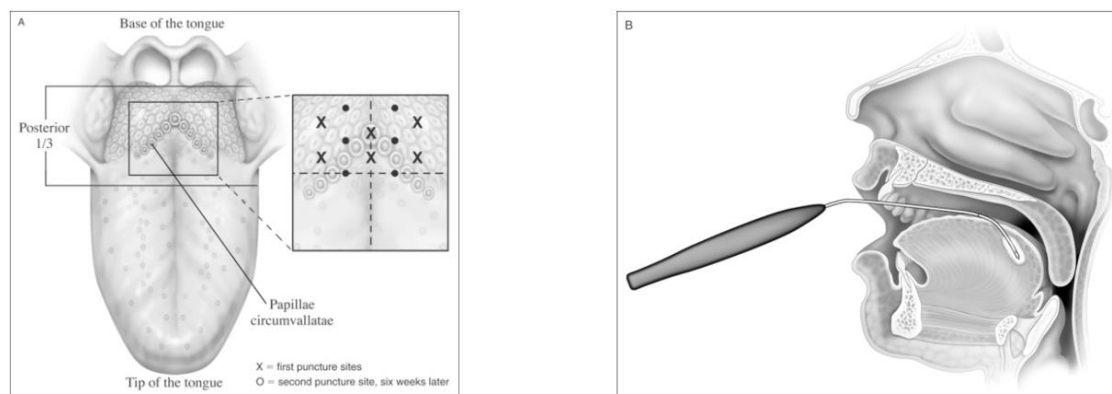
Figure 2- 21 Radiofrequency ablation puncture sites. Energy was delivered with an exclusive needle device through the dorsal surface of the tongue after the initial surgical procedure, on indication a second and sometimes third additional RFT was performed [34].

2.4.7.6 Tonsil RF ablation

Over the last 10 years, surgeons have recognized the advantages of minimizing injury to the tissues surrounding the tonsillar fossa and have described procedures to preserve the overlying mucosa to avoid or lessen the problems associated with complete tonsillectomy. Nelson determined that the tonsil volume shrinks by 30%–70% after RF ablation and that this technique is superior to cold-knife tonsillectomy in terms of postoperative pain and complications [23]. RFITT also allows the shrinkage of oversized tonsils under local anesthesia. However, that comes in adults are rare. In the frequently affected children with oversized tonsils tonsillectomy (Mandel reduction) is preferred in general anesthesia.

2.5 RF frequency and real time impedance monitoring

The main goal of this project is volumetric tissue reduction of upper airways which is discussed in the previous section by RF in the range of 4MHz via real time impedance measuring. There are some reason to choose the 4MHz as a working frequency based on theoretical and clinical experiments which are discussed in the following.

2.5.1 Clinical approaches to choose a desire RF frequency

Based on a research on Comparative study of four radiofrequency generators for the treatment of snoring by Blumn et la. Radiofrequency decreased the snoring sound intensity from 7.9 ±1.7 to 4.4 ±2.7 (P< 0.0001). The four radiofrequency generators had a statistically comparable efficacy. The generator with 4MHz caused less discomfort and required less anti-inflammatory drugs [2].

Four radiofrequency generators were compared (Table 3-2). Radiofrequency parameters were determined according to the distributor's/manufacturer's instructions, except for the Somnus generator for which higher energy doses were delivered (700 J vs 350 J), based on a study conducted in one of the departments (not published) that revealed no difference in terms of discomfort or pain between the two energy doses. Treatment parameters are shown in Table 3-3.

Table 2- 2 Characteristics of the four RF generator [36].

Characteristics of the four RF generators					
Generator	Wavelength	Feedback control	Action	Mode	Use
Coblator	100 kHz	No	Co+Se	B	S
Ellman	4 MHz	No	Co+Se	M	S
Select Sutter	470 kHz	No	Ce+Se	B	Re
Somnus	476 kHz	Yes	Co	M	S

Coblator (Arthrocare Corp, Sunnyvale, CA); Ellman (Oceanside, NY), Select Sutter (Fribourg, Germany), Somnus (Gyrus, Memphis, TN).
Co, coagulation; Se, section; B, bipolar; M, monopolar; S, single use; Re, sterilizable.

Table 2- 3 RF treatment parameters [36].

RF treatment parameters			
	Application time (seconds)	Power	Energy (Joules)
Coblator	14	5	
Ellman	30	20	
Select Sutter	9	2	
Somnus	Variable	15 W max	750

W, watts.

Results on snoring were comparable for the four generators (Ellman, Select Sutter, Coblator, Somnus), with different technical characteristics in terms of snoring sound intensity and level of satisfaction. In terms of safety, the Ellman generator induced less discomfort and required less anti-inflammatory drug intake than the other three generators [2].

2.5.2 Theoretical approaches to select a desire RF frequency

Frequency dependent behavior of the tissue impedance is an important issue. The most well-known model for representing a tissue's electrical characteristics is the three-element model depicted in Figure 2-22. It is a simple and easy model to understand from a biological aspect. This model was reported to be a good representation of the electrical properties of biological materials due to relaxation phenomena throughout the frequency range [2]. The simplified equivalent three-element model was applied for the interpretation of the electrical properties of biological tissues, with R_e (extracellular resistance), R_i (intracellular resistance), and C_m (membrane capacitance). R_e is contributed by the extracellular matrix (which is made up of mostly water), R_i by intracellular complex substances of the cytoplasm, and C_m by changes in cell membranes [24].
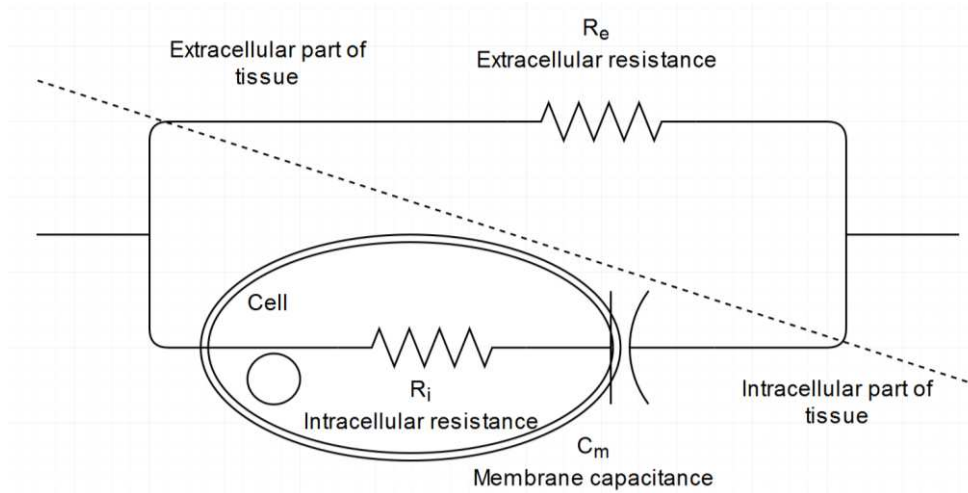
Figure 2- 22 The simplified equivalent three-element electrical circuit model for tissues. The simplified equivalent three-element model to interpret the electrical properties of biological tissues, with R_e(extracellular resistance), R_i (intracellular resistance), a and C_m (membrane capacitance) [24].

Impedance (Z), from an electrical point of view, is the obstruction to the flow of an alternating current and, hence, is dependent on the frequency of the applied current, defined in impedance magnitude ($|Z|$) and phase angle (φ) as shown in Equations (1) – (3)[25]. Bioimpedance is a complex quantity composed of resistance (R) which is caused by total body water and reactance (X_c) that is caused by the capacitance of the cell membrane.

$$Z = R_e. \ (R_i + jX_c \ )/ \ R_e + R_i + jX_c \tag{1}$$

$$|Z| = \sqrt{R^2 + Xc^2} \tag{2}$$

$$\varPhi = \tan^{-1}(X_c/R) \tag{3}$$

Resistance of an object is determined by a shape, that is described as length (L) and surface area (A), and material type, that is described by resistivity (ρ), as shown in Equation (4). Reactance (X_c) of an object as shown in Equation (5), is defined as resistance to voltage variation across the object and is inversely related to signal frequency (f) and capacitance (C). In biological systems resistance is caused by total water across the body, and reactance occurs due to the capacitance of the cell membrane.

$$R = \rho \ L/A \tag{4}$$

$$X_c = 1/2\pi fC \tag{5}$$

Capacitance (C) is defined as the ability of the non-conducting object to save electrical charges, that is equal to the ratio between differentiation in voltage across object (dV/dt) and current that is passed through the object (I(t)), as shown in Equation (7)[25]. In the parallel capacitor module, capacitance is in direct proportion to the surface area (A) in meters square and inversely proportional to distance (d) in meters between the charged plates, and is dependent on the permittivity constant of vacuum ($\varepsilon_0 \approx 8.854 \times 10^{-12}$ F·m^{-1}) and the relative dielectric permittivity constant (ε_r) that is defined based on the material between the plates (for a vacuum space, $\varepsilon_r = 1$), as shown in Equation (6) [25]:

$$C = \varepsilon_0 \varepsilon_r A / d \tag{6}$$

$$C = (dV(t)/ dt)I(t) \tag{7}$$

Body composition estimation using bioimpedance measurements is based on determination of body volume (V_b) through the basic means of resistance measurement. From Equation (4) that gives the relation between resistance and ratio of length (L) to surface area (A), body volume (V_b) can be obtained by substituting the surface area (A) with the numerator and denominator of the length (L), as in Equation (8):

$$V_b = \rho L^2 / R \tag{8}$$

2.5.3 Bioimpedance Spectroscopy

Analysis of bioimpedance data obtained using a broad band of frequencies is known as bioimpedance spectroscopy (BIS). The BIS method is based on the determination of resistance at zero frequency (R_0) and resistance at infinite frequency (R_{inf}) that is then used to predict ECF and TBW, respectively [26].
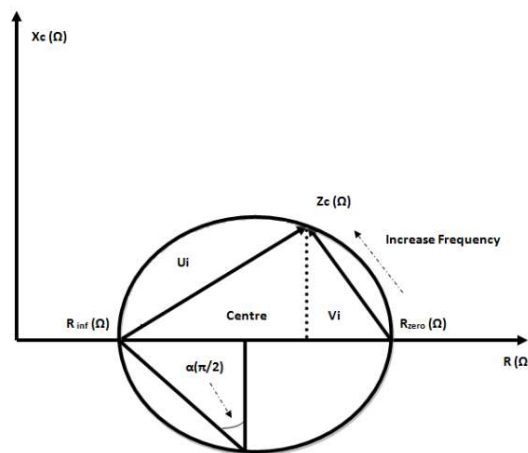
Figure 2- 23 Module plot and Cole module parameters [39].

As can be seen in BIS by increasing frequency the capacitive reactance changes and then the final impedance will be decreased Figure 2-23. In other words current can pass through both intra and extracellular space which means lower impedance based on the electrical model and relaxation effect [24].

By summarizing above mentioned electrical impedance properties of the tissue a lower current density as a result of the lower impedance is needed to ablate the tissue. In other words, the lower current density leads a lower and more controlled thermal effect in ablative tissue and less thermal distribution to the adjacent tissue. Therefore, a very focused and directed ablation region facilities the healing process and recovery time which was discussed in previous section by 4MHz Elman generator [2].

2.6 Clinical recommendation for RF volumetric tissue reduction procedure

The soft palate is sprayed with 20% benzocaine as a topical anesthetic. A local anesthetic as a gel (2% lidocaine) is placed on a cotton-tipped applicator at the initial soft palatal injection site. A 27- or 30-gauge needle is used to inject 2.0 mL of 0.25% bupivacaine (Marcaine) 1:100,000 with epinephrine at this superior palatal midline site. The local anesthetic diffuses over approximately 5 to 7 minutes caudally, making additional inferior and lateral injections nearly painless. The soft palate from the uvular base to the posterior nasal spine and the paramedian area extending approximately 2 cm laterally from the midline is selected for treatment [21].

To diminish the risk of infection, the following precautions can be taken:

(1) Pre-treatment with oral antibiotics, usually cephalexin, and a 3-day prophylactic antibiotic course;
(2) Instructing the patient to gargle with 0.12% oral chlorhexidene (Peridex) for at least 1 minute immediately before treatment;
(3) Use of sterile technique as much as possible;
(4) Use of a new sterile needle with each injection site;
(5) Avoidance of steroids, which may lower the immune response;
(6) Ensuring that the electrode is seated completely into the tongue or soft palate musculature to prevent a superficial ulceration
(7) Checking the curvature of the tongue or palate base to prevent the electrode tip from being placed close to the superficial aspect of the tongue
(8) Wiping the [21]electrode tip using sterile technique between treatment lesion sites to remove debris
(9) Not delivering greater than 1000 J of energy per treatment site
(10)   Considering other treatment alternatives in patients with diabetic mellitus

Following these recommendations limits the incidence of tongue superficial ulcerations and infection

2.7 Theoretical background

2.7.1 Historical aspects from beginning to now

One of troublesome issues in surgery is bleeding in operation area, to avoid bleeding during operation, there are different methods, and a common method is utilizing thermal biological effects of high frequency current which is called electrosurgery (diathermy).

For hundreds of years, heated metal was used to burn or destroy tissue and control bleeding. Heating the metal was originally accomplished with fire; later the metal was heated with electricity, and this procedure was termed electrocautery. Electrocautery involves passage of a current through a filament. The filament resists the flow of current and becomes red-hot. The disadvantage of electrocautery is that its use on human tissue results in a third degree burn with scarring and prolonged healing [27].

From 1889 D'Arsonval did the first research on the physiological effects of alternating current on the body. He discovered that currents with frequency over 5,000 Hz did not cause the muscular contractions and nerve stimulation effects of electric shock. Instead they seemed to have beneficial effects. He pioneered the therapeutic application of high frequency current to the body, founding the field of electrotherapy. He developed a spark-excited resonant circuit to generate currents of 0.5-2 MHz called "D'Arsonval currents" for therapy, which became known as "D'Arsonvalization". It was later used for diathermy[28] .

In 1892, Arsene d'Arsonvall failed in his attempt to cause neuromuscular stimulation or tetanic response in humans by application of electric currents with frequencies greater than 10,000 Hz. In 1899, Oudin modified d'Arsonval equipment and was able to generate sparks that caused superficial tissue destruction. In 1907, de-Forest invented a radio tube known as the triode that amplified and modified electrical output[27].

As of 1970 the technique which was used to manufacture such devices, was spark-excited resonant circuit. They used spark solenoids, LC filters or triode vacuum lamps or combination of them.

When the electrical output exceeded 70 W and the frequency surpassed 2 MHz, he found he was able to make skin incisions [29]. Harvey Cushing was eager for a practical electrosurgical unit that could be used in neurosurgery for both cutting and coagulation. In 1926, William Bovie, a physicist at Harvard, developed for Cushing a prototype of the modern electrosurgical generator capable of both coagulation and cutting [30]. In 1978, Maness, et al [31]. found 3.8 MHz was an optimal frequency for cutting soft tissue.

Today's popular electrosurgical instrument is often incorrectly referred to as electrocautery. Rather than the electrode serving as the resistance for the passage of current and itself becoming hot, the modern high-frequency electrosurgical apparatus transfers current to the patient via a cold electrode tip. Human tissue in contact with the electrode tip offers resistance to passage of this current, with the result that electrical energy is converted to heat energy in the tissue. Depending on the characteristics of the wave frequency and power output, the result can be excision of tissue, control of bleeding, or destruction of tissue.

By developing high power semiconductors in 1970-1985, transistors based generators were manufactured commercially. One of significant advantages of these generators was smaller size and weight in comparison to the spark gap or vacuum lamp system [32].

Recently, microprocessor based systems can offer considerably better methods and meet completely standard requisites in both application and safety issues. That is why surgeons prefer electrosurgery to the other techniques and this devices have become compulsory parts of operating rooms. The frequency range often is between 300KHz – 4MHz in which the biologic non-thermal effects are negligible and thermal effects are dominant.

High frequency output can be applied either monopolar or bipolar. In monopolar mode, the patient is connected to the generator by a relatively large conductive electrode and the second pole is a tiny surface electrode which is called active electrode. Current through the tiny surface electrode (active electrode) enters the tissue, passes through the whole body and flows through a large surface electrode (neutral electrode) and returns to the generator. By that, a huge temperature increase in the active electrode and contacted tissue is generated, which causes cut or coagulation in tissue and blood vessels.

Physical and practical principle of high frequency surgery

Main principle of high frequency surgery is utilizing thermal effects of high frequency on biological tissues which provide coagulation along with incision. In this chapter, it is explained how the thermal effects of electrical current are used and different methods of electrosurgery are illustrated.

Generally biological tissues have considerable conductivity and electrical current can easily pass through them and causes multiple effects.

2.7.2 Biological effects of current on biological tissue

These effects can be categorised in three main effects:
- Electrolysis effects
- Faradic effects
- Thermal effects

2.7.2.1 Electrolysis effects

The movement of ions of opposite polarities in opposite directions through a medium is called electrolysis and can be made to occur by passing DC current through body tissues or fluids. If a DC current is passed through body tissues for a period of minutes, ulceration begins to occur. Such ulcers, while not normally fatal, can be painful and take long periods to heal[6].

By passing electrical current, ions of electrolytic compositions of cell entities move and with DC current positive ions move towards negative electrode and negative ions toward positive electrode Figure 2-24. Ion accumulation close to the electrodes can destroy the tissue and electrolysis of intra and extra electrolyte of the cells. If the frequency is increased enough, ions cannot move towards electrodes, but resonate in their places and in very high frequency they cannot even vibrate Figure 2-25. Therefore, the ion accumulation close to electrodes will not happen and the electrolysis effect is eliminated.
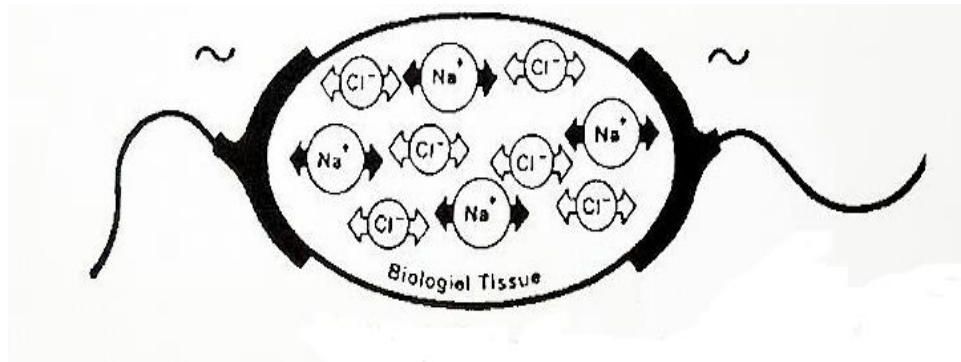
Figure 2- 24 Electrolysis effects with alternative current (AC) [33]
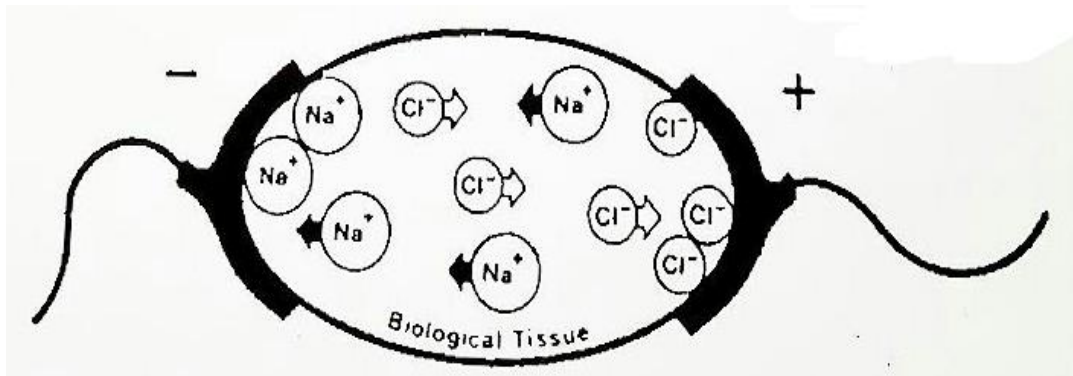
Figure 2- 25 Electrolysis effects with direct current (DC) [33]

2.7.2.2 Faradic effects

Stimulation of nerve and muscular cells by electric current is called faradic effect. These stimulations can cause muscular contraction and pain as a result and in higher range causes irregular heart muscle contraction.

For the sinusoidal oscillation stimulus Figure 2-26, the level of I_T increases for a long oscillating period T (or a small oscillating frequency $1/T$), which is due to the accommodating mechanisms. In the range from 30Hz up to 100Hz the sinusoidal stimulus is sufficiently dynamic with a depolarizing positive half period which has a sufficient duration for the excitation of the cell. It is notable that the most commonly used technical frequencies of 50Hz and 60Hz in power lines fall into this critical frequency range. By increasing the frequency, the association between the stimulus and the corresponding action potential begins to disappear. For frequencies higher than about 500Hz, the depolarizing half period starts overlap with the absolute refractory period, impeding the generation of new action potentials. In the KHz range, mainly capacitive currents bridge the membrane. Practically, no action potentials can be triggered for frequencies higher than 30KHz [6] .
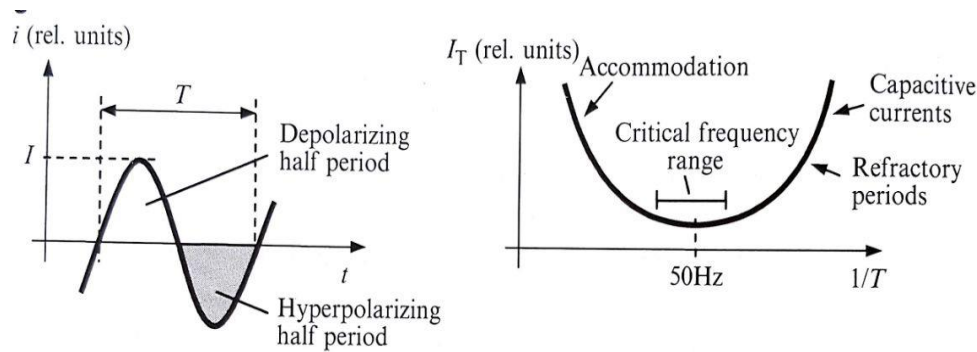
Figure 2- 26 sinusoidal current stimulus with the oscillating period T [34]

Therefore, frequencies over 300KHz are more preferential for electrosurgery.

2.7.2.3 Thermal effects

Current passage through tissue like every other conductive component generates heat energy. Energy amount depends on current value, time duration and electrical resistance of the tissue in equation (1-1).

$$Q = I^2 . R . t \qquad (1\text{-}1)$$

Q= energy, I= current intensity, R= electrical resistance of tissue, t = time

For instance, if R = 100 Ω, I = 1 A, t = 1s, 100 J energy will be produced. As each calorie equals with 4.18J, 23.9 calorie thermal energy is generated in the tissue. If this energy in 1 cm^3 of tissue uniformly concentrates, by assuming that specific thermal capacity and density of the tissue is the same as water, by considering Q= $m.c.\Delta\Theta$, temperature increase rate in tissue is 23.9 °C/s.

Need to mention that, using equation (1-1) would be possible when tissue impedance can be assumed as a pure resistive kind, which is not always a true assumption and on the other hand, tissue impedance depends on frequency. Therefore, thermal effects of electrical current on tissue are not independent from the frequency.

Therefore, by utilizing electrical current with more than 300KHz, faradic and electrolysis effects are negligible and thermal effect is dominant. In Figure 2-27 electric current effects in different frequencies and applications are shown.
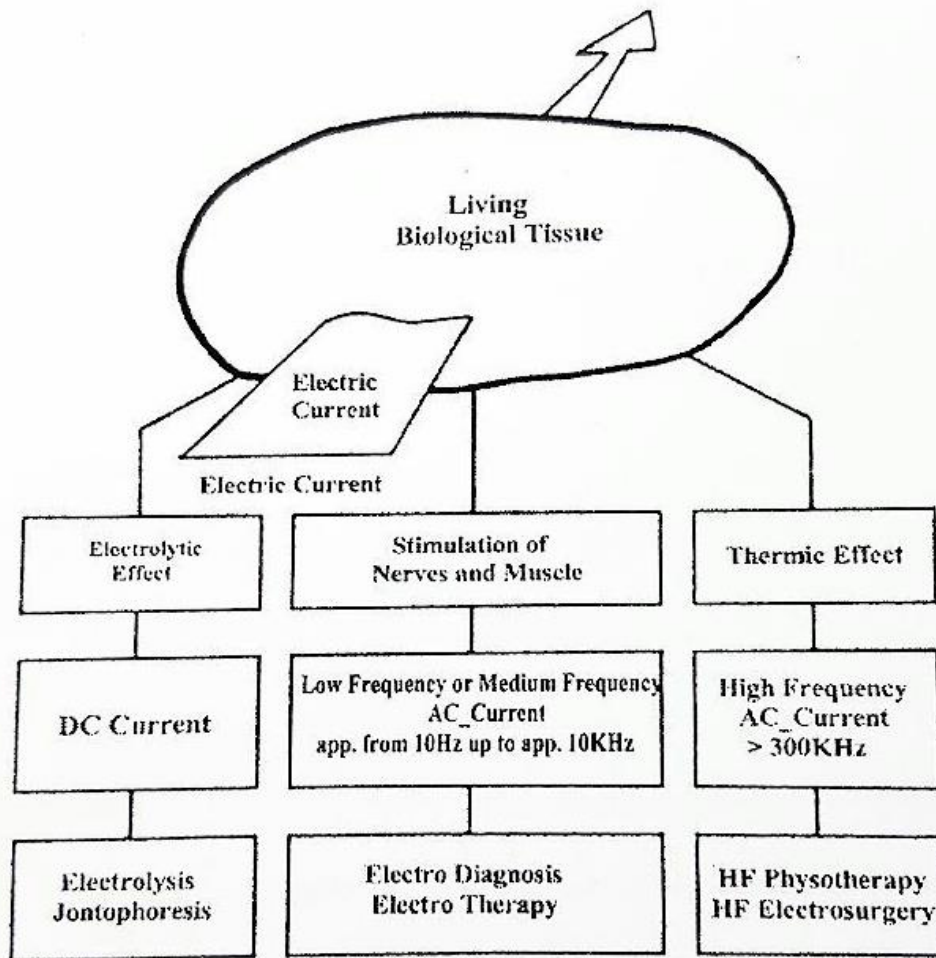
Figure 2- 27 Electrolysis effects with DC current passage, electro diagnoses/therapy by nerve and muscle stimulation with AC current in the range of f=10-10KHz, thermal effects of AC current in the range of f> 300KHz in HF electrosurgery [1].

2.7.3 Application of thermal effects of electrical current in high frequency surgery

Thermal effects of high frequency currents are used in order to cut or coagulate tissues with bleeding control. If the current density through the tissue would be high enough, intra cellular liquids rapidly are heated and evaporated Figure 2-28. When a high-frequency alternating current is applied to tissue, molecular heat is generated and produces a motion of electrons. One theory regarding the effects of high-frequency electrical current on tissue is that within each cell intramolecular fluids are heated to the point of volatilization, and the cell explodes. This explosive vacuolization is thought to result from intra-cellular steam pressure. When moving the electrode through the tissue, this electrical energy is applied to individual cells, sequentially separating the tissue and producing a cutting effect. Although heat produces the cellular effect, the end result simulates mechanical disruption as seen when surgical blades are used in cutting. A second theory postulates that the to-and-fro oscillations produced by the electrical current eventually disrupt and cleave the cell wall. Some electron microscopy evidence seems to support this theory. The cutting effect produced is known as electrosection [3].

If the current used is less concentrated and the heat is produced over a relatively larger area, the cells become dehydrated and their protein contents denaturized. Cell outlines are lost, blood vessels are thrombosed, and a coagulating effect is produced.

Higher voltage but less current, which causes cell dehydration with shriveling but maintenance of cell outlines and preservation of nuclei, produces a desiccating effect. When the electrode tip is moved above the surface of the skin and a strong high-frequency alternating current is applied, a spark gap is produced. The evaporated tissue contents due to spark leads carbonization and charring, which insulates the tissue from deeper destruction. This is known as fulguration.

2.7.3.1 Cut

Electrical current in the configuration of a continuous, pure sine wave with a smooth and uniform appearance is known as an undamped current. When such an electrical current is applied at high frequency through an electro surgical tip, cutting, or electro-section will result. Electro-section is comparable to a cold steel surgical incision except for a small amount of heat-induced tissue damage. When an electrosurgical tip is used in the electro-section mode with a brushing or cursive motion at minimal power settings, there is so little tissue damage that this disadvantage is compensated by the resulting rapid hemostasis (particularly in the blended mode described below) and the decreased manipulation of tissue.
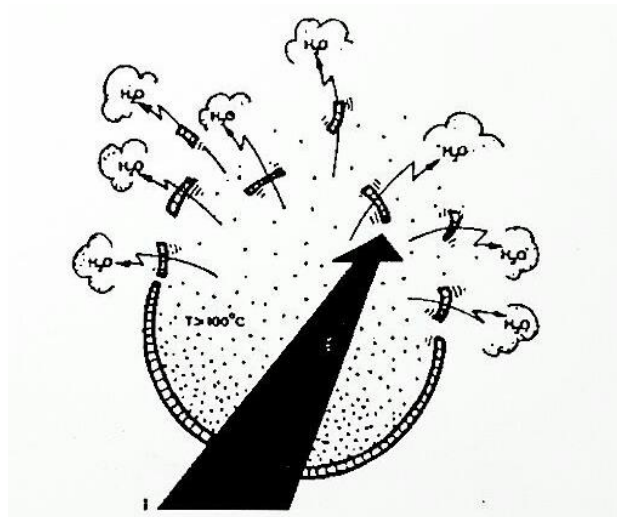
Figure 2- 28 Explosion of cell wall by current passing through it [1].

Effective factors in cut quality

In order to cut a biological tissue, the voltage difference between tissue and cut electrode should be as much as enough to make an electrical arc, so that through this electrical arc, high frequency current, in a certain point of tissue can be concentrated. (Figure 2-29)
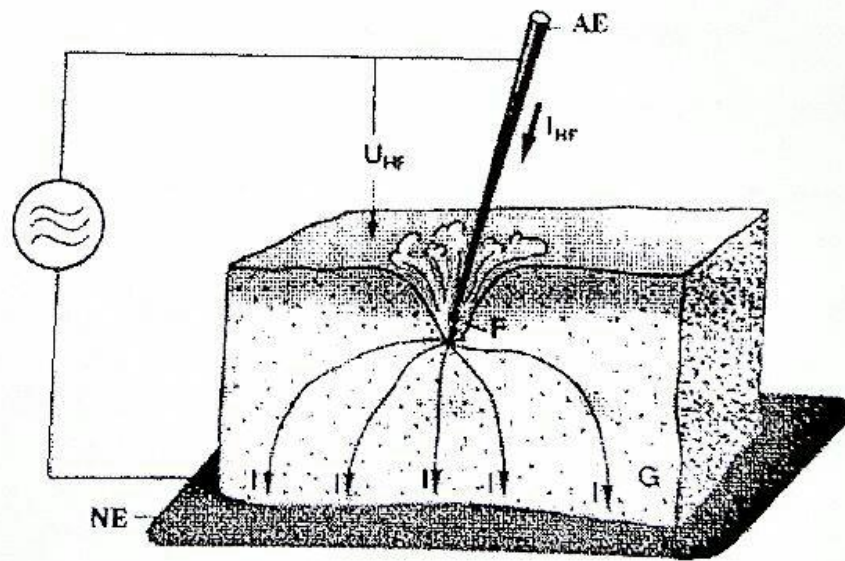
Figure 2- 29 Cut effect on tissue and current distribution [35].

Voltage amplitude

At least 200 V_{peak} are needed to generate an electrical arc between the active electrode and tissue. With lower voltage amplitudes, electrical arc will not happen and with higher amount of voltage, intensity of electrical arc will increase. Experiences show that by increasing electric arc, coagulation depth (K) will increase. (Figure 2-30)
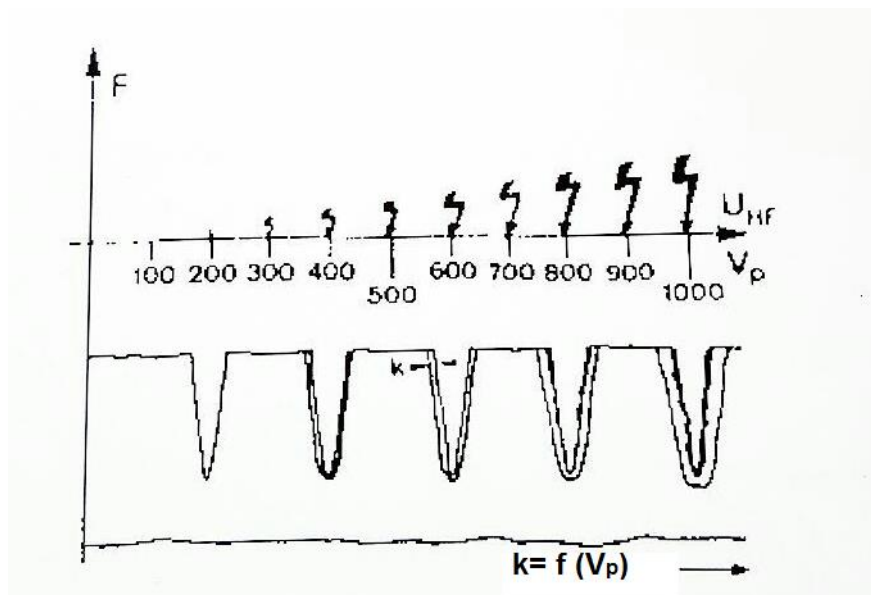
Figure 2- 30 Voltage amplitude effect on coagulation depth [1].

In fact, with increasing voltage, tissue temperature will be more and generate more thermal effect in both sides of sectioned tissues. Then, coagulation K can be defined as a function of high frequency power. (Figure 2-31)

$$K=f(P_{HF}) \qquad (1\text{-}2)$$
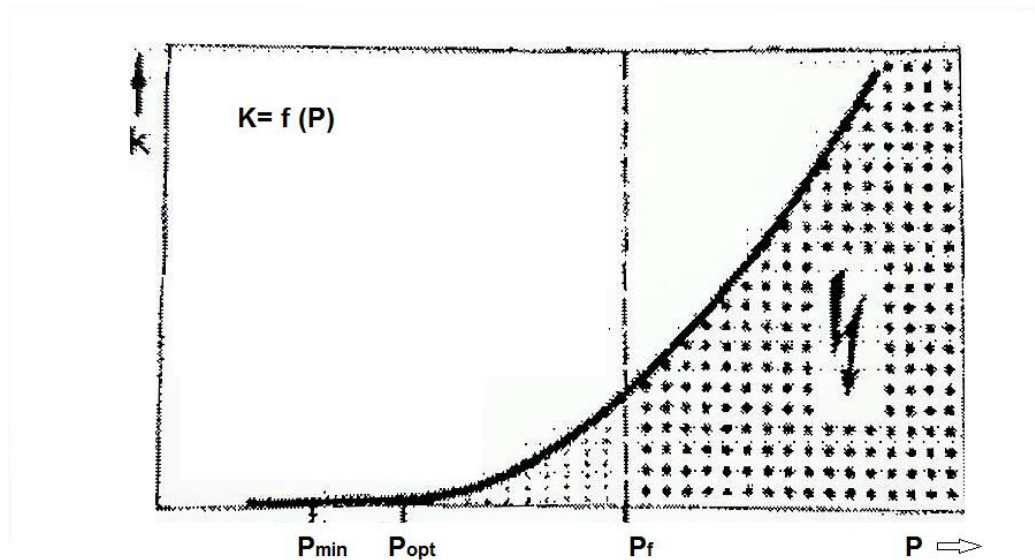
Figure 2- 31 Power required for coagulation effects [1].

P_{min} in Figure 2-31 is minimum the required power to cut and P_{opt} is the optimum power to cut the tissue with minimum coagulation effects in adjacent tissues , by increasing power more than P_{opt} coagulation depth will increase and with drastically increase in P_{HF}, a sever arc between electrode and tissue leads carbonization in adjacent cut tissues.

Frequency modulation of current wave shape

Coagulation of cut tissues also depends on current wave shape through the tissue. Experiences show that by increasing crest factor of applied voltage, coagulation depth will increase. *C.F* is defined by equation (1-3).

$$C.F= V_{peak} / V_{rms} \qquad (1\text{-}3)$$

Crest factor for a pure sinusoidal wave shape is 1.41 for a symmetrical square wave, it is 1.00, and for an undistorted triangle wave, it is 1.73.

A very common method of manipulating the crest factor is adjusting frequency modulation, which by increasing modulation rate, crest factor will also increase. Figure 2-32 shows 3 different wave shapes with different crest factors.
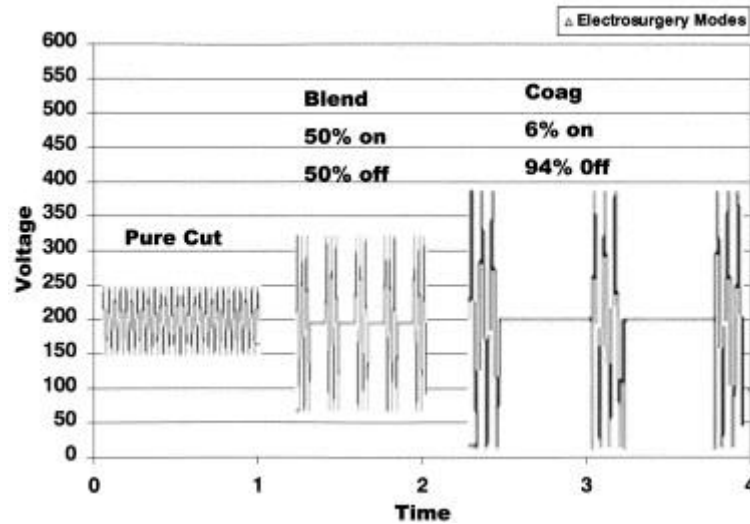
Figure 2- 32 Frequency modulation for electrosurgery modes [36].

Therefore, if 2 wave shapes with the same power but different crest factor compare, the one with more C.F has more coagulation effect. This phenomenon can be so justified that, the wave shape with more C.F, because of more voltage peak, can generate stronger electrical arc between active electrode and adjacent tissues which causes deeper coagulation. Figure 2-33
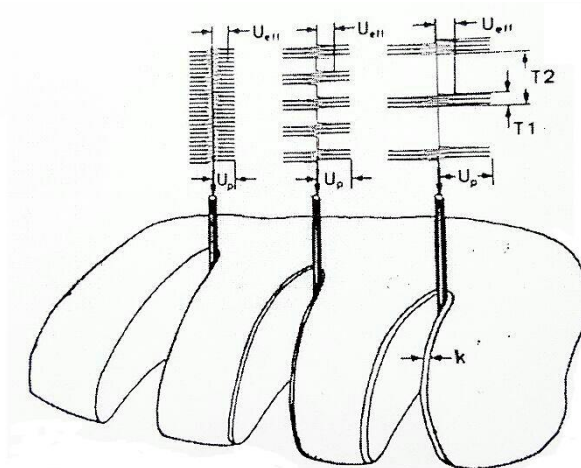
Figure 2- 33 With the same V_{eff} and more V_{Peak}, coagulation depth (k) has been increased [1].

Tissue properties

Electrical conductance of different tissues is variable. Certain tissues with more water content like muscles, skin and rich blood regions have more electrical conductance, and certain of them like fat, cartilage and bones less conductivity. Coagulation and carbonization effects during less water content tissues cutting, is more than in wet tissues. Moreover, electrical conductance

of tissue which is in contact with the active electrode has been considered in HF generator output impedance.

2.7.3.2 Coagulation

By current flow through the tissue with a relatively low density, in contrast to cut, adjacent tissue temperature gradually increases and causes intra and extracellular liquid evaporation Figure 2-34.
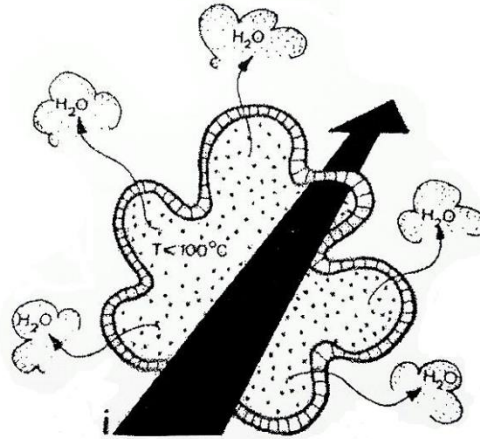
Figure 2- 34 Gradually temperature increase of tissue and slow evaporation of cells leads to coagulation effect [33].

To coagulate a biological tissue, at least 70 °C is required. Although tissue temperature can be increased by other simple methods in contrast to HF, creation of controlled thermal effects, in a way that minimally destroys other tissues, is not a simple issue.

Critical temperatures with biological effects are:

- Up to 40 °C not considerable damages to cells
- Up to 49 °C reversible damages to cells
- Up to 70 °C tissue coagulation in which collagens (Albominoid which is the most important protein of connective tissue) convert to the glucose
- Up to 100 °C evaporation of intra and extra cellular liquids, which dries the tissues and afterward glucoses become more viscose and are contracted
- Up to 200 °C tissue carbonisation (4th burn grade)

ΔT or tissue temperature increase depends on 3 factors:

1) Their resistance against current flow (r)
2) Current density which passes through the tissue (i_{rms})
3) Current time duration (Δt)

$$\Delta T = f(r, \Delta t, i_{rms}) \hspace{2cm} (1\text{-}6)$$

Temperature increase in different regions of tissue, because of heterogeneous tissue, and their different electrical impedance, and current distribution pattern in them, change. As the current density in electrode vicinity is more, temperature increase is also more. Farther from electrode and tissue contact temperature decreases Figure 2-35.
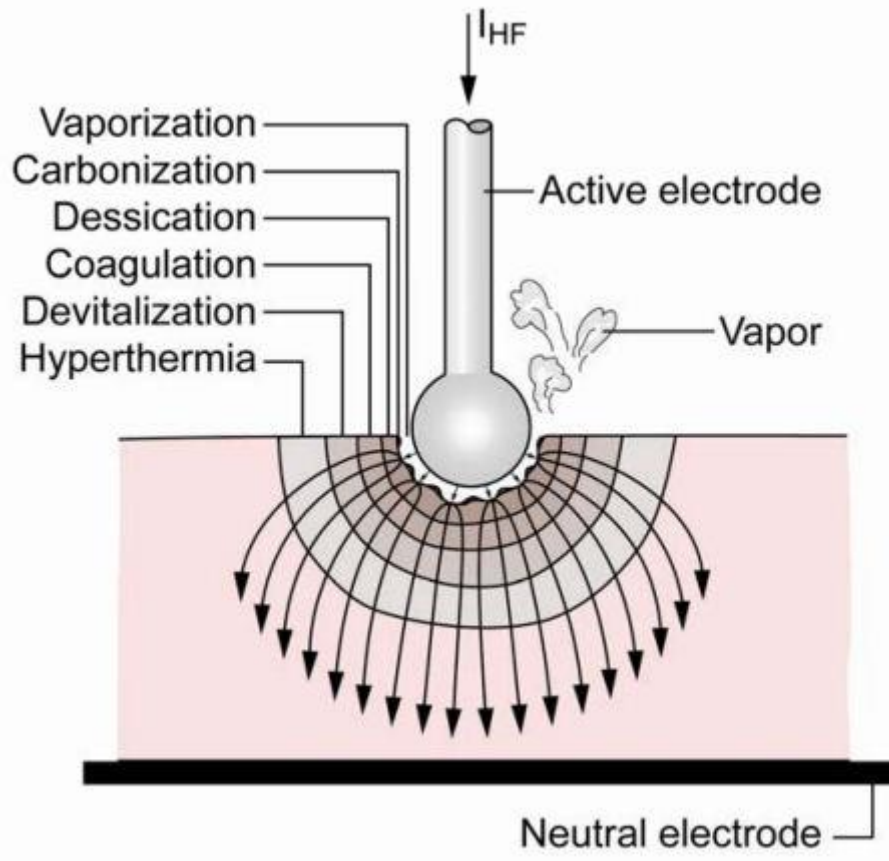
Figure 2- 35 Equi-thermal lines in a coagulation process [37].

As shown in Figure 2-36, according to temperature increase in tissue, and biological effects of temperature increase, different layer and regions are created:

- **A1**: temperature increase is not considerable
- **A2**: cellular damages are not reversible
- **A3**: tissue coagulation
- **A4**: tissue are dried
- **A5**: cellular liquids are evaporated
- **A6a**: in this region because of collagen to glucose conversion in area 3, and tissue are dried in area 4, electrical conduction of tissues become very low and crossing current will decrease.
- **A6b**: if voltage difference between tissue and active electrode would be more than 200 V_{peak}, after a while the tissue around the electrode will be carbonized.
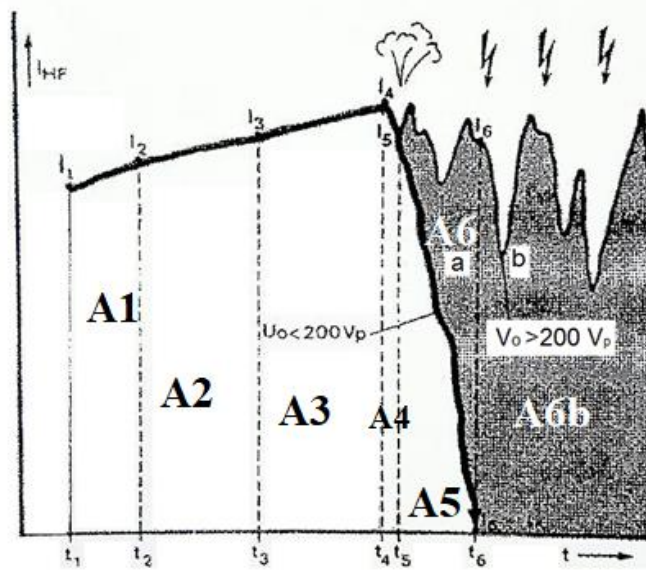
Figure 2- 36 HF current variations during a coagulation process [1].

If voltage difference between tissue and electrode would be less than 200 V_{peak}, after reaching 5th area, because of creation of isolating layer between electrode and tissue, as a result of reaching tissue temperature to the boiling point of cellular liquids and drying adjacent tissues, no more current can pass.

But in case that voltage difference between tissue and electrode is more than 200 V_{peak}, there is no significant change till t_5 (Figure 2-36), except that coagulation process reaches faster to this point, but after t_5 , electrical arc between electrode and tissue starts and carbonizes the tissue. If the generator is not switched off, a carbonized layer covers the electrode surface, and sometimes this layer is enough thick not to let current pass.

By considering above mentioned illustration, if the electrode is supposed to be in contact with the tissue to coagulate, the higher voltages than 200 V_{peak} are used if:
- low Coagulation time,
- area for coagulation be relatively broad,
- electrodes have relatively small surface,
- tissue carbonization hazard are accepted.

Electrocoagulation is used when rapid haemostasis is desired without cutting. An example for which this application might be used is treatment of vascular skin lesions, such as telangiectasia, haemangiomas, dilated venules, or other vascular structures that require coagulation rather than excision. Also, following electrosection, when pinpoint bleeding remains that is not resolved by the initial electrosection, switching to electrocoagulation will produce haemostasis of small blood vessels of up to 1/16th inch in diameter [1].

Soft coagulation (electrodesication)

In this method there is no electrical arc between electrode and tissue, and tissue carbonization is avoided. Therefore, V_{peak} should not exceed more than 200 V_{peak}. A wave shape with a

relatively low crest factor is suitable so that unlike relatively low V_{peak} can provide enough energy to coagulate the tissue (Figure 2-37).
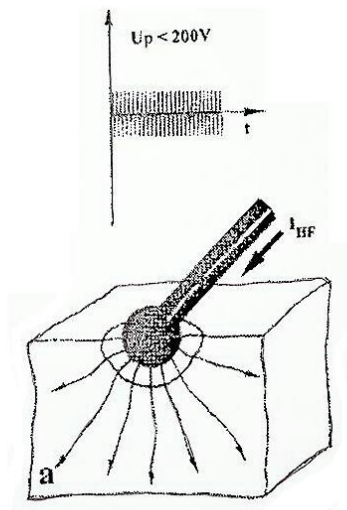
Figure 2- 37 Soft coagulation [36].

Electrodesiccation is produced also by the damped oscillation described under electrocoagulation. In this case, voltage and current are varied to generate heat that desiccates tissue. When using minimal power, most of the damage is confined to the upper layers of skin, and there is minimal risk of scarring. When using this modality with higher power settings, deeper tissues can be coagulated, and subsequent scarring can occur. Electrodesiccation is useful for treating superficial skin lesions, such as actinic or seborrheic keratosis. Warts can also be treated by this method. Combining scalpel or shave excisions with electrodesiccation of the base of pigmented nevi or malignant skin lesions, such as in removal of basal cell carcinoma, is also popular in cutaneous surgery. [1]

2.7.4 Clinical Applications

Most frequent application of electrosurgery in clinical applications is treatment of cutaneous lesions. In cutaneous surgery, it is important to know the type of skin lesion being treated to determine the electrosurgical modality to be used. Table 2-1 lists examples of cutaneous lesions and the electrosurgical mode suggested for treatment. If a lesion is to be destroyed by electrodesiccation or fulguration, a small punch biopsy specimen can be removed first if there is uncertainty about the nature of the superficial lesion. A lesion that is excised using electrosection or shave techniques can be submitted for pathologic evaluation. Most hyper-pigmented lesions should be submitted for pathologic evaluation.

Table 2- 4 Cutaneous lesions and the electrosurgical mode suggested for treatment [7].

Lesion	Electrosurgical Modality
Nevus **Basal cell carcinoma** **Keratoacanthoma** **Pedunculated fibroma** **Acrochordon (skin tag)** **Papilloma** **Dermatofibroma**	Electrosection or blended setting
Telangiectasia **Hemangioma**	Electrocoagulation
Seborrheic **keratosis** **Condyloma** **Actinic** **keratosis** **Common wart Basal cell** **carcinoma (after shave biopsy)**	Electrodesiccation or fulguration

Lidocaine or another anesthetic agent is locally infiltrated or administered by nerve or field block before electrosurgery. Adding epinephrine to the anesthetic agent is recommended, except at the digits or tip of the nose, as the additional hemostatic effect is beneficial. There are a wide number of applications of electrosurgery technology in addition to cutaneous surgery. Those family physicians whose skills include gynecologic surgery may use this equipment to perform a type of conization of the cervix known as large loop excision of the transformation zone (LLETZ). Following total or partial avulsion of a toenail, the nail matrix can be destroyed with electrodesiccation using specially adapted electrodes that are insulated on the side facing the skin fold when the electrode is placed between the skin fold and the nail matrix at the base of the nail. Electrosurgical equipment can be used in hair removal and has applications in a wide range of other surgical procedures [38]

3. Methodology

Regarding the previous sections, a RF system in the range of 4MHz should have designed which was able to control the output power given to the tissue with feedback sensing. Hence, a RF system based on microcontroller with high voltage DC/DC switching convertor would be the best choice, because through this system a very precise and fast control is possible to follow the impedance change in the output section (tissue impedance change). In the following first of all a RF generator (4MHz) for general purpose will be explained, and later on will be customized corresponding to the method which is offered in this approach.

3.1 General design of RF-Therapy devices

In this section, based on what was already discussed in the previous sections, the design procedure will be considered. In order to follow the design procedure a whole system block diagram can be seen in Figure 4-1(see also Fig A-1).
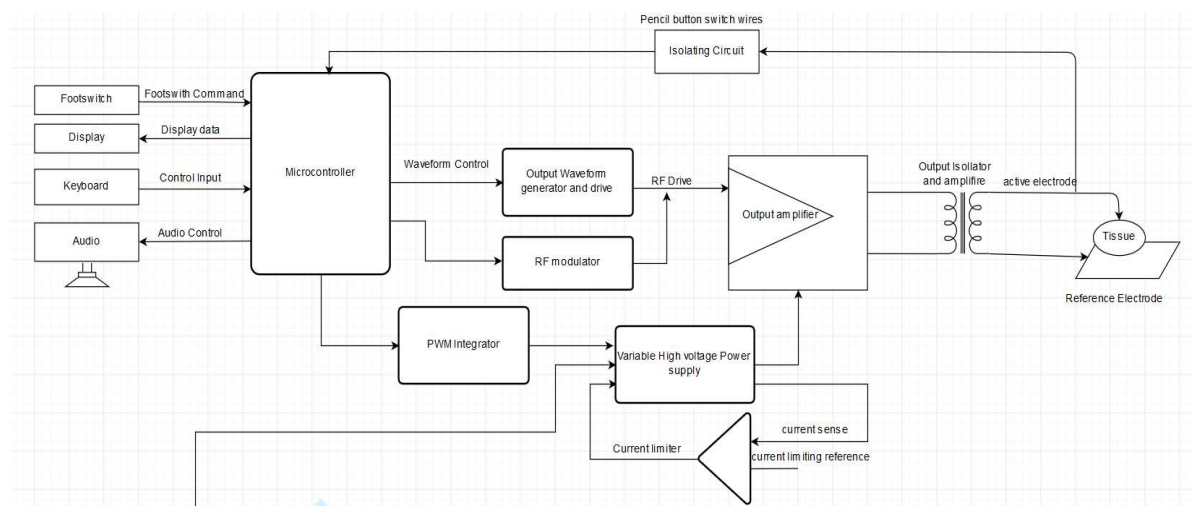
Figure 3- 1 System block diagram.

A microcontroller ATMEGA 32 is used to process the system and interface between different parts of the system. It receives the data from keyboard to set the values and define the setting mode of device in Cut, Coagulation or set the device in standby or ready to use. The signals are shown by LEDs or 2 Digit 7-segments. A signal modulator is used to alarm or notify the active RF output and activation of RF output is done either with Footswitch or knobs on handpiece. In order to meet IEC isolation regulations, the output system is isolated by optocoupler transistors.

Low voltage transformer provides the low voltage for +12VAC and +5VDC regulators to supply the control unit , while variable high voltage power supply directly connects to the line and uses a push-pull fly-back converter to maximize the efficiency and is of course isolated from amplifier and control unit by a high frequency ferrite core transformer. Variable power supply is connected to the microcontroller via PWM integrator. By that, microcontroller dictates the desired value for the amplifier section. Signal is generated by crystal and oscillator 4MHz signal is the input for RF driving system. Microcontroller controls the activation of the 4MHz and modulate it in case of need by a 30KHz signal which is generated by

microcontroller. Output amplifier is driven by 4MHz oscillation pulse and supplied with voltage from variable high voltage power supply and output isolation and amplifier transformer will amplify and is the last stage to apply it to the tissue. To protect the system from short circuit, a continuous current sampling compares the current with a reference value to shot down the power supply as long as the system is in the short circuit situation.

3.1.1 Variable high voltage power supply

Variable power supply provides a wide range of DC supply from 2-85 VDC. Although there is a power amplifier at the end stage, a variable output power can be achieved only with variable DC power supply. In the following circuit Figure 3-2 (see also FigureA-2) a control unit to adjust and drive the power MOSFETs are described:
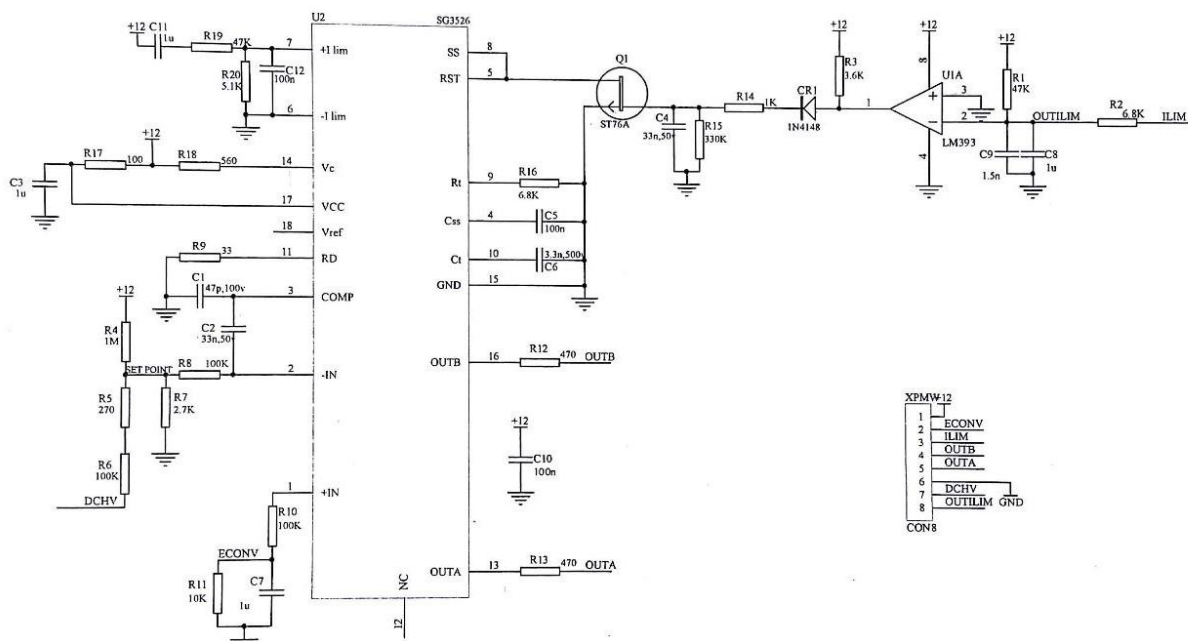
Figure 3- 2 Control unit for variable power supply.

The SG3526 is a high performance pulse width modulator integrated circuit intended for fixed frequency switching regulators and other power control applications. The versatility of this device enables implementation in single−ended or push-pull switching regulators that are transformerless or transformer coupled and two high current totem pole outputs ideally suited for driving the capacitance of power FETs at high speeds.

U2 as a PWM controller provides diving pulse for transformer the 2 signal at the OUTA and B with variable pulse width based on the difference voltage at the input (pins 1,2), the more ECONV can increase the pulse width on the output (pins 13,16). These 2 signals are digital signal with 12V amplitude in flip flop mode.

U1A is a comparator which shuts down the U2 in case that the current sensing (ILIM) goes to the short circuit area.

3.1.2 High voltage Power Switching

Driving signal provided by the control signal is applied to the high voltage power switching in Figure 3-3 to switch the DC-DC convertor circuit (see also FigureA-3).
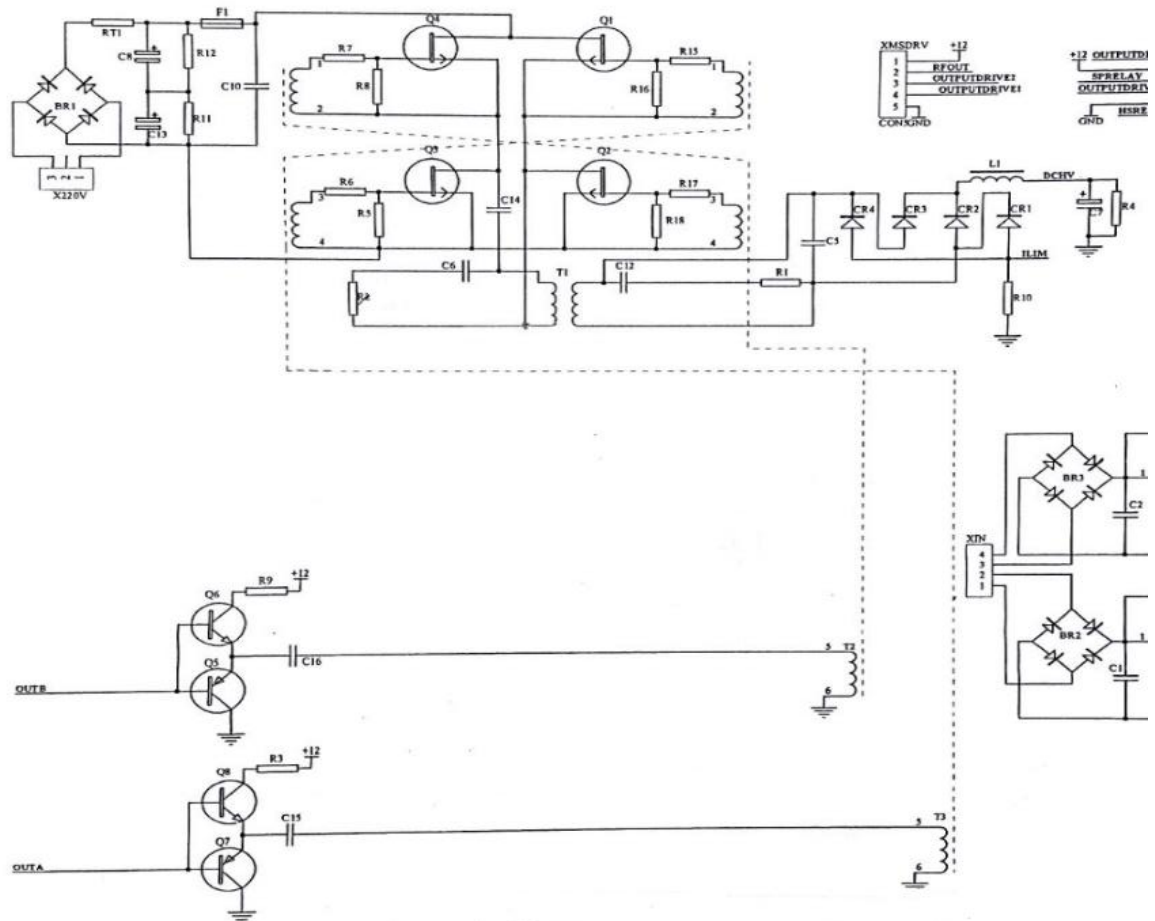
Figure 3- 3 Switching high voltage DC-DC convertor

Q1-Q4 are power MOSFETs which are driven by T2 and T3 pulse transformer to isolate the control unit from the line voltage. As can be seen the switching structure is a push-pull one to increase the efficiency in high current situation for very low impedance loads. T1 is the switching transformer which works in 68KHz. CR1-CR4 are high speed diode to rectify the DC-DC switching and filter by C7. L1 acts as a booster to compensate the switching mode. R11 and R12 discharge the main filtering capacitors in off mode and RT1 is a NTS to reduce the sudden shock current when the system turns on to charge C8 and C13. U1 and U2 regulates the low voltage power supply for the control unit.

3.1.3 Control unit

In order to control the whole system an AVR microcontroller was used to communicate between keyboard and display in one hand and control the power supply function on the other hand. in Figure 3-4 control unit can be seen (see also Figure A-4).
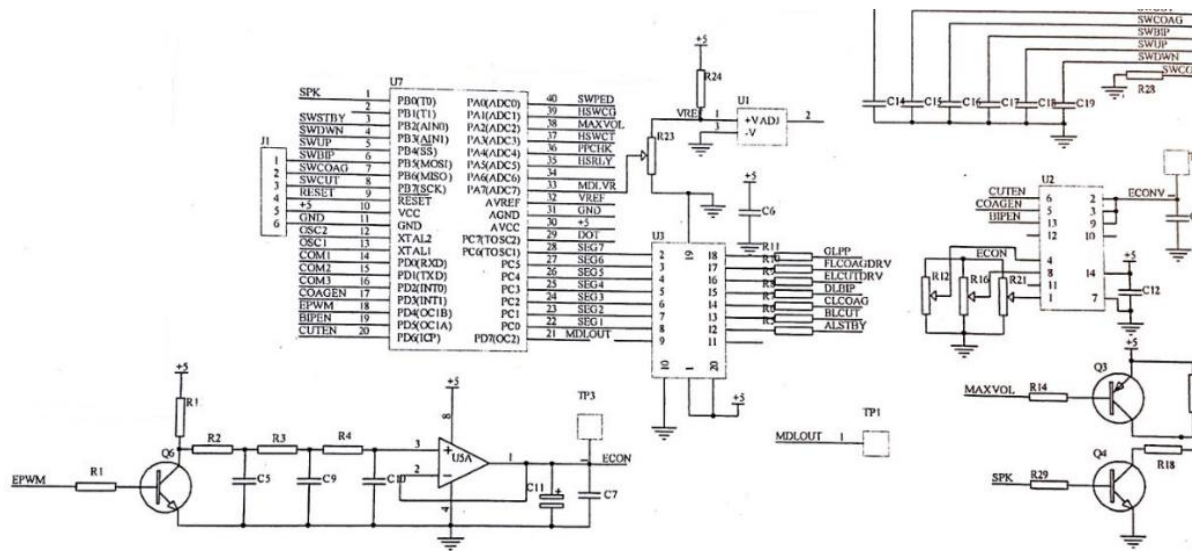
Figure 3- 4 Control unit

U7 is AVR family 8453 which works with 8MHz clock and in port B connects to the keyboard and in port c connects to the U3 as a buffer to drive the 7-segments. U5A, ladder RC and Q6 act as an Integrator to generate a DC voltage form a variable PWM which is produced by the AVR to apply control unit of the Variable high voltage power supply base on the pre-set value by user. U1 is a reference voltage for the micro to use in ADC7 pin . X1 connects the keyboard and display to the micro and C14-C15 debounce and remove the noise. U2 acts as an analogue switch to define scale the setting values for the different modes of the system. Q3 and Q4 drive the speaker to alarm during the activation on RF and Q3 bypasses the R13 in case of fault alarm to the max value.

3.1.4 Isolation from the patient

In order to meet the IEC regulations for medical equipment, the output section was isolated from the control unit in case the electro shock device is not be damaged. Therefore an isolation circuit Figure 3-5 was considered (see also Figure A-5).
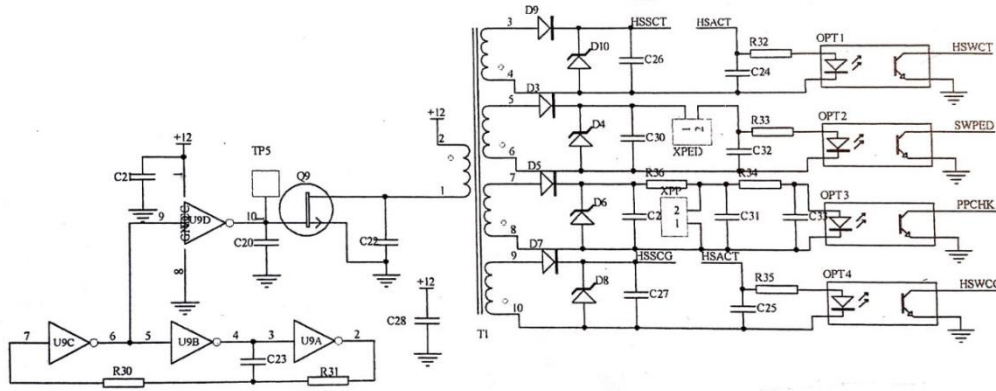
Figure 3- 5 Isolator module

U9 acts as a bi-stable resonator at 80KHz and supplies secondary circuit. Optocouplers OPT1-4 in emitter side are connected to the control board and microprocessor via buffer and LED which drives the base depending on the output switches turn on and off. T1 is high frequency isolator transformer and provides AC signal which is rectified with diode at secondary part. Q9 is a MOSFET to switch the +12VDC on primary coil of the T1.

3.1.5 Keyboard and display

Interface between user and device is done with the keyboard and display. Hence, a 2 digit 7-segment show the pre-set values as power from 1-50 watt and different keys allow the user to set the power or mode of user between Cut and Coagulation (see also FigureA-6).
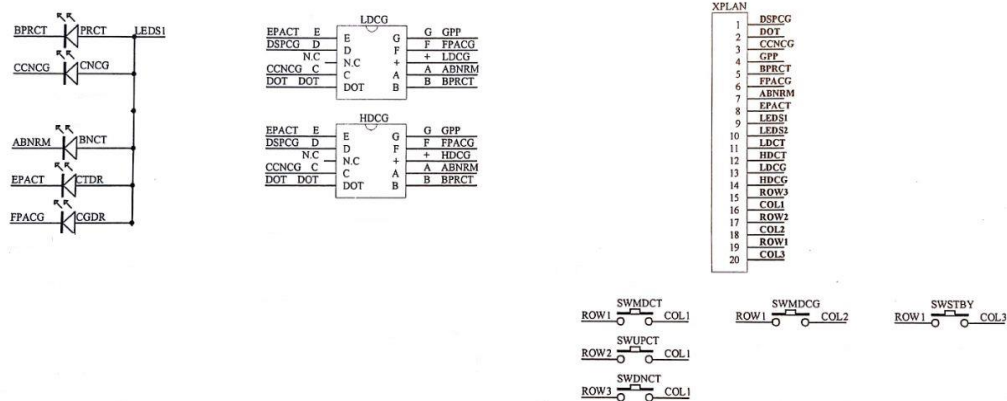
Figure 3- 6 Keyboard and display module

3.1.6 RF power amplifier

At the final stage the 4MHz oscillated signal is amplified with a RF transformer to be applied to the tissue. Figure 3-7 shows the RF power amplifier stage.
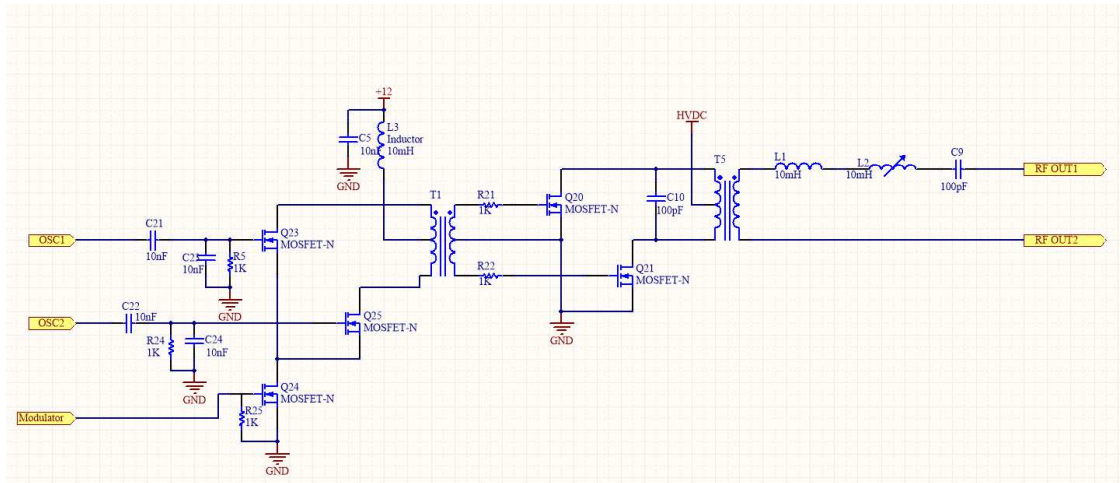
Figure 3- 7 RF power amplifier

T1 is a driving transformer to drive Q20 and Q21 in push-pull mode and guaranteed to have complementary switching at the output stage. Q24 modulates the switching signal with a pulse in the range of 30KHz for the coagulation mode and activate the cut mode with a continues high signal. As can be seen HVDC comes from the variable high voltage power supply and can be tuned by the user via keyboard and finally microcontroller dictate the power supply to generate corresponding supply voltage at the output. L1, L2 and C9 stabilize the output oscillation.

3.2 RF generator results

4.2.1 Output for Cut and Coagulation mode

Output signal for an ohmic load was scoped in Cut and Coagulation mode and the results are shown in Figure 3-8 and Figure 3-9.
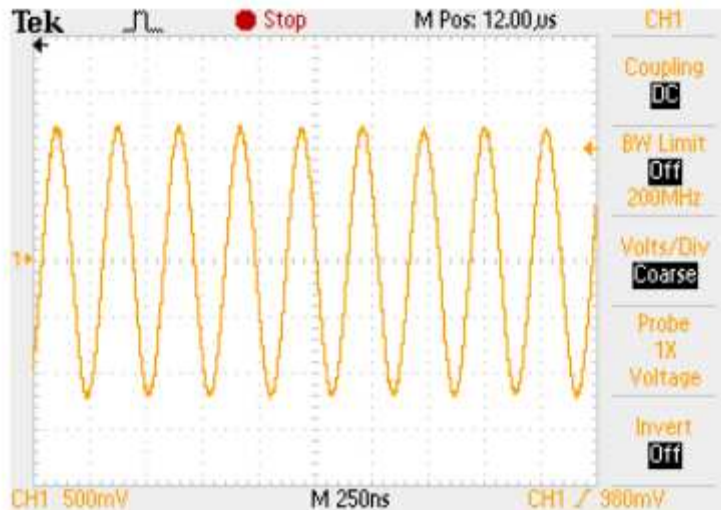
Figure 3- 8 Cut signal at the output with 580 Ω load
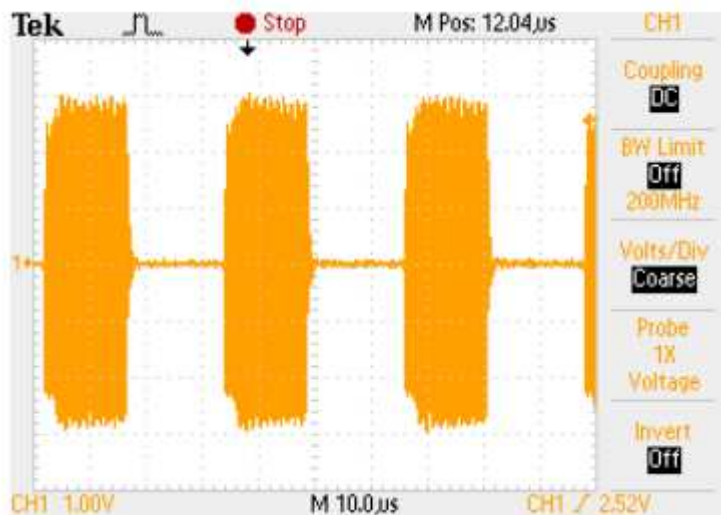
Figure 3- 9 Coagulation signal with 30KHz modulation with 580Ω load

3.2.2 Output power

In order to verify the results, a reference ohmic impedance was placed at the output and measured the voltage across this load. As the system output will be loaded with a wide range from short circuit to open circuit, first of all, power over load for a wide range of the load can be seen in Figure 3-10 for 50Watt and 25 watt in Figure 3-11 .

POWER VS LOAD IMPEDANCE
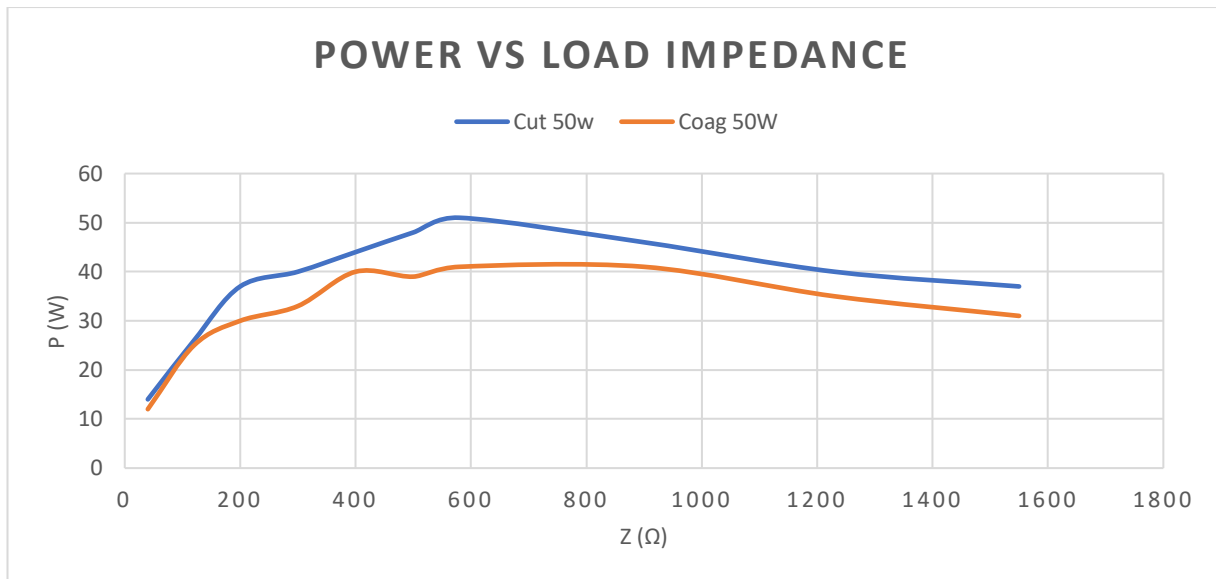
Figure 3- 10 Power curve at 50Watt

POWER VS LOAD IMPEDANCE
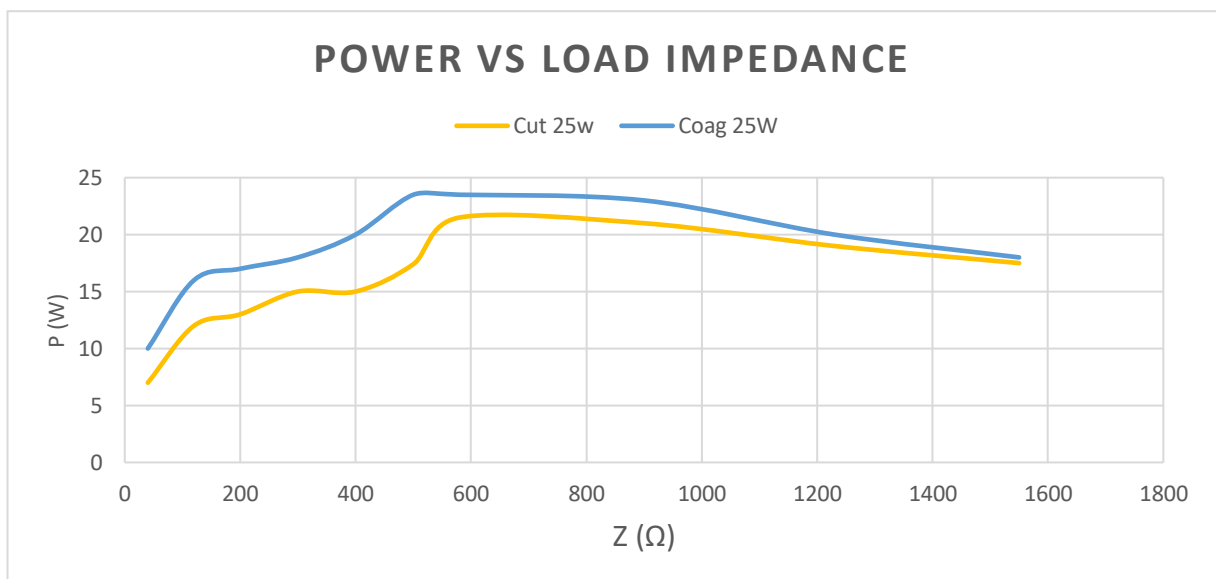
Figure 3- 11 Power curve at 25Watt

3.2.3 Output voltage

Then an output voltage change across the different loads was scoped and the resulted curve can be seen in Figure 3-12 and Figure 3-13 .
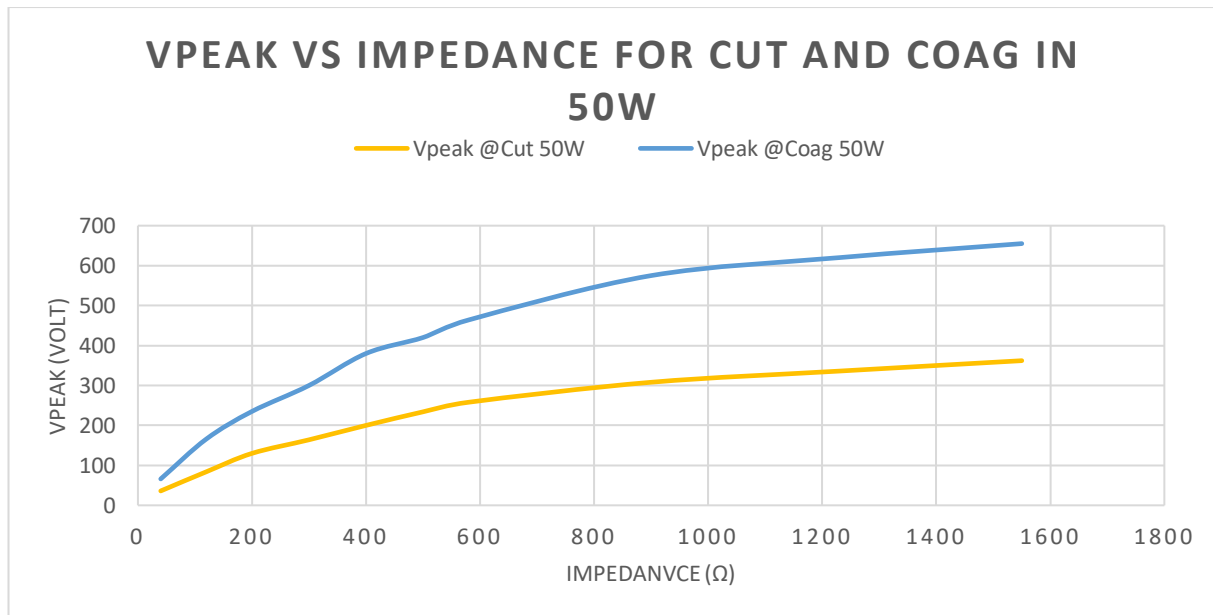
Figure 3- 12 Peak voltage at 50 watt for different loads

At the next step a survey of the open circuit voltage for different power setting was extracted in the Figure 3-13.
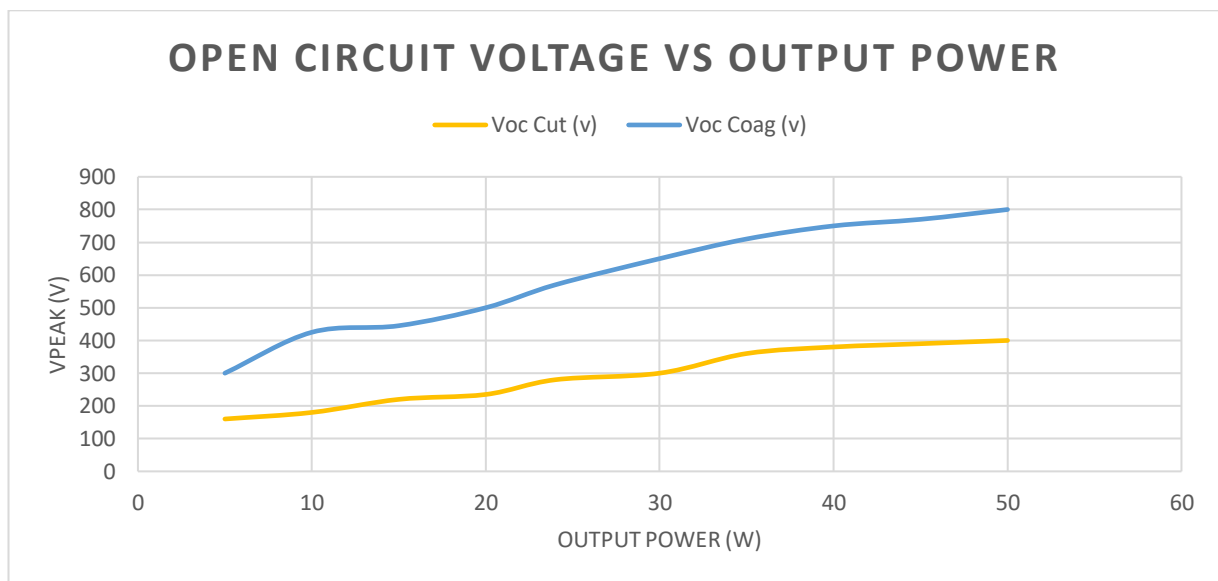
Figure 3- 13 V_{peak} for Cut and Coagulation with open circuit output

3.3 Power adjustment process and calibration

Figure 3-10 and Figure 3-11 show that the maximum power is located at 500-600 Ω. Therefore, this impedance would be the setting impedance to adjust the power, since for the other

impedances, power will be surely lower. In other word, output power which is set will not be exceeded for unknown impedance. In order to determine the power the voltage RMS on load was measured and power adjusted. The final adjustment for Cut and Coagulation can be seen in Figure 3-14.
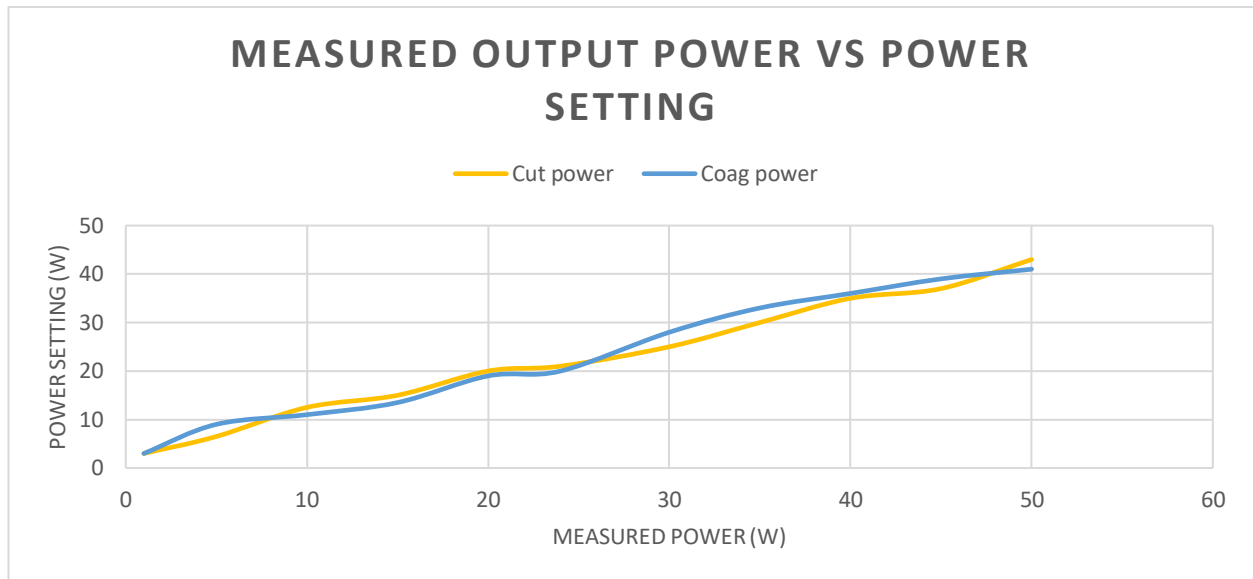
Figure 3- 14 Output calibrated power for Cut and Coagulation

RF generator design discussion

The signal generation and amplification was completely clear and noiseless and the calibration process verified it. As can be seen in the voltage curve for open circuit there is no control on output to keep the power constant for a certain impedance domain, which could be troublesome in case that applying the RF from the open circuit (non-contact situation with the patient) to the tissue, which could be along with electrical arc. Therefore, a feedback system can sample from the output and correct it to avoid overshoot and downshoot (with very low impedance loads).

Duty cycle for coagulation is 50% and the voltage curve proves it, since the voltage RMS for the same power setting shows the double amplitude for the peak voltage in coagulation mode.

Output power in the range of 200-800 Ω shows a roughly constant value but in open circuit and short circuit decreases remarkably. Therefore, a system with a current constant for the very low impedances and voltage constant for very high impedances is an ideal option to protect the system in very low impedances and for the patient for very high impedances.

3.4 System Design with real time impedance monitoring

Before starting system design, it is necessary to define input and output parameters of the system. Regarding to the superior effect of the 4MHz on tissue ablation [2], the system which was already designed as a base generator was used, and a developed block diagram is introduced to cover all requirements and connections between different blocks Figure 3-15.
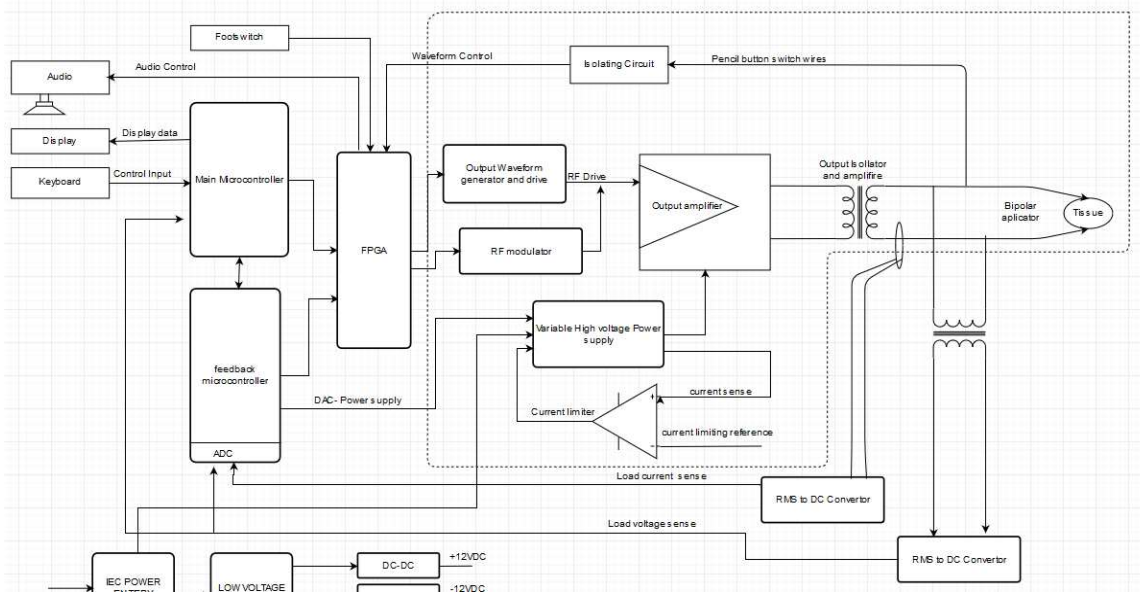
Figure 3- 15 RF generator with real time impedance monitoring.

Dashed line region in the block diagram is similar to the section 4.1 with a little change with a new processing system, which will be described later. The whole RF generator is responsible to generate an amplified RF. Therefore, it requires to be supplied by switching power supply and RF driving signal. A protective system senses the current in power supply stage not to exceed a certain level (close to the short circuit value) and shuts down PWM repeatedly, which is sensed by process unit and alarmed short circuit fault for the power supply unit.

3.4.1 Voltage and current sampling

Voltage and current sampling section is the first step in impedance monitoring. As discussed in section 3 the impedance is a combination of ohmic and capacitive Figure 3-16. therefore, a RMS value of them would be an appropriate and reliable measure of them to determine the tissue impedance in this frequency. Sampling section should be isolated from control section and internal circuit as a safety policy due to avoid any possible current leakage to the patient or high voltage shock to the control circuit in return. Hence, the current and voltage are sampling with isolation transformer which will be explained latter. Voltage is sampled directly on the load (tissue) in the last stage where the RF is applied to the tissue, while current is sampled at the final stage where the current is returned to the generator by inductive ferrite core transformer. This current and voltage are real values which represent real tissue impedance in particular frequency.
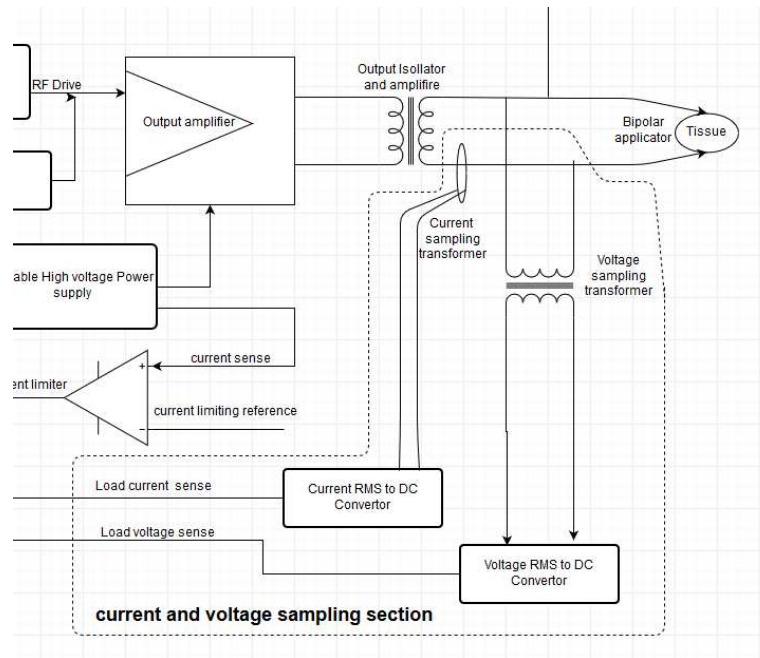
Figure 3- 16 Current and voltage sampling section (dashed line region).

RMS to dc converter circuit is shown in Figure 3-17 Which is the same for current as well. Sampling signal is fed into the RMS/DC, and D1 and D4 protect the op-amp input against overshoot voltage, U1 and U2 rectify the signal and finally R1 amplifies the DC level to calibrate the output. Although the LT1364 is an ultrafast op-amp with 1000V/µS Slew Rate, a really considerable offset can be seen in 4MHz which can be compensated with R1 in final stage. Zener diode D3 protects process unit against overvoltage.
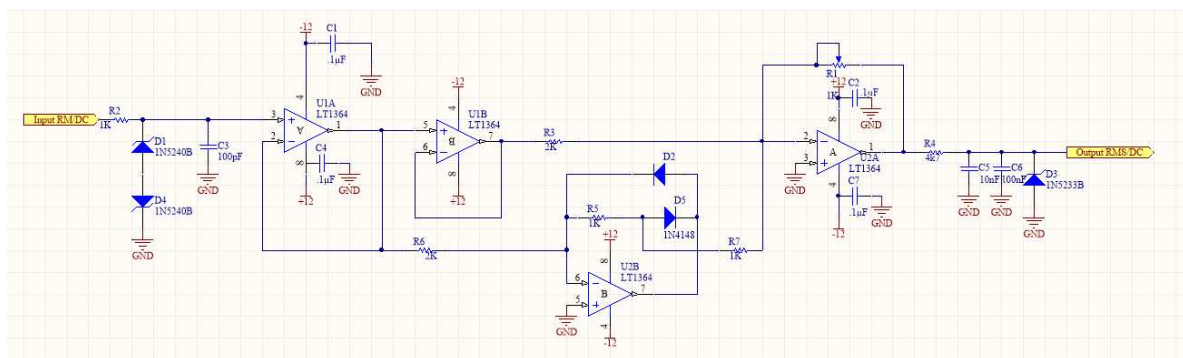
Figure 3- 17 RMS/DC convertor schematic

Voltage sampling transformer consist of a coreless double winding, which is shown in Figure 3-18. This transformer is designed base on output specification, by considering maximum power (50 watt) the output voltage peak is 700V and maximum voltage can be applied to the op-amp is limited to the supply voltage (12 V). therefore the attenuation coefficient is 70 (700/10 = 70).
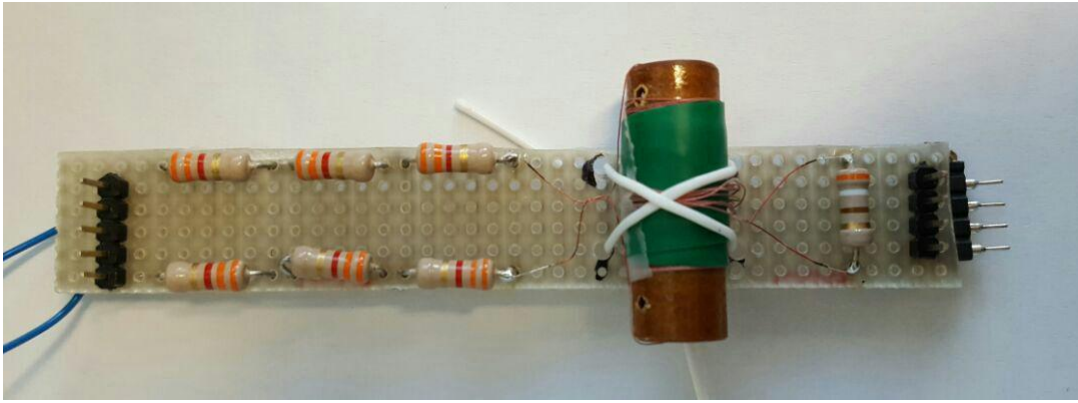
Figure 3- 18 Voltage sampling coreless transformer

Capacitor C6 filters out low frequency distortions and ripples to provide the ADC in microcontroller with a smooth DC input.

RMS/DC was calibrated with a function generator at 4MHz with variable amplitude and verified with oscilloscope Tektronix TDS 2024B.

Current sampling was done with a ferrite core inductive transformer which is shown in Figure 3-19. This ferrite core is needed to induce current perfectly into the transformer so that it can be sensed precisely for low current, since the current flow is really low.
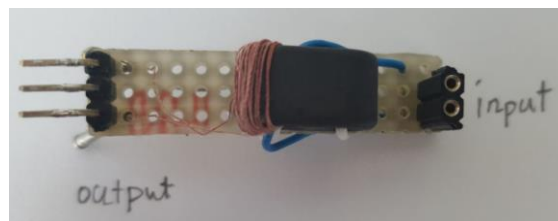
Figure 3- 19 Current sampling inductive transformer blue wire is shunt and red wire output

Winding turns was calculated at the worst case and maximum current flow. This point would be open circuit at maximum power output (50 watt). Final structure of current and voltage sampling is shown in Figure 3-6 schematic.
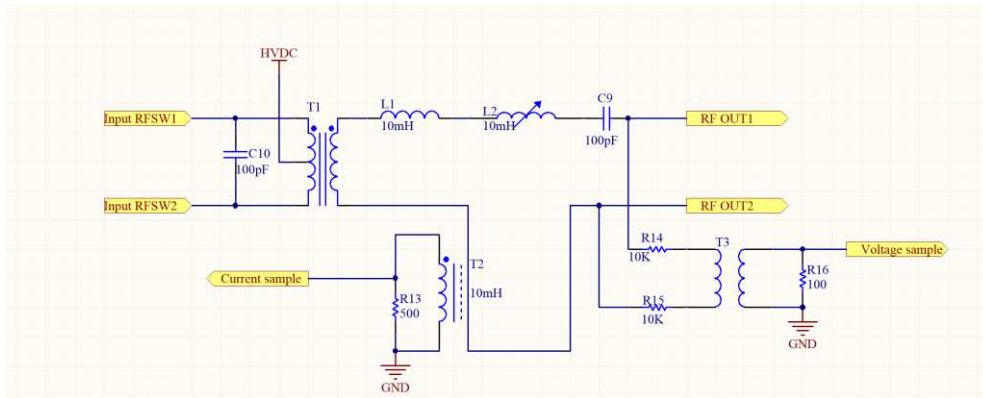
Figure 3- 20 Current and voltage sampling structure

According to Figure 3-20 sampling was recorded and calibrated. The result can be seen in Figure 3-21. A relatively precise measurement for the voltage was gained. A linear behavior of the measured and real values prove a precise sampling over whole ranges of output power.
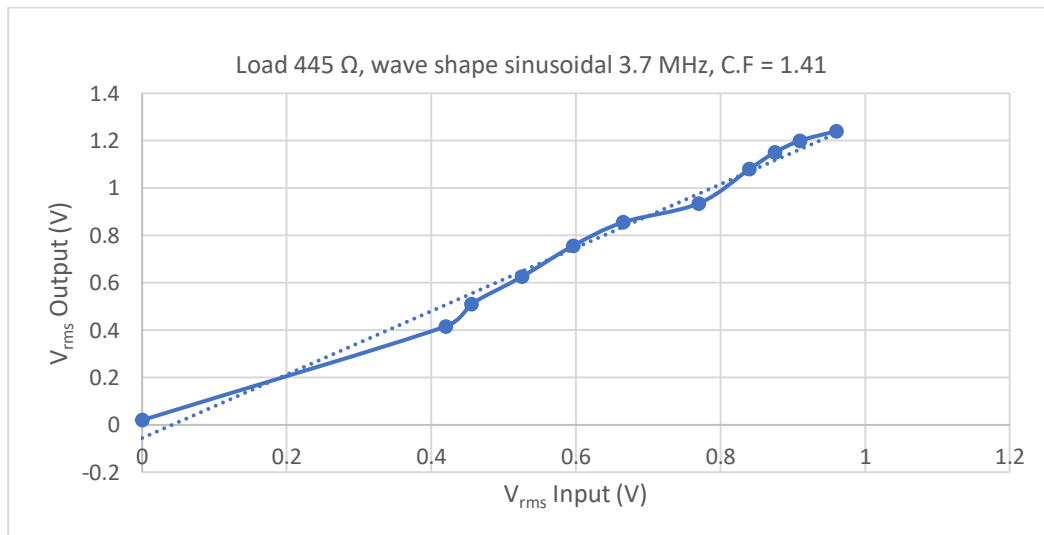
Figure 3- 21 V_{rms} input is the calibrated real voltage and V_{rms} output is RMS/DC values for a sinusoidal waveform at 3.7 MHz for 445 Ω load

The same method was used for the coagulation waveform with 31KHz modulated in 50% duty cycle Figure 3-22.

Load 445 Ω, 3.7 MHz sinusoidal modulated with 31KHz with 50% duty cycle, C.F = 2.8,
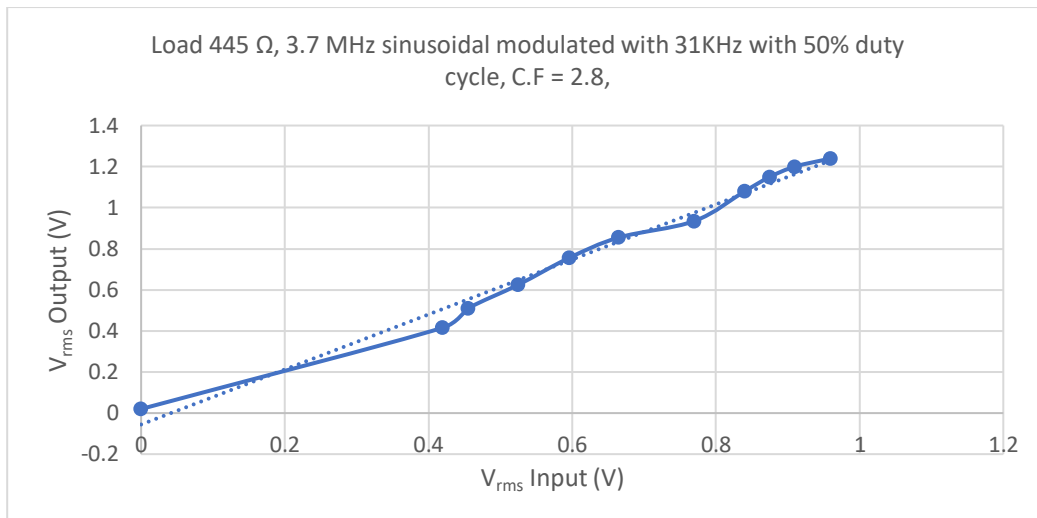
Figure 3- 22 V_{rms} input is the calibrated real voltage and V_{rms} output is RMS/DC values for a sinusoidal waveform at 3.7 MHz for 445 Ω load with 31KHz and 50% duty cycle

The sampling signals correspond to the output as input for the RMS/DC is shown in Figure 3-23 and Figure 3-24.

Current sampling return line 50 cut
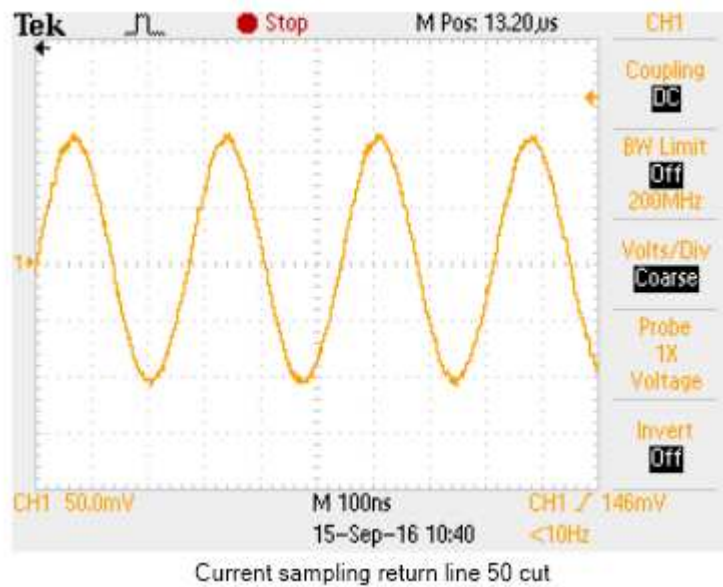
Figure 3- 23 Current sampling return line 50W cut , Vpp = 120 mV

Current sampling return line 50w coag
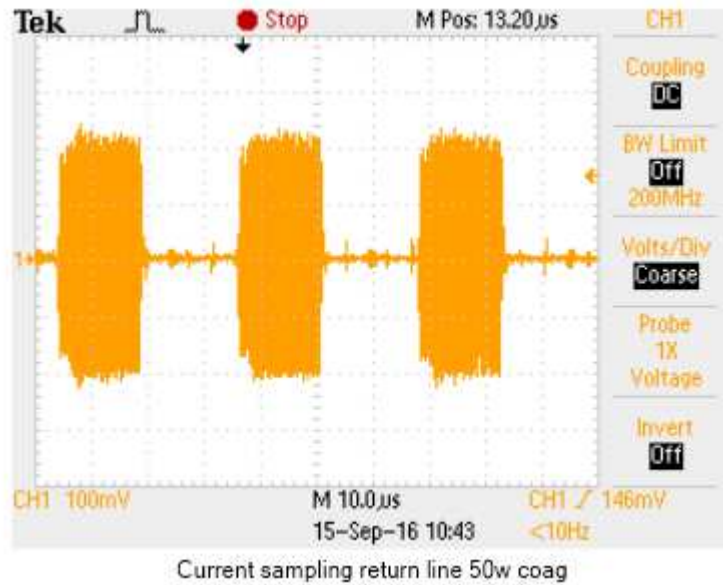
Figure 3- 24 current sampling return line 50W cut , V_{pp} = 420 mV, with 31KHz modulation and 50% duty cycle

4.4.2 Developed Control unit

Impedance control as an approach to control the coagulation rate over volumetric reduction needs a process unit and algorithm which is indicated in block diagram in Figure 3-25.
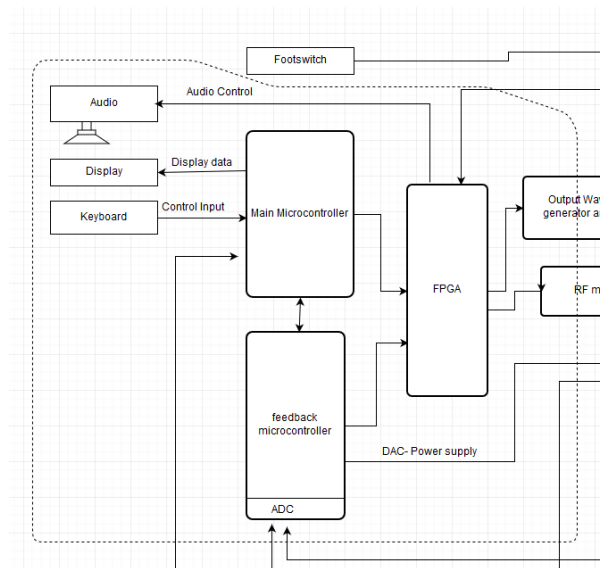
Figure 3- 25 Developed process unit block diagram

Process unit consist of an evaluation board and complementary part to meet all the requirements and support input and outputs. In Figure A-7 (appendix) and Figure 3-26 evaluation board with a STM32F103VET6 microcontroller and peripheral units is shown.
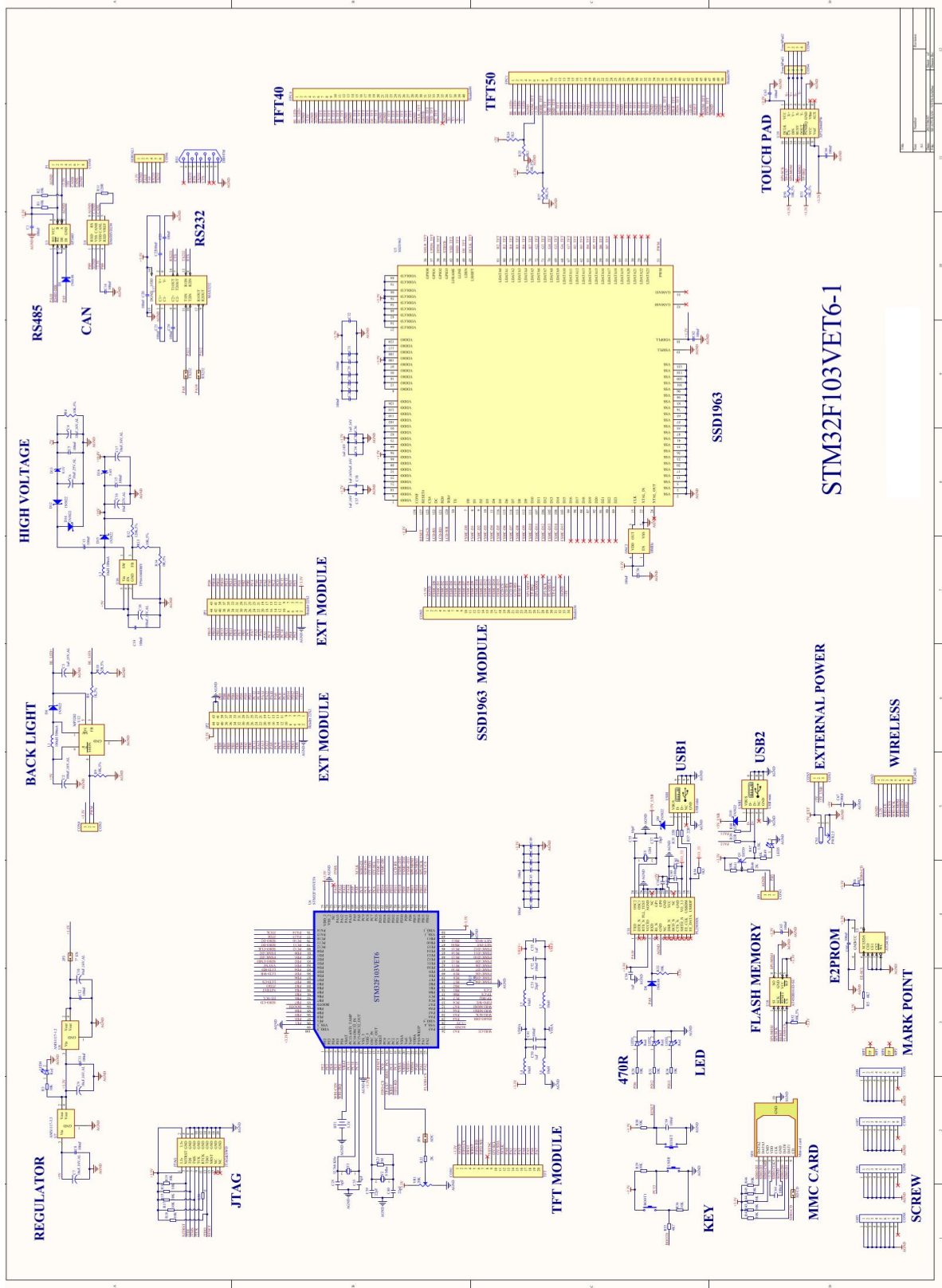
Figure 3- 26 Evaluation board of STM32F103VET6-1 schematic

This DEV BOARD contains the STM32F103VE:

STM32F103 devices use the Cortex-M3 core, with a maximum CPU speed of 72MHz. The portfolio covers from 16 Kbytes to 1 Mbyte of Flash with motor control peripherals, USB full-speed interface and CAN Figure 3-27.
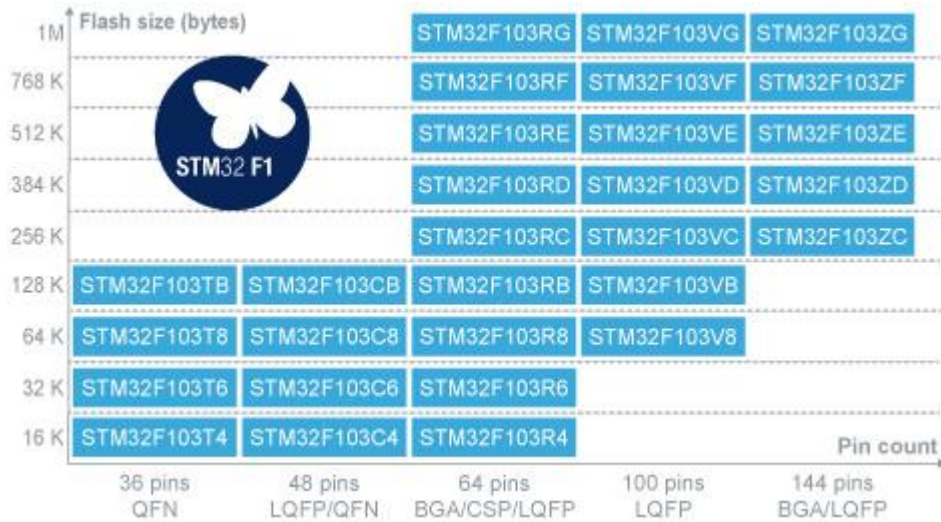
Figure 3- 27 STM family microcontrollers and size of flash memory which can support

As can be seen in the Figure 3-28 this microcontroller supports the 512kbyte of flash. The STM32F103xx is a complete family whose members are fully pin-to-pin, software and feature compatible.

Pinout	Low-density devices		Medium-density devices		High-density devices		
	16 KB Flash	32 KB Flash	64 KB Flash	128 KB Flash	256 KB Flash	384 KB Flash	512 KB Flash
	6 KB RAM	10 KB RAM	20 KB RAM	20 KB RAM	48 KB RAM	64 KB RAM	64 KB RAM
144	-	-	-	-	5 × USARTs 4 × 16-bit timers, 2 × basic timers 3 × SPIs, 2 × I2Ss, 2 × I2Cs USB, CAN, 2 × PWM timers 3 × ADCs, 2 × DACs, 1 × SDIO FSMC (100 and 144 pins)		
100	-	-	3 × USARTs 3 × 16-bit timers 2 × SPIs, 2 × I2Cs, USB, CAN, 1 × PWM timer 2 × ADCs				
64	2 × USARTs 2 × 16-bit timers 1 × SPI, 1 × I2C, USB, CAN, 1 × PWM timer 2 × ADCs						
48					-	-	-
36					-	-	-

Figure 3- 28 STM32F103xx family

Facilities which are included in this evaluation board:

1. LCD driver SSD1963 to drive coloured LCD 3.6 inch up to 9.0 inch
2. 40 pin LCD connector to connect 3.6 and 5 inch LCD

3. 50 pin LCD connector to connect 7 and 9 inch LCD
4. 2x4 pin touch connector to support both right and left cable touch panels
5. CON1 camera connection
6. JTAG standard port 20 pin
7. Serial port connector
8. USB device
9. USB to serial port convertor in order to program and debug
10. CAN,RS485 OUTPUT
11. NRF24101 connection
12. Micro SD
13. XPT2046 touch driver
14. Battery backup socket
15. User and Reset key
16. EEPROM AT24C02
17. SPI FLASH AT45161D

3.4.3 Complementary feedback hardware design

In order to use DEV board and develop it to this project, a complementary circuit in accordance with the input and output section was designed to develop this DVR and play a role as an interface between DRV and RF generator. This complementary hardware called Feedbak module Figure 3-29 , Which connects input and output signals to the processing unit and analogue section. Therefore, feedback part was designed to receive the feedback signals from the analogue section and process them separately from the main microcontroller.

Feedback module description:

STM32F103VBT6 is used as feedback microcontroller to process the feedback signals and calculate the impedance. XC95144 is a Complex Programmable Logic Devices (CPLD) to reduce the digital gates in the circuit and increase the flexibility in design procedure and lower the cost of redesign and correction in hardware design.

The XC95144 is a high-performance CPLD providing advanced in-system programming and test capabilities for general purpose logic integration. It is comprised of eight 36V18 Function Blocks, providing 3,200 usable gates with propagation delays of 7.5 ns.
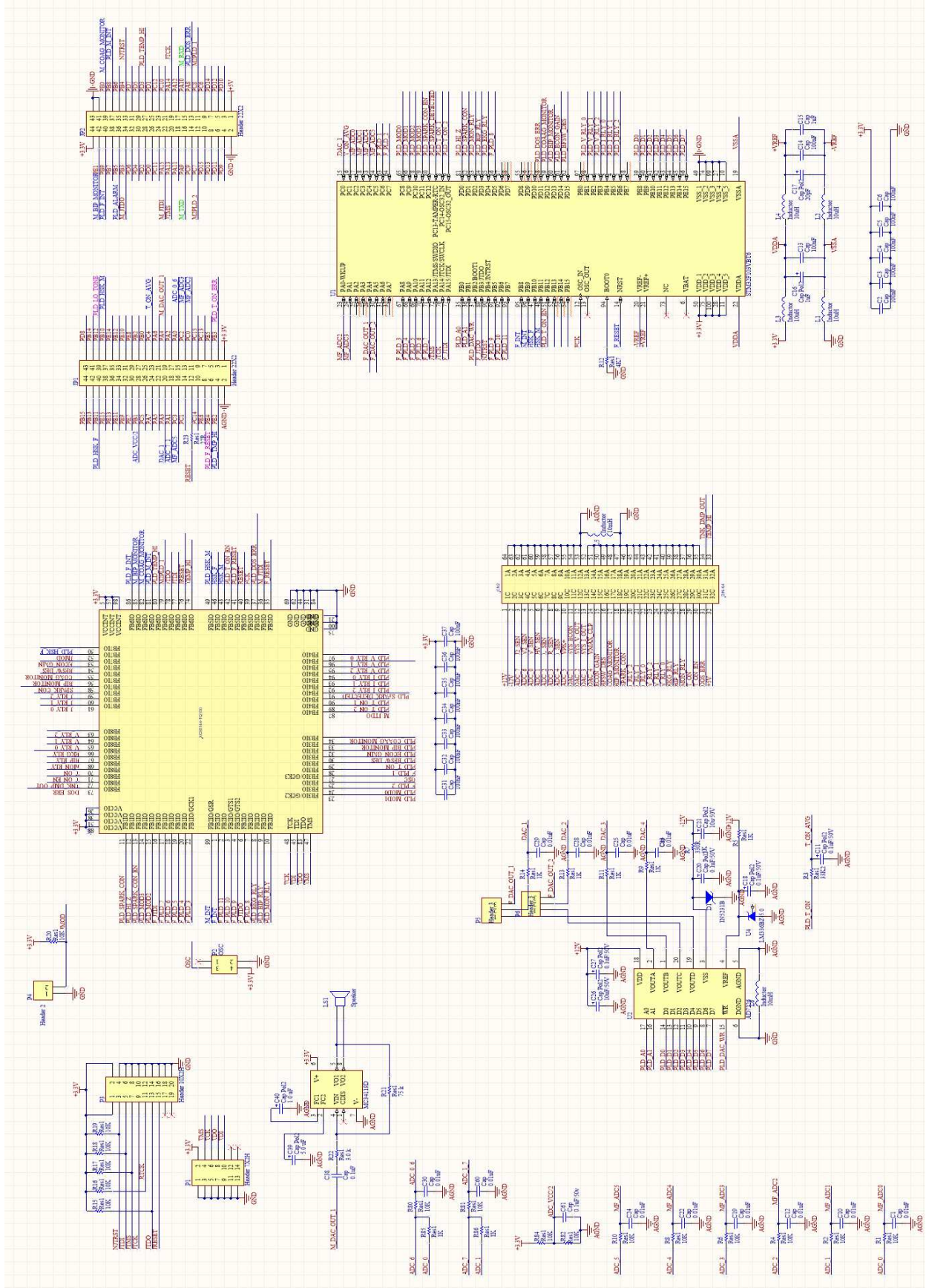
Figure 3- 29 Feedback module

Startup process

In order to simulate the keyboard and display a virtual terminal was used to input the setting data via PC and display reports. Hence, a test program was prepared to run the system with minimum requirements:

1- Receive an activation digital signal as input
2- Generate a DC voltage on DAC port
3- Receive following inputs from the PC via serial port by USB connection
   - help
   - u   ---- fine up   +1.6 m volt
   - U   ---- coarse up   +16 m volt
   - d   ---- fine down   -1.6 m volt
   - D   ---- coarse down   -16 m volt
   - n   ---- fine scroll forward   +1
   - N   ---- coarse scroll forward   +5
   - p   ---- fine scroll backward   -1
   - P   ---- coarse scroll backward -5
   - s,S ---- Save current configure to flash
4- generate a flip flop 4 MHz signal for RF output
5- generate an activation signal
6- read the voltage and current output sample

In the next step the supply DC was calibrated :

A DC voltage (with PSSV label) was generated on DAC pin of microcontroller so that PWM in power supply can be set and drive power supply switching like what is stated in section 2. This DC voltage labeled with PSSV pin at feedback microcontroller (pin 29) by two fine (1.6 mv) and coarse (16 mv) incremental and decremental steps.
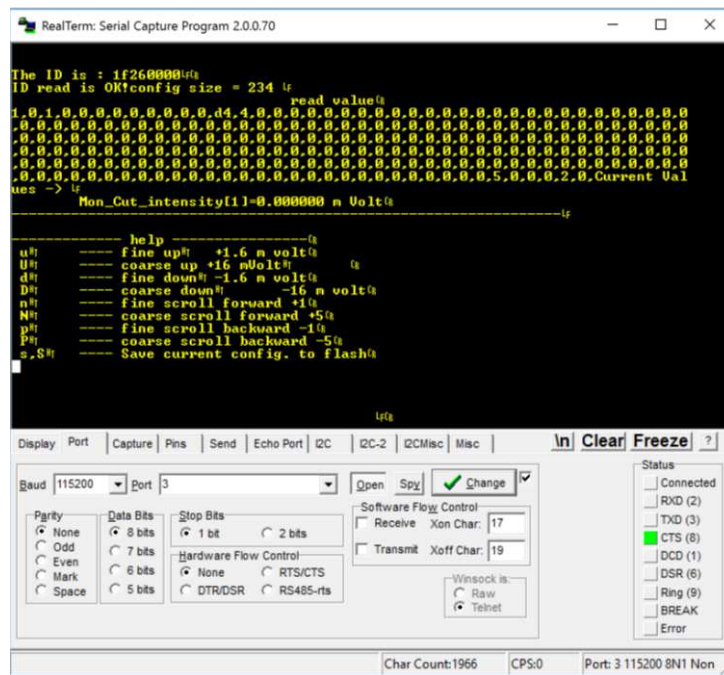
Figure 3- 30 RealTerm serial capture program 2.0.0.70 was used as virtual keyboard and display

Adjustment was done by a virtual keyboard and display (RealTerm serial capture program 2.0.0.70), which can communicate with the microcontroller instead of using a real keyboard and display Figure 3-30.

As can be seen the baud rate was set to 115200 bps without parity with one stop Bit and 8 data Bit without hardware flow control.

To verify the performance of the communication, if you press the (H,h,?) keys the help menu will be appear.

-------------- help ----------------

u   ---- fine up   +1.6 m Volt

U   ---- coarse up   +16 m Volt

d   ---- fine down   -1.6 m Volt

D   ---- coarse down   -16 m Volt

n   ---- fine scroll forward   +1

N   ---- coarse scroll forward   +5

p   ---- fine scroll backward   -1

P   ---- coarse scroll backward   -5

s,S   ---- Save current configure to flash

in case that:

- the upper case or lower case U is pressed, the PSSV will increase 16 mV or 1.6mV
- the upper case or lower case D is pressed, the PSSV will decrease 16 mV or 1.6mV
- the upper case or lower case N is pressed, the setting level will be incremented 1 or 5 upward
- the upper case or lower case P is pressed, the setting level will be decremented 1 or 5 backward
- The upper case or lower case S is pressed, both will save the adjusted value in flash memory corresponds with the setting level

Now the PSSV was set to the switching PWM IC and monitor the DC supply.

RF driving signal

This signal is generated basically at frequency of 8 MHz in feedback microcontroller and via CPLD transformed to two separated 4 MHz signal in flip flop form. In fact this two signals are representing to the output. Figure 3-31 shows RF driving signal which is generated by CPLD.
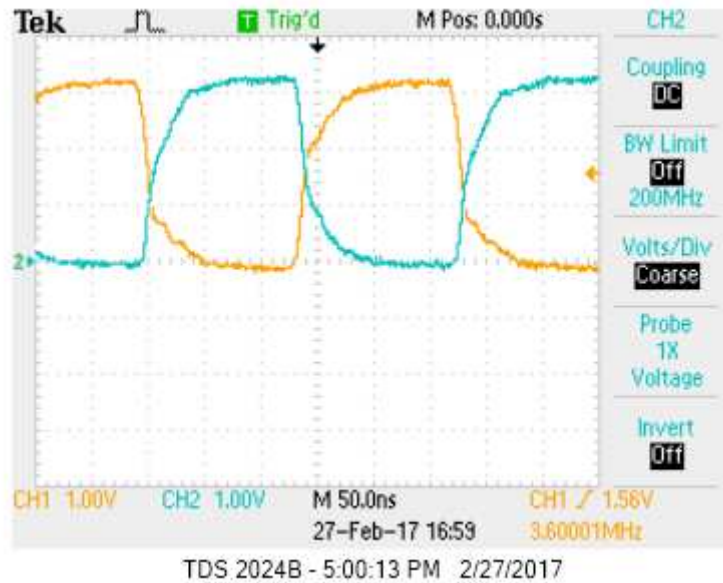
Figure 3- 31 RF1 (pin70 CPLD) and RF2 (pin74 CPLD)at 3.6 MHz in CPLD

Feedback voltage and current sampling

In this step, voltage and current sensing circuit outputs were applied to the feedback microcontroller. As already mentioned, the current and voltage sampling circuits are connected to the output part of the system, where the system is connected to the tissue. Through the current and voltage transformer RMS values are measured. This V_{RMS} And I_{RMS} are used by the feedback system to calculate the tissue impedance by feedback microcontroller.

Voltage and current sample were read at ADC port and the impedance value were calculated (sample rate is 10KHz). Voltage, current and impedance were reported and displayed every 50ms.

The voltage sensed from output was tuned proportional to the RMS value of the load voltage, but the sampling scale was set to a certain level not to damage the Microcontroller ADCs. Therefore, In order to show the real value, in coding the coefficient values for both voltage and current was considered. Then a specific resistive load (580 Ω) was applied to the output to calibrate the system.

The voltage and current sampling was calibrated by the oscilloscope TEKTRONIX TDS2024B voltage and current in Figure 3-32, 4-33 show the linearity to the load variation.
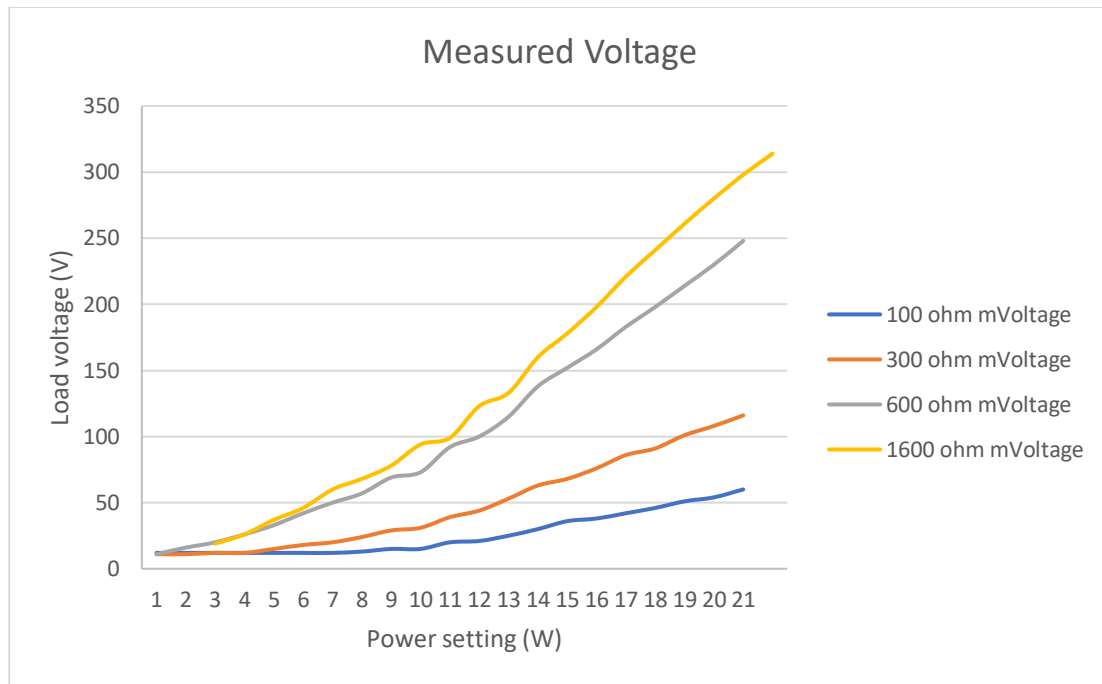
Figure 3- 32 Measured voltage for different loads shows a linear behavior
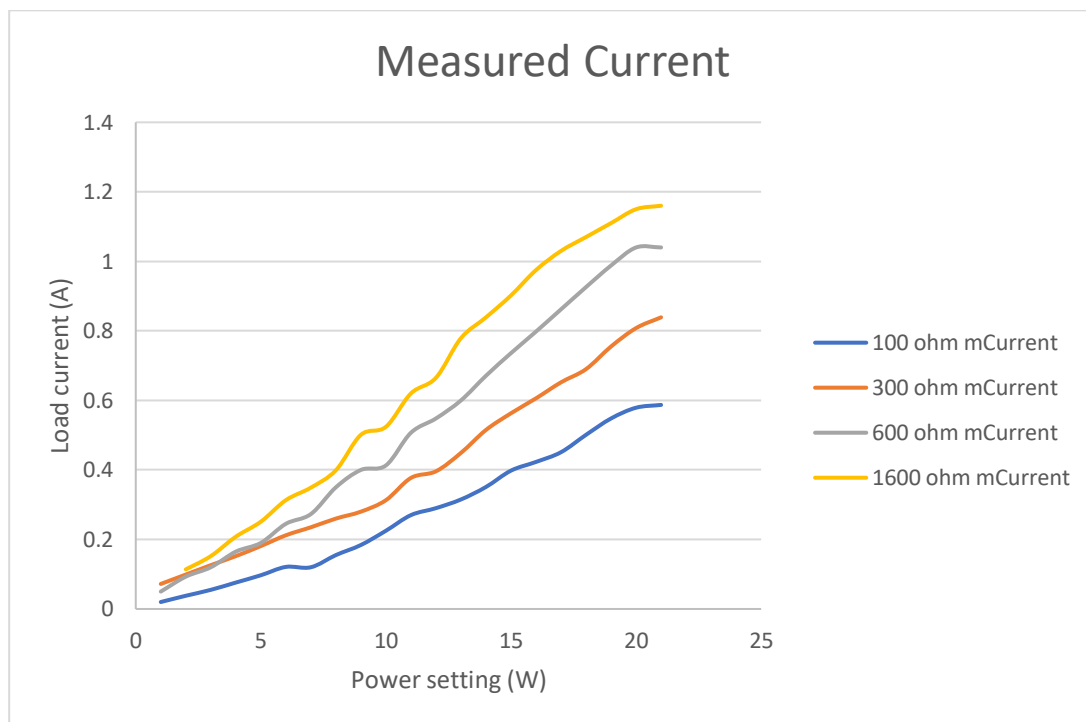
Figure 3- 33 Measured current for different loads shows a linear behavior

With a rough overview, it is clear that voltage and current have a proportional relation with power setting which helps to determine impedance. Therefore, next step would be impedance determination during coagulation to control the rate of coagulation.

Impedance monitoring

Impedance monitoring could be done by sensing the voltage and current of load in microcontroller. Therefore, a continues variable load which simulates the tissue coagulation was designed and made Figure 3-34. This load block with sliding knob provides a variable resistive load in the range 50-1600 Ω. In order to be most similar to the tissue coagulation, in each step the impedance will increase gradually without disconnecting during switch to the next (higher) or prior (lower) impedances.
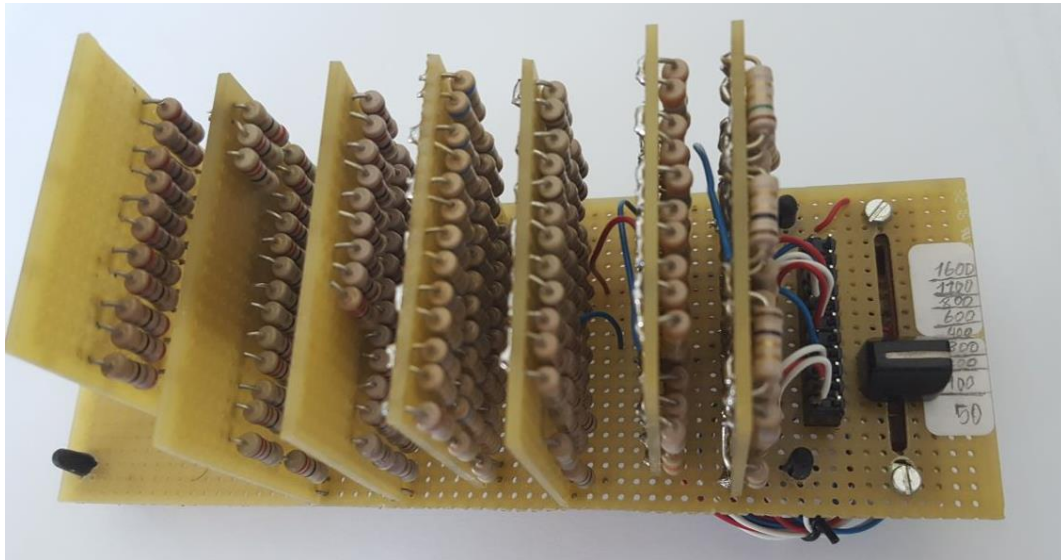
Figure 3- 34 Variable resistive load bank to simulate tissue coagulation

This resistive load with carbon film resistors has no inductive effect which is quite equivalent for coagulative tissue since in this frequency membrane capacitive effect is negligible and can be neglected.

In fact this resistive variable load is used to calibrate the real time impedance monitoring. The results with varying the impedance for different power setting yielded fault in impedance monitoring. Although the current and voltage sensing are quiet precise, the possible fault can be due to the fault in current sensing. This could initiate as a result of capacitive coupling of output with device chassis and load in this frequency, which cannot be sensed completely or nonlinearity of the current for variable power setting and load. This capacitive current leakage in the following will be found indirectly, when the transfer function of the system elicited by mVolatge and PSSV based on the calibrated load. In fact system recognizes the output load in a feedback loop by solving an equation which is function of mVoltage and PSSV as defined values. This process will be discussed later in detail.

3.5 Impedance calibration

Impedance calibration requires at least two calibrated parameters for voltage and current or load related parameters indirectly.

4.5.1 Voltage calibration corresponds to the impedance

As measured voltage by microcontroller and scoped voltage with Tektronix TDS 2024B for different loads and power setting in Figure 3-35 shows a constant offset, a simple function

Figure 3-36 could calibrate the voltage based on measured voltage. This voltage will be used in control process and power calculation.
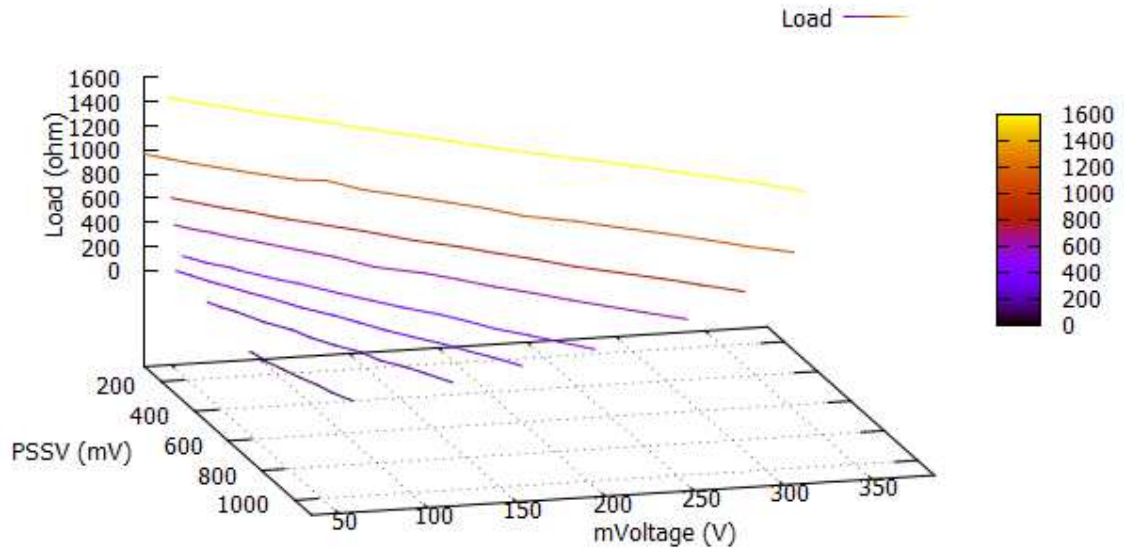
Figure 3- 35 Measured voltage vs PSSV and impedance which shows a linear variation

Although a polynomial function of voltage would be more fit and precise but would take time and decrease sampling rate for controlling the coagulation, therefore a linear interpolation is more preferential. (V_{Load}=2.15 $mVoltage^{0.781}$)
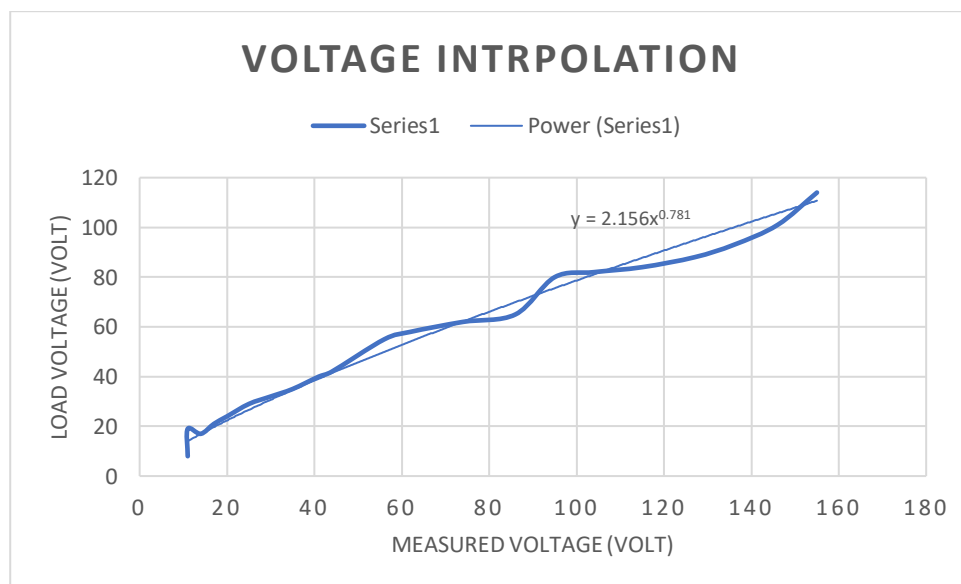
Figure 3- 36 Measured voltage

3.6 Experimental setup

The whole experimental setup is shown in Figure 3-64. This setup includes RF generator and peripheral devices and meat as a biological tissue.
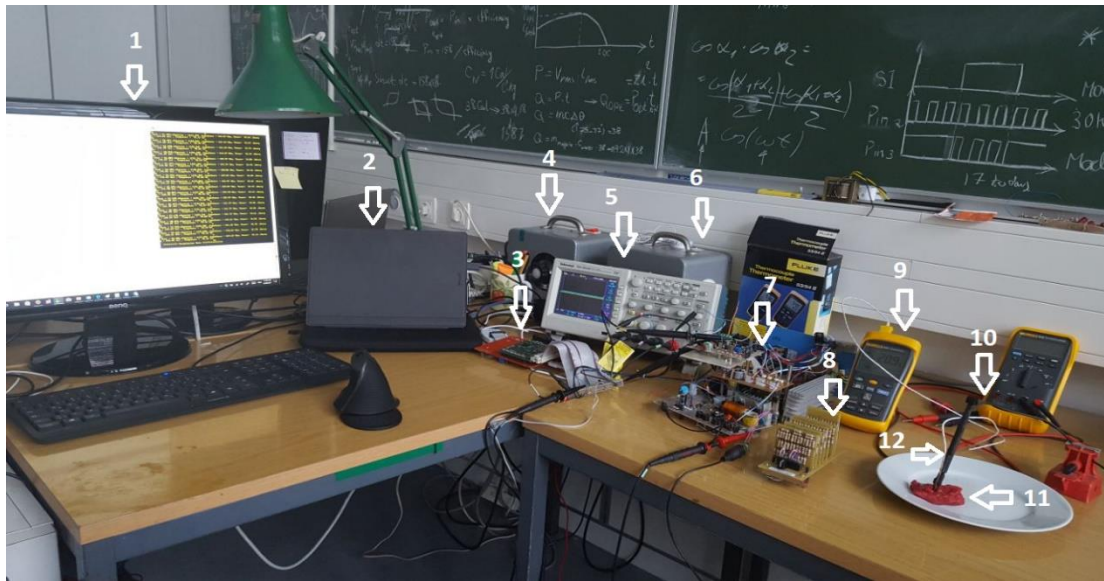
Figure 3- 37 Experimental setup for meat coagulation

Experimental setup description:

1- Report screen which is connected to the PC and shows the parameters like impedance, temperature and power real time
2- PC which is in communication with evaluation board with serial port to use keyboard and display via serial terminal interface.
3- Evaluation and feedback module which are responsible for the impedance control
4- Auto transformer which regulates the line power to the pre-set voltage, in fact with this auto transformer stability of the system to the line voltage can be considered
5- Tektronix TDS2024B oscilloscope which is used as calibrated measurement to scope the measured feedback parameters like voltage drop on load and ADC input of feedback module
6- Isolator transformer which isolates the line power. As this experimental system has many exposed parts, an isolation from power line can reduce the risk of electric shock considerably.
7- RF generator which generates the RF energy and sample the voltage drop on load for feedback module
8- Calibrated variable resistive module which is used to verify the sensed impedance
9- Thermometer FLUKE 54II which monitors the temperature in the site of the applying RF energy between to bipolar tips of applicator.
10- Bipolar applicator to apply the RF energy into the Tissue (meat)
11- Fresh meat as biological tissue muscle which corresponds to the muscle structure in soft palate, tongue base and turbinate tissue

12- Thermometer sensor which is located inside the meat where the bipolar applicator tips are inserted to monitor the temperature of the tissue during the RF apply

4. Results

4.1 Current calibration corresponds to the impedance

current sampling and calibration needed another strategy, since the current sensing had no calibrating reference like the voltage. As can be seen in Figure 4-1 current has a nonlinear behaviour for different impedances, therefore a bended surface was extracted based on calibrated voltage and load at the output Figure 4-2. Current nonlinearity especially for higher impedances caused an unacceptable prediction for calibrating, therefore another approach was considered to calculate the impedance by an indirect parameter, which is explained latter.
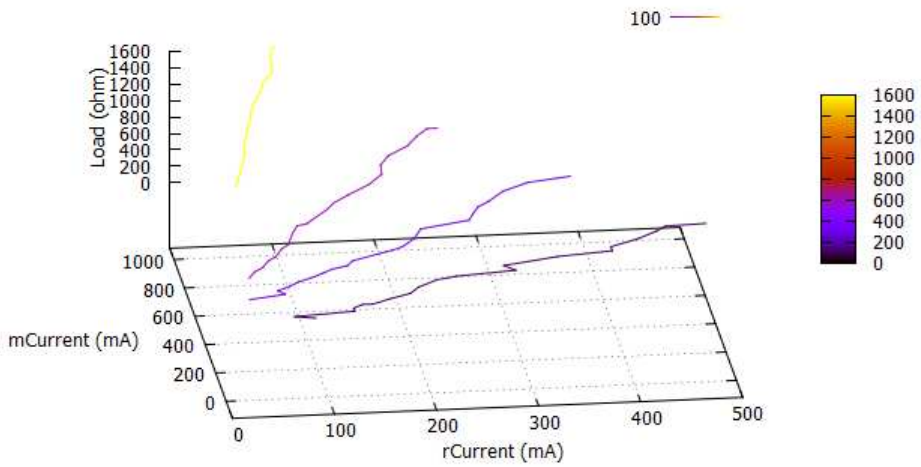
Figure 4- 1 mCurrent (measured current) and rCurrent (real current) vs load
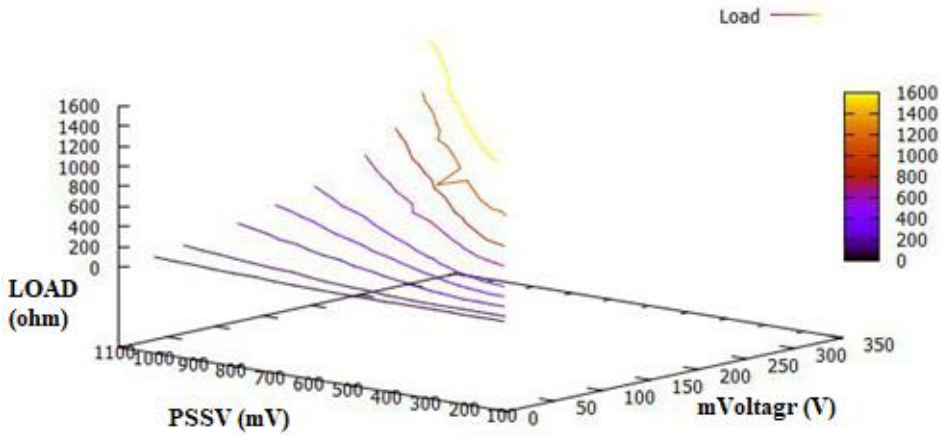
Figure 4- 2 Measured current b)PSSV (X axis mv),mVoltage (Y axis volt), load (Z axis Ω)

71

4.2 Impedance calibration with indirect parameter

A substitution parameter instead of current comes from setting power supply for a defined impedance. By assuming that a predefined load has a define voltage drop then power can be calculated. Likewise, This setting parameter for power supply stands for the second parameter to calculate unknown impedance at the output. In order to make it more clear, system behaves as a power constant in a particular impedance range (100- 1200 Ω), if we set the system for a particular power then impedance will change by time due to coagulation, for instance impedance increases, then power will decrease and system in a control feedback tries to compensate it by increasing the voltage at power supply. This compensation and impedance change are related together by a specific function to the impedance. Therefore, In order to find this function a complete measurement was done and power supply setting voltage (PSSV) scoped for different measured voltage setting separately for each impedance from 50-1600 Ω, which are shown in Figure 4-3 – 4-10.
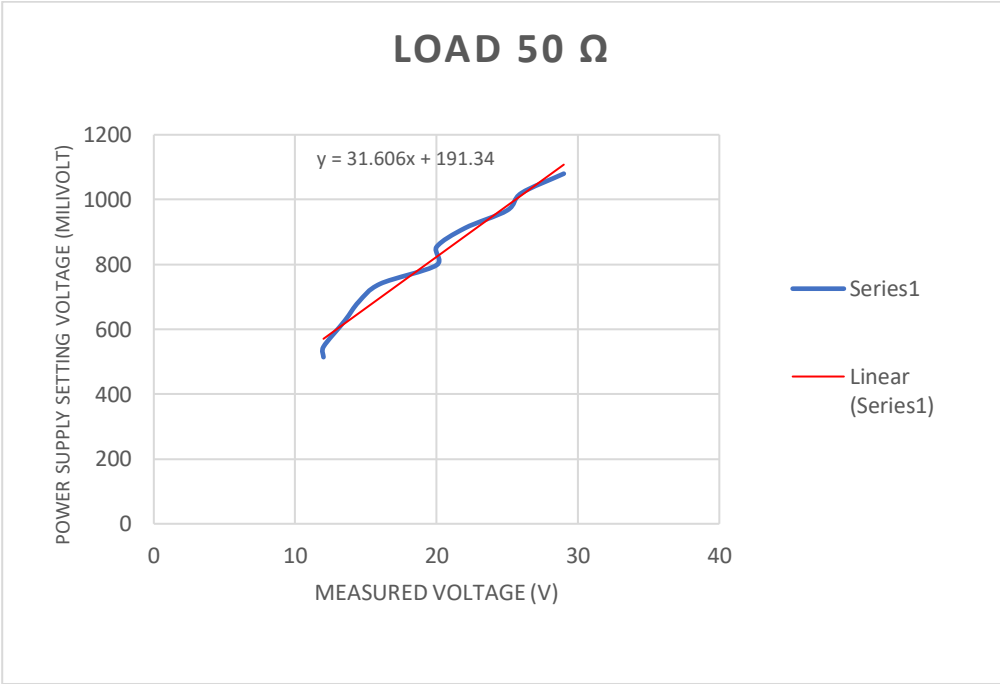
Figure 4- 3 Power supply setting voltage (PSSV) vs measured voltage for 50 Ω load
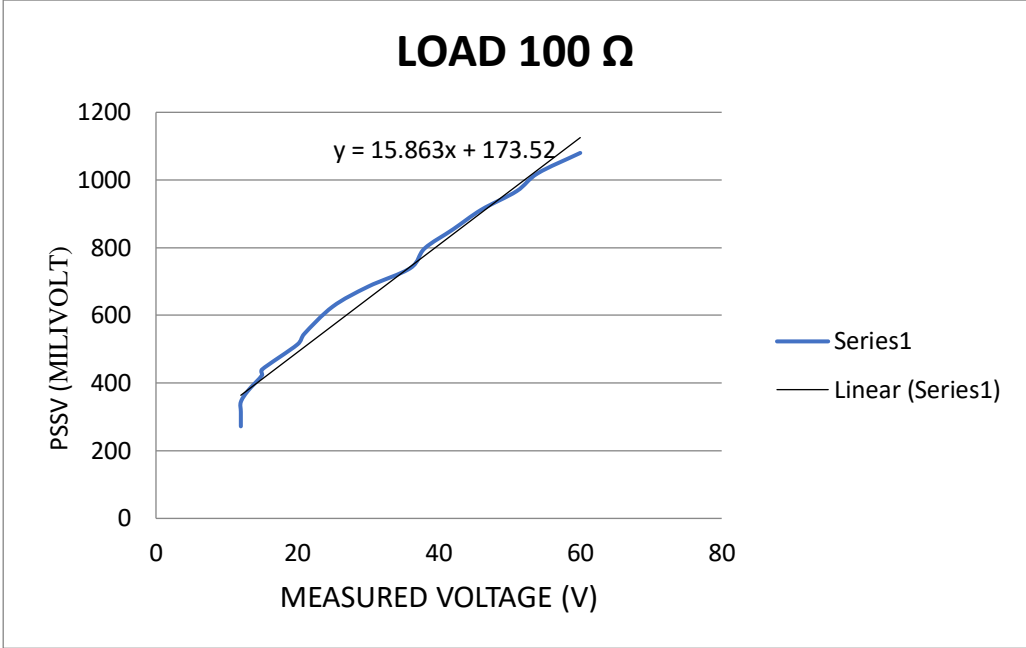
Figure 4- 4 Power supply setting voltage vs measured voltage for 100 Ω load
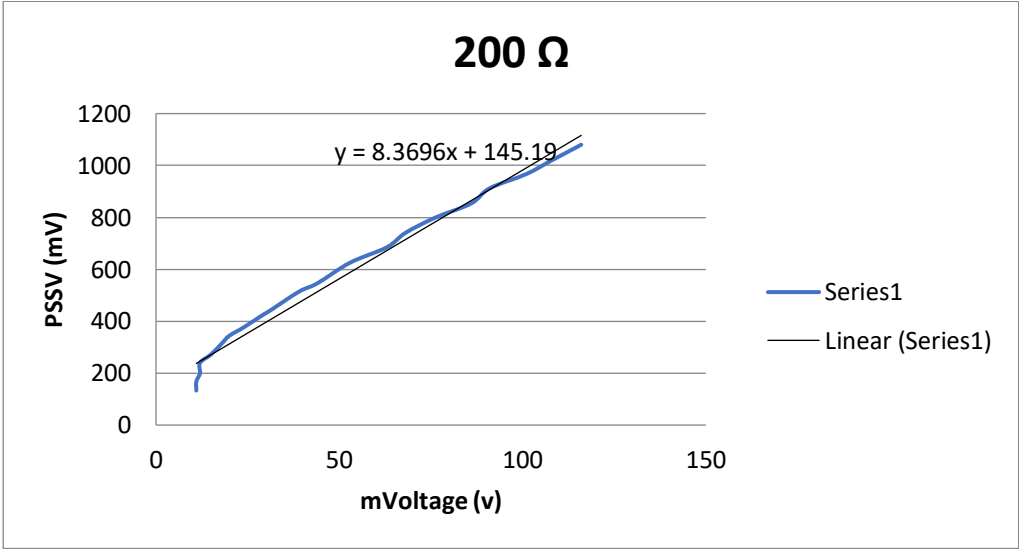
Figure 4- 5 Power supply setting voltage vs measured voltage for 200 Ω load
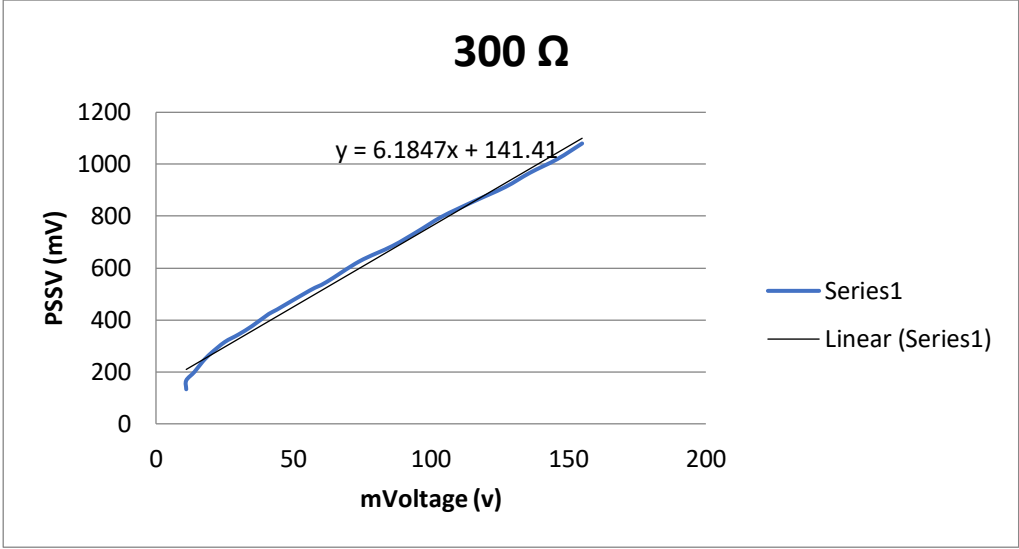
Figure 4- 6 Power supply setting voltage vs measured voltage for 300 Ω load
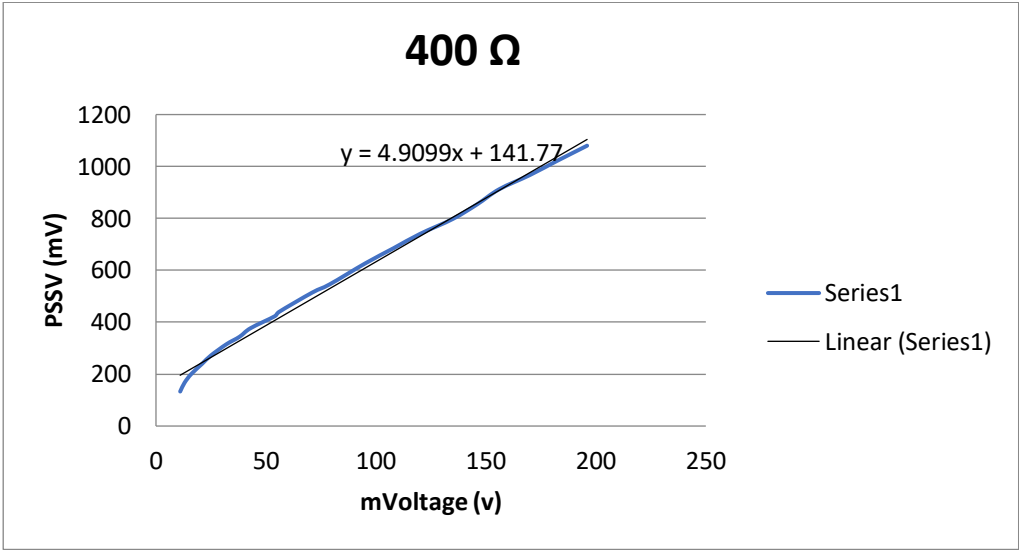
Figure 4- 7 Power supply setting voltage vs measured voltage for 400 Ω load
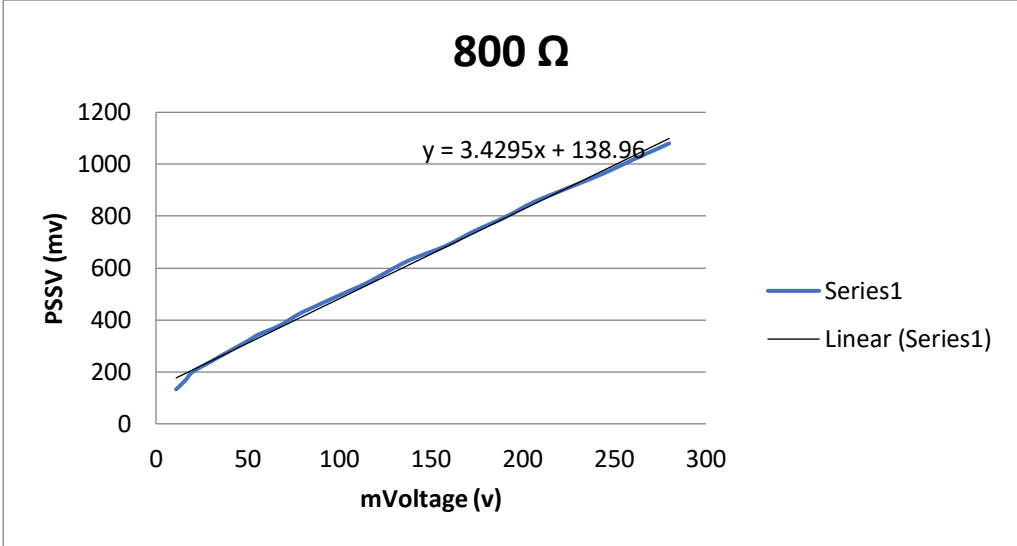
Figure 4- 8 Power supply setting voltage vs measured voltage for 800 Ω load
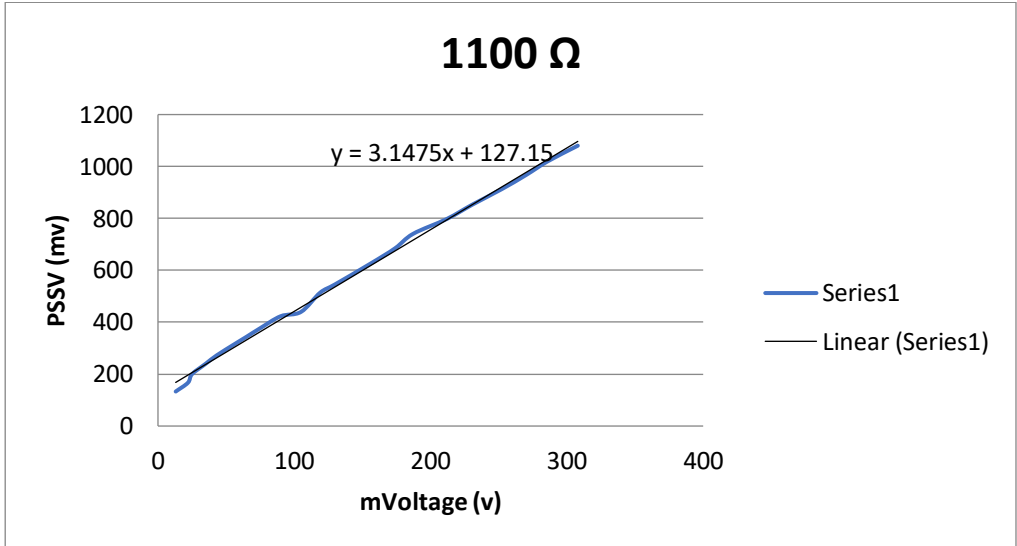
Figure 4- 9 Power supply setting voltage vs measured voltage for 1100 Ω load
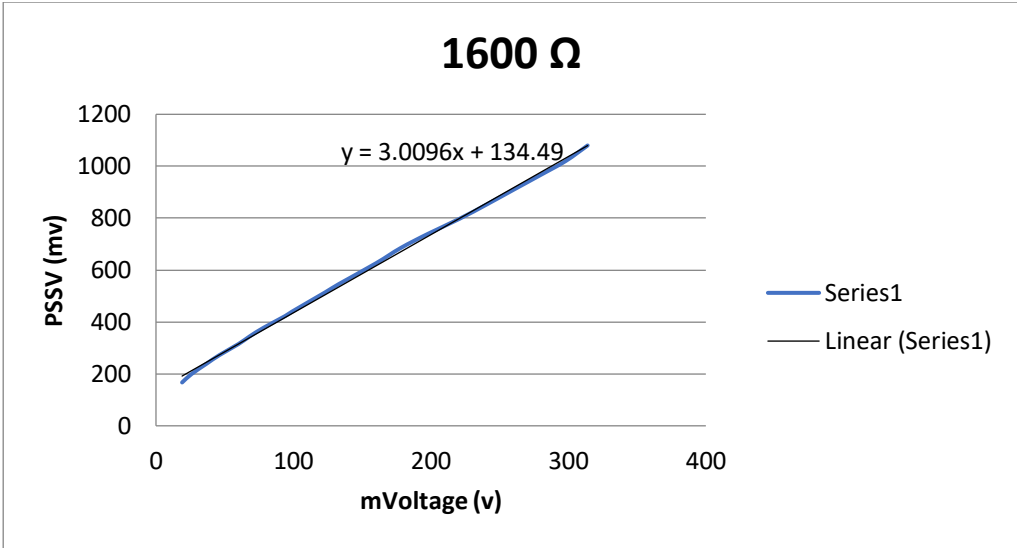
Figure 4- 10 Power supply setting voltage vs measured voltage for 1600 Ω load

A linear trendline (y= ax+b) shows an appropriate interpolation, which x stands for measured voltage (mVoltage) equation (4-1), a and b are functions of R_{load}.

$$PSSV = G(R_{Load})\ mVolatge + H(R_{load}) \qquad (4\text{-}1)$$

$G(R_{load})$ and $H(R_{load})$ as function of load are shown in Figure 4-11 and Figure 4-12.
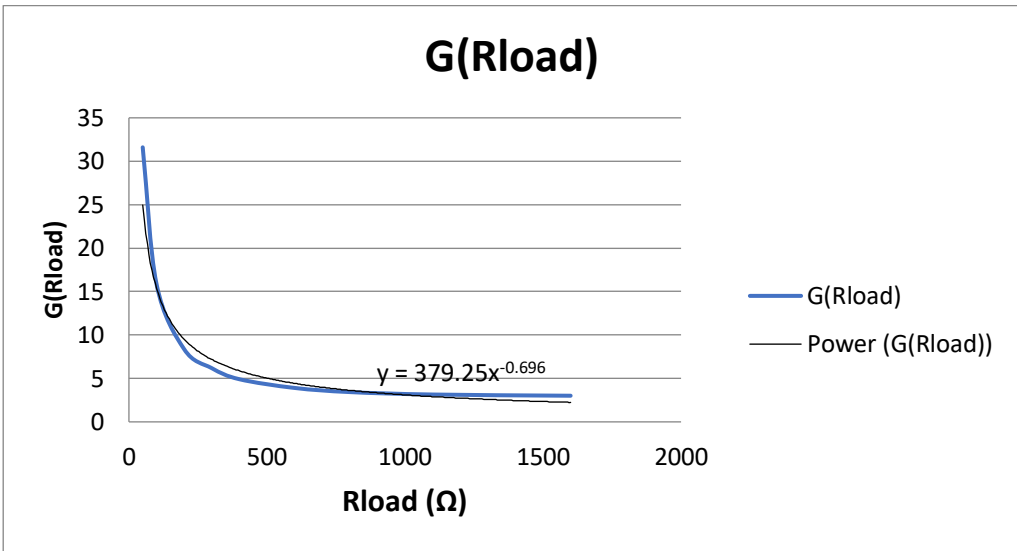
Figure 4- 11 $G(R_{load}) = G'(R_{load}) +2.4$
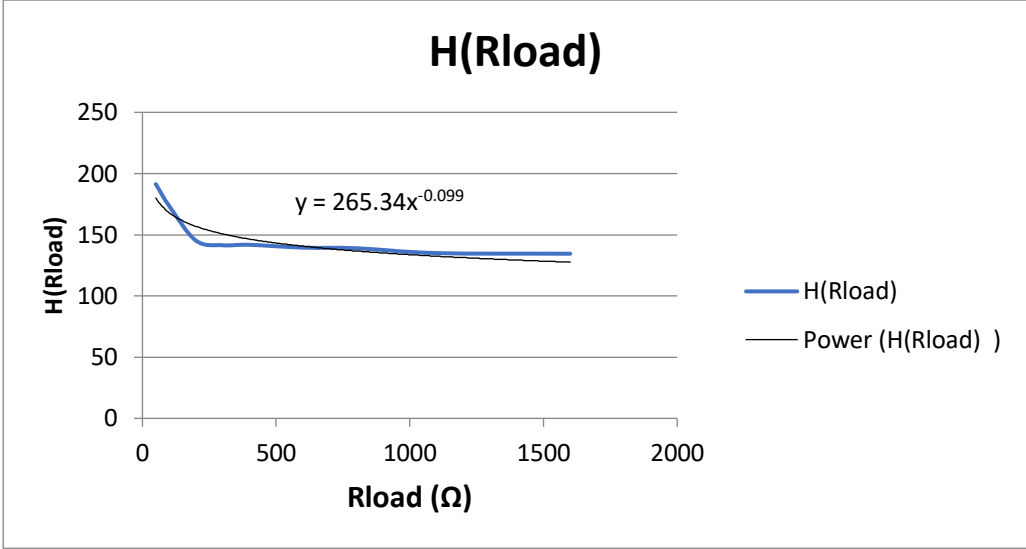
Figure 4- 12 $H(R_{load}) = H'(R_{load}) + 132$
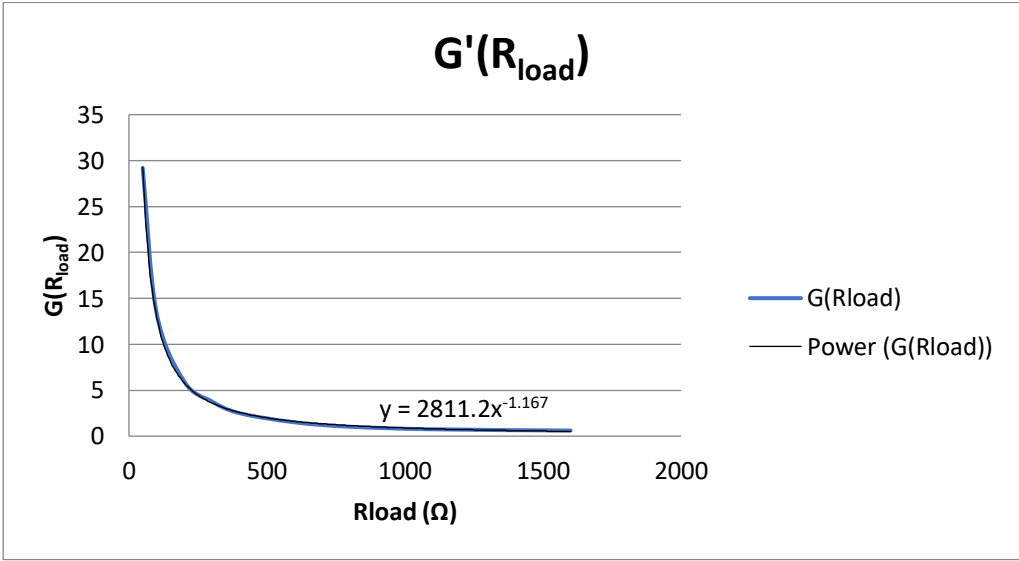
Figure 4- 13 $G'(R_{load})$
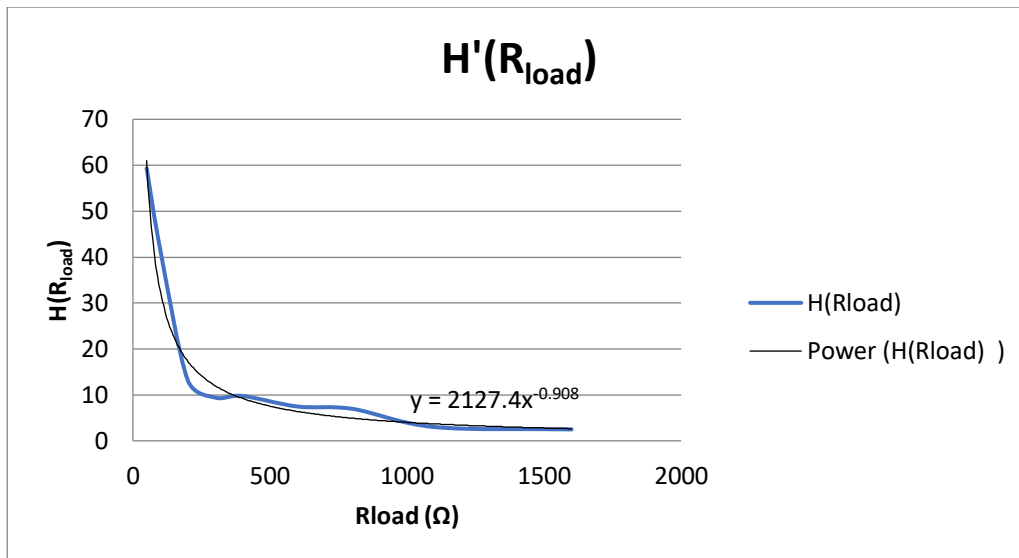
Figure 4- 14 H′(R_{load})

Equation (4-1) defines the whole function based on elicited graphs:

$$F(PSSV, mVoltage, R_{load}) = (2811.2 R_{Load}^{-1.167} + 2.4)* \ mVoltage + 2127.4 R_{Load}^{-0.908} + 132 - PSSV \quad (4-1)$$

R_{load} is the only unknown in this equation, since PSSV and mVoltage are definite values. R_{load} can be calculated by False position method and bisection method. R_p and R_m are minimum and maximum possible values for Load, which are used to calculate the R_c as output load Figure 4-15.

```
double CalcImp(float vSys,float mVolt)
{
  int i;

  Rp=2000;
  Rm = 1;
  Rc = 0;


  for(i=0;i<10;i++)
  {
    Rc = ( Rp + Rm )/2;
    Equ = -PSSV + (2811.2*pow(Rc,-1.167) + 2.4)*mVolt + 2127.4*pow(Rc,-0.908) +132;
    if(Equ > 0)
      Rm = Rc;
    else if(Equ < 0)
      Rp = Rc;
    else
      break;
  }
  return(Rc);
}
```

Figure 4- 15 Code function based on false position method to calculate R_{load}

Impedance calibration was done with calibrated variable resistive load.

4.3 Power control algorithm

Impedance calculation procedure detects the unknown load in output. Therefore, power on tissue can be calculated exactly. As discussed already, system behavior for wide range of the load is current constant for very low impedances (<50 Ω) to protect the system against short circuit and voltage constant for very high impedances (>1600) to protect the tissue against high voltage spark and power constant in between (50< load >1600) Figure 4-16.
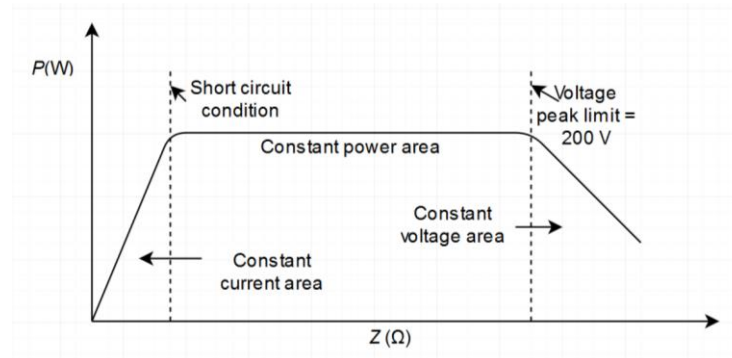
Figure 4- 16 Output power based on impedance, current in low impedance, power constant between 50-1600 Ω and constant voltage for impedance higher than 1600 Ω

In order to apply this behavior to the system a control loop system Figure 4-17 is required. This control loop calculate the power by measuring voltage drop on definite load. If the power increases or decreases rather than preset value correct it via adjusting PSSV.
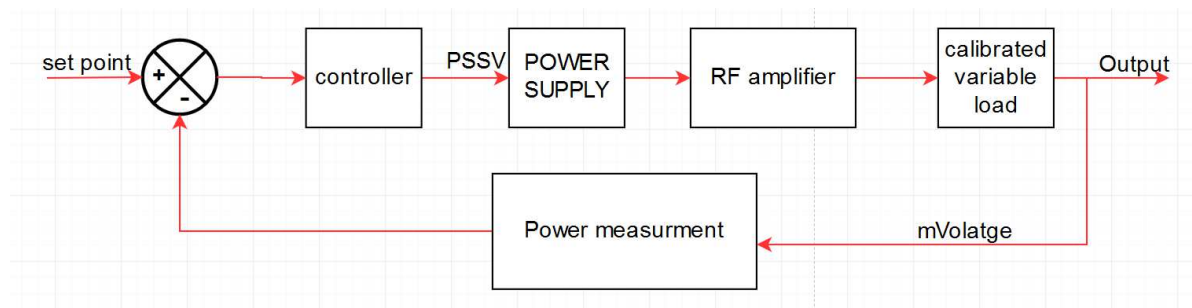
Figure 4- 17 Control loop to set the parameters based on impedance variation in output stage

4.4 Boundary conditions

Boundary conditions are related either to system or tissue and are very important to control the system. This boundary conditions are mentioned in the following:

- Tissue impedance which is a function of power and should be less than coagulation impedance $Z= f(\text{p}) < Z_{coagulation}$
- Tissue temperature is function of power and biological properties which should be less than 85 °C
- RF apply duration to the biological tissue should be set in a secure domain and is function of energy which is given to the tissue $T= f(Q)$

- Threshold voltage defines a certain level of voltage in which no spark can be created $V_p < 200$
- Threshold Current defines a certain level of current which represents short circuit in output of system and can be define less than 50 Ω < short circuit impedance range(less than 50 Ω)

4.4.1 Tissue impedance

In order to analyze the tissue impedance during RF apply, a piece of meat was prepared to find out impedance change over the time for a constants power 25 watt. The result on a muscle tissue is shown Figure 4-18 (initial meat temperature was 22 °C and mass 20 gr).
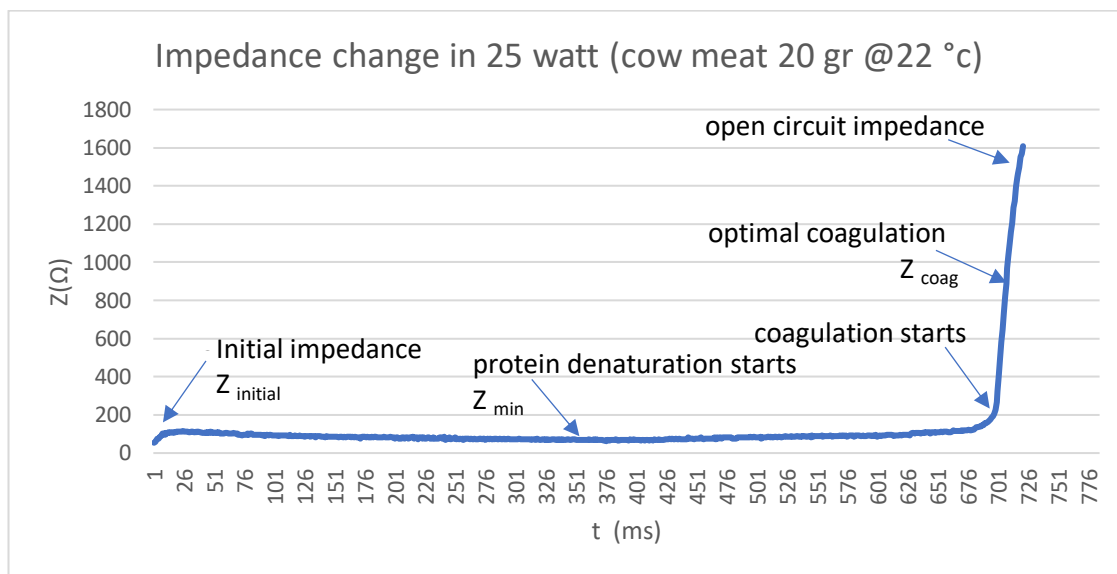
Figure 4- 18 Meat tissue impedance over time at 25 watt 4 MHz RF

This tissue impedance model is an appropriate approximation to prepare an algorithm for coagulation process. Once the RF is applied to the meat tissue impedance is detected in the range of 100- 150 Ω then energy continuously is given to the tissue and ionic vibration increased and for a while the conductivity of the tissue is increased and impedance decreased. This process goes on up to a certain level that energy which is applied continuously increases tissue temperature and consequently protein denaturation starts. This biochemical changes causes a lower RF current conductivity and consequently impedance starts to rise to a certain level that current cannot pass through the tissue structure and impedance dramatically rises. Likewise, impedance rise in coagulation region is very steep and sampling rate should be quiet fast to protect tissue against excess coagulation and consequently open circuit situation (>1600 Ω). Impedance in the steep region is more critical and increases the coagulation region markedly, therefore the faster this region is sensed the better control on coagulation rate will be achieved. Otherwise open circuit or high impedance situation is more prone to create spark in coagulation region and as a result perforation in tissue specially in the soft palate region with a very thin tissue layer will be increased.

4.4.2 Tissue temperature

RF energy which is given to the tissue, escalates the tissue temperature with a simple model equation (1-1). For a different constant power setting temperature increase is shown in Figure 4- 19. Temperature boundary is defined around 85°C since in this level all kind of muscle tissue proteins are denatured and increasing temperature leads to boiling water content of intra and extra cellular space and bursting effect close to the applicator and tissue contact. Likewise, Bursting effect increases impedance and starts sparking which is out of control and perforation risk will increase markedly.
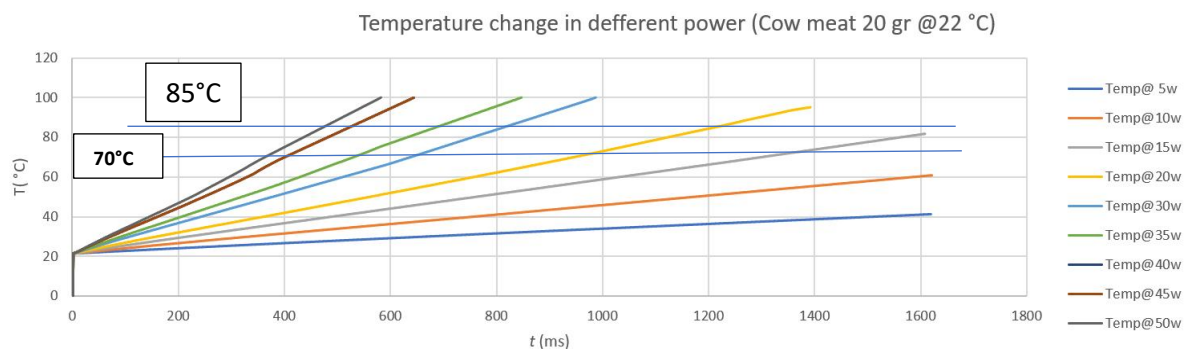
Figure 4- 19 Temperature rise for different power setting vs time

Figure 4-19 experiment was done for a piece of meat with 20 grams mass and 22°C initial temperature. Therefore, for body temperature 70°C determine the required time for coagulating tissue. In other words, time will be restricted by power setting time and is a function of setting power. A proper power setting over coagulation should consider the time during volumetric reduction tissue operation so that physician can do consecutively coagulation in different regions with an optimum time. A time period between 3-6 second could be more tolerable for the surgeon and patient to coagulate a point.

Given energy also as a product of power and time is shown in Figure 4-20.

Energy in defferent output power (Caw meat 20 gr @22 °C)
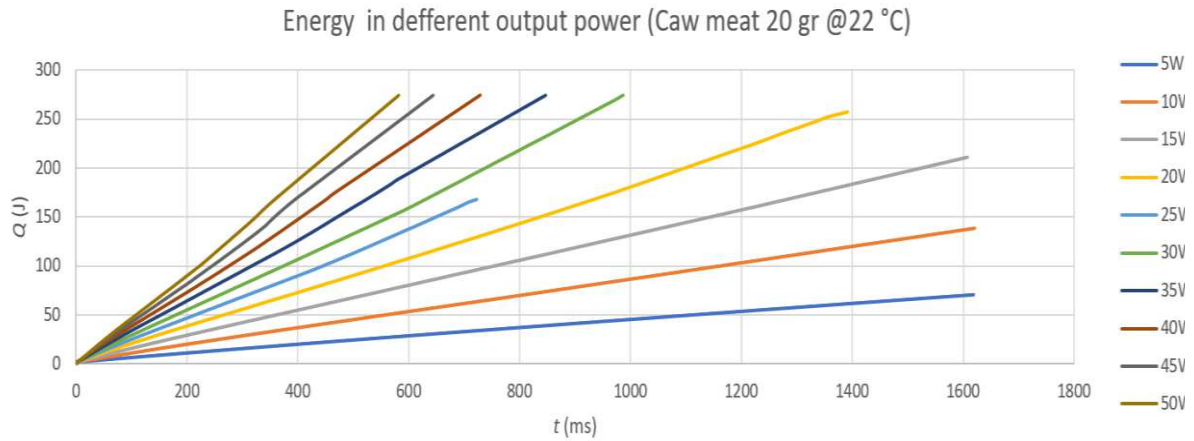
Figure 4- 20 Given energy to the tissue in time domain

4.4.3 RF apply duration

RF apply duration is a function of RF power energy , Figure 4-21 shows that with lower RF power duration is increased. At 5 and 15 watt coagulation will not happen at all while with 50 and 45 watt this duration decrease to 1 second, therefore an optimum power range is between 20-40 watt. Consequently, physician has an optimum time, not too much which is time consuming , no too short which leads scare and perforation.

Impedance change in defferent power (Caw meat 20 gr @22 °c)
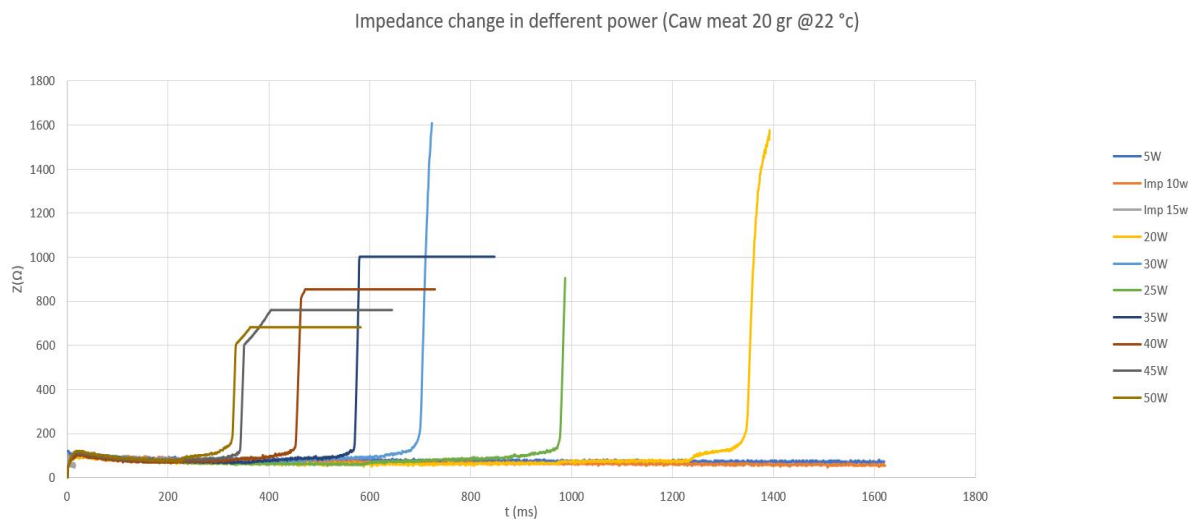
Figure 4- 21 Coagulation curve for different RF power energy

4.4.4 Threshold voltage

As discussed in section one, voltage drop over tissue should be controlled over whole coagulation process not to exceed 200V (V_p rms < 200). This boundary condition protects

tissue against spark and perforation. In fact voltage drop over tissue is a function of tissue impedance during coagulation process. Since power control algorithm changes the amplitude of RF at output to keep the power constant, therefore by increasing impedance over coagulation process feedback system increases the RF amplitude.

4.4.5 Threshold current

It is possible due to any reason a short circuit condition at output happen, like applicator short circuit which its tips would be in touch with a metal part in surgery environment; therefore, a current threshold which stands for short circuit should be considered. As the system can detect real time impedance at the output, impedance could be a control factor to define a short circuit as a current boundary, which is assumed less than 50 Ω as short circuit condition.

4.5 Coagulation process

4.5.1 Coagulation rate function

Coagulation for different tissues depends on biological tissue properties and is a relative amount. Therefore, system needs a function (4-2) base on the impedance to determined coagulation impedance. This function is based on minimum impedance Figure5-41 as a definite value.

$$f(Z_{min})= Z_{min} + K. Z_{min} \tag{4-2}$$

k is determined based on clinical approaches on biological outcomes. On the meat sample with a very small change for k factor a great impact on coagulation amount was observed. As the initial impedance changes after a short period to Z_{min} and Z_{min} is constant for a relatively long period of time Figure 4- 1, Z_{min} is used as variable for this function.

4.5.2 Coagulation algorithm

Upon boundary condition an algorithm was considered to follow the impedance behavior for preset power to fulfill coagulation qualitatively and quantitatively.

START 200

201
Initialize variables
Z_{min}, V_{thresh}, I_{thresh},
Time over, $Z_{initial}$

The system continues to look for the activation
of the RF switch (block202)

202
Is RF switch active?   No

Yes   203
set interrupt for RF switch

204
set interrupt for short circuit

205
set interrupt for open circuit

206
start timer

207
RF amp health check

208
Is
AMP okay?   No

Yes   209
send request to turn on RF

210
send request to
turn off RF

211
hardware failure
alert

B

A

When the RF switch is turned on, the interrupts are
set for RF Switch(block 203), for Short Circuit
(block 204), and Open Circuit (block 205) so that
when one of these interrupt conditions occur,
the microprocessor automatically goes to the
instructions associated with block 234.

After the interrupts are set, the timer is started
(block 206). Asequence is run to check the
RF amplifier health (block 207), e.g., to look for an
Amplifier On signal or to check if certain voltages
are in a suitable range.If the amplifier is operating
properly, RF energy is turned on (blocks 208 and209).
If the amplifier is not operating correctly, an RF Off
request is made(blocks 209 and 210) and a Hardware
Failure Alert flag is set (block 211).

look for an Amplifier On signal or to check
if certain voltages are in a suitable range

a Hardware Failure Alert flag is set

The system looks for a hardware failure flag
(block 233). When the hardware failure is detected,
the controller provides a hardware failure
alert indication and shuts off. (blocks 243 and 244).

If RF energy is turned on (block 209), then the V_{rms}mvoltage and PSSV are read and the impedance, Z, is calculated by $_{equation\ via\ False\ position\ method}$ (block 212). The controller checks to see if the V_{enable} and I_{enable} flags are set. (block 213).

These flags are set when a minimum threshold voltage is present and a minimum threshold current is delivered through the electrodes of the device

After looking for a time over condition, the controller checks for a short circuit or open circuit condition. If a short or open circuit exists, the corresponding short circuit or open circuit bit is set (block 220), RF energyis turned off (block 221), and a hardware failure check is run (block 233).

The controller checks again for V_{enable} and I_{enable} in block 222, before proceeding to the threshold determining portion of the circuit illustrated. If the voltage or current did not exceed V_{thresh}or I_{thresh} in blocks 214 and 216, the controller iterates the sequence beginning at block 212 for detecting time over, short circuit, opencircuit, i.e., the coagulation complete detection enable. This enables the device to wait until enough RF energy is delivered to the circuit to check for the coagulation complete condition.

If the V_{enable} and I_{enable} flags are set, the short circuit and open circuit bits are not set (block 220), and the time overcondition does not yet exist (block 219), the measured impedance used to determine if coagulation is complete as follows

The Z initial flag is set during the first iteration and Z_{min} is initially assigned the measured impedance value (blocks223-225).
Initially, Z_{min} is the same as the measured impedance and thus block 227 is bypassed at block 226.

A calculation is made of $f(Z_{min})$ (block 228). As long as the measured impedance is less than the $f(Z_{min})$, the sequence is iterated (229, 231). In the next iteration of blocks 223−231, the newly measured impedance is compared to the previous measured impedance which has been assigned Z_{min} (block 226)

As long as the impedance is decreasing, Z_{min} will be reassigned the new value of the measured impedance (blocks 226 and 227) and the steps repeated. When the measured impedance is greater than or equal to $f(Z_{min})$, i.e. the threshold impedance, the coagulation complete flag is set (block 230). If coagulation complete flag is set, the RF is turned off (block 232) and the hardware failure check is run.

4.5.3 Coagulation control process

A complete control system is required to secure the whole process not only for patient and quality of the coagulation process, also protect the system against overload Figure 4- 22.

For a couple of milliseconds regardless of the system setting for an appropriate coagulation impedance measurements loop with assistance of Z_{min} detection applies a very secure voltage and find out whether the current situation is a short circuit , open circuit or normal condition(50-1100 Ω). In case that impedance is in the normal range, the other control units contribute to achieve a complete control.

In the next step, system samples the mVoltage on the output stage and calculate the impedance and regulate the given power to the load constantly. Therefore, a closed loop control tries to adjust the PSSV voltage corresponds to the load variation as result of the coagulation process. This regulation process follows completely the load variation and impedance measurement block calculates the impedance as a transfer function which was yielded in equation (4-1). Likewise, mVolatge monitoring does not let the system exceeds over the threshold voltage to make the arc between applicator tips and tissue.

As can be seen in control diagram duration of coagulation and given energy as well as temperature are function of impedance and can contribute as additional control parameters. Moreover, coagulation rate is function of minimum impedance which is calculated at the beginning and k Coefficient defines the rate of coagulation, the higher k values the larger coagulated area and vice versa.
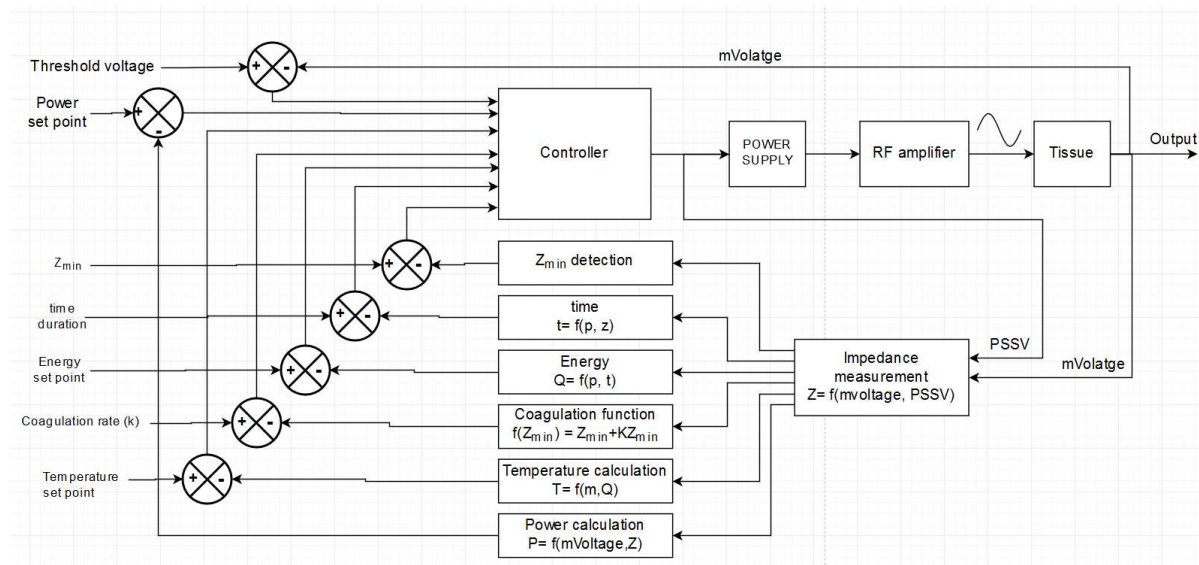

Figure 4- 22 Control system diagram to control the coagulation process with multi parametric input

4.5.4 Time response of the system

Time response of the system is really crucial especially if the rate of the coagulation is considered in Figure 4-54. Therefore, a quiet fast sampling and impedance calculation can follow the changes as precise and fast as possible, since a slow system cause an over estimated energy and unwanted coagulation rate. Here sampling and impedance calculation by counting the instruction clock is given in the range of 0.5 msec. Corresponds to the Figure5-54 :

$$\text{Slew rate of coagulation curve} = (1600-200) \ \Omega/25mS = 56 \ \Omega/ms \qquad (4-3)$$

By taking into account the time response of the system in the range of 0.5 ms and equation (4-3) , each sampling can detect impedance of tissue with 23 Ω resolution.

A report during the coagulation of the meat shows the impedance change rate and impedance monitoring in Figure 4-23. This test was done with a switch on a resistive load to switch output impedance from 300 Ω to 400 Ω abruptly. As can be seen the system after 10 times sampling reached to the 400 Ω. This experiment determine the time response of the system. Certainly the report procedure by serial port is a time consuming process and this lag in system will not exist, since we do not need to report it.

```
= 109.68 Jul , Tempature =  53.61 ClF
CRLF                                          CR
Uout = 96.379,vSysecon = 949.072 ,Impedance = 303.58 Ohm, Power=  30.60 ,Energy
= 110.20 Jul , Tempature =  53.76 ClF
CRLF                                          CR
Uout = 96.804,vSysecon = 949.072 ,Impedance = 307.49 Ohm, Power=  30.48 ,Energy
= 110.72 Jul , Tempature =  53.91 ClF
CRLF                                          CR
Uout = 97.441,vSysecon = 949.072 ,Impedance = 311.39 Ohm, Power=  30.49 ,Energy
= 111.21 Jul , Tempature =  54.05 ClF
CRLF                                          CR
Uout = 101.398,vSysecon = 949.072 ,Impedance = 334.82 Ohm, Power=  30.71 ,Energ
y = 111.73 Jul , Tempature =  54.20 ClF
CRLF                                          CR
Uout = 103.523,vSysecon = 949.072 ,Impedance = 350.43 Ohm, Power=  30.58 ,Energ
y = 112.25 Jul , Tempature =  54.35 ClF
CRLF                                          CR
Uout = 106.044,vSysecon = 949.072 ,Impedance = 369.96 Ohm, Power=  30.40 ,Energ
y = 112.74 Jul , Tempature =  54.49 ClF
CRLF                                          CR
Uout = 107.277,vSysecon = 949.072 ,Impedance = 377.76 Ohm, Power=  30.46 ,Energ
y = 113.26 Jul , Tempature =  54.64 ClF
CRLF                                          CR
Uout = 109.035,vSysecon = 949.072 ,Impedance = 389.48 Ohm, Power=  30.52 ,Energ
y = 113.77 Jul , Tempature =  54.79 ClF
CRLF                                          CR
Uout = 109.523,vSysecon = 949.072 ,Impedance = 393.38 Ohm, Power=  30.49 ,Energ
y = 114.29 Jul , Tempature =  54.94 ClF
CRLF                                          CR
Uout = 110.133,vSysecon = 949.072 ,Impedance = 401.19 Ohm, Power=  30.23 ,Energ
y = 114.78 Jul , Tempature =  55.08 ClF
CRLF                                          CR
Uout = 111.026,vSysecon = 949.072 ,Impedance = 405.09 Ohm, Power=  30.43 ,Energ
y = 115.29 Jul , Tempature =  55.23 ClF
CRLF                                          CR
Uout = 111.107,vSysecon = 949.072 ,Impedance = 409.00 Ohm, Power=  30.18 ,Energ
y = 115.81 Jul , Tempature =  55.37 ClF
```

Figure 4- 23 Impedance are detected with the rate of 10 Ω per report

4.6 Applicator design

Applicator geometry can affect the range and size of coagulation area. As already discussed, in this approach a bipolar method is used to apply RF energy to the tissue. Therefore, a bipolar structure is needed to circulate the current flow in tissue in between tow conductive tips. While in monopolar technique current enters in one tip and exit from large reference electrode on the other side and current flows through the large portion of the body Figure 4-24.
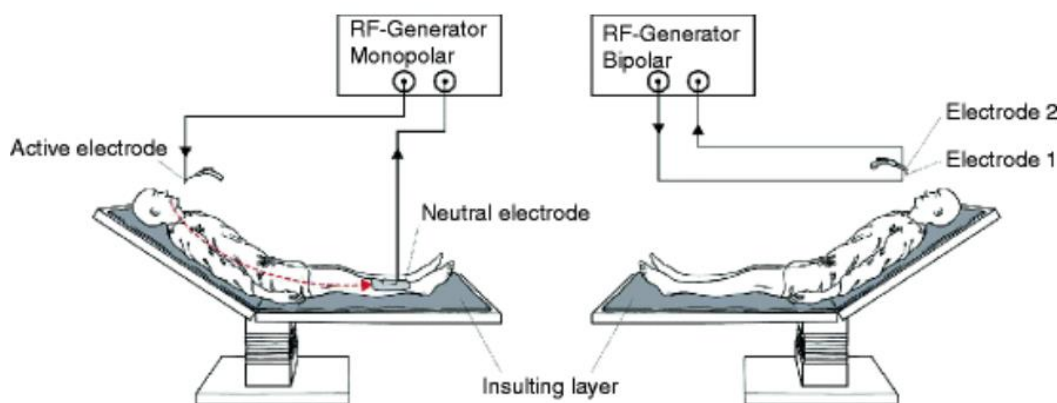

Figure 4- 24 Bipolar and monopolar technique in RF application [39]

There are many different bipolar applicators at the market. Nevertheless, depends on site of ablation in soft palate, nasal turbinate or tongue base an ergonomic design of the applicator facilitate the maximum flexibility for physician and less unwanted ablation for patient. On the other hand, no need to mention that post-operative healing process with the best ablation result is achieved with contribution of all related factors including physician, generator and appropriate applicator. As this project does not aim to focus on applicator design, a simple

bipolar applicator Figure 4-25 was made to perform the experiments. Tipps are made of stainless steel profile and insulating layer is thermos shrink tube. Distance between 2 tips are about 5 mm and each tip is 1mm in diameter, which were sharpened to push easily into the tissue mechanically to some extend that insulated layer is places under mucus. This insulated cover protects mucus layer against ablation.
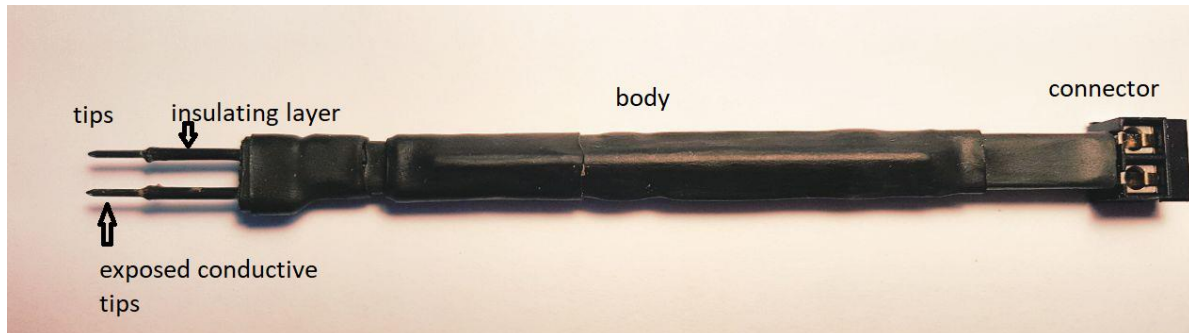

Figure 4- 25 Bipolar applicator for experimental application on meat tissue

4.7 Biological results

Experiments were done on fresh cow meat at initial temperature 22°C and 4-5mg mass, Figure 4-26 , Figure 4-27.
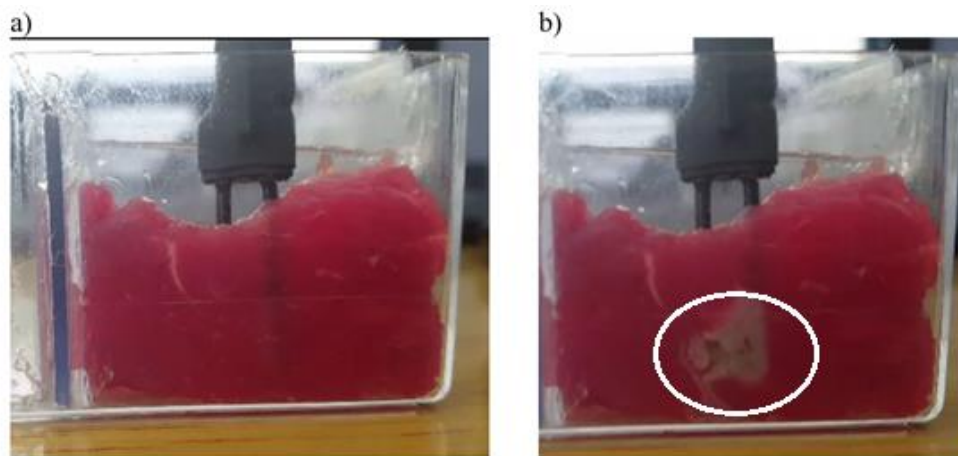

Figure 4- 26 Coagulation experiment with real time impedance monitoring on meat inside a transparent cavity so that the changes to be observable   a) meat with inserted bipolar applicator before applying RF energy b) coagulation process was done automatically by coagulation algorithm and feedback ($Z_{coag}= Z_{min}+200\ \Omega$), white region in the right picture.

A coagulation was defined based on minimum impedance Figure 4-26 plus 200 Ω, as can be seen in Figure 4-26b the white region represents the coagulated tissue. During this process there were no electrical arc and the process was done automatically based on the above mentioned algorithm. The size of white region corresponds to the Z_{coag} which is function of Z_{min}. In Figure 4-27 this value was decreased 100 Ω less than prior experiment ($Z_{coag}= Z_{min} + 100\ \Omega$), the coagulated region between bipolar region markedly decreased. This process was

monitored over the coagulation process by reporting the feedback sensed parameters and calculated impedance on the screen.
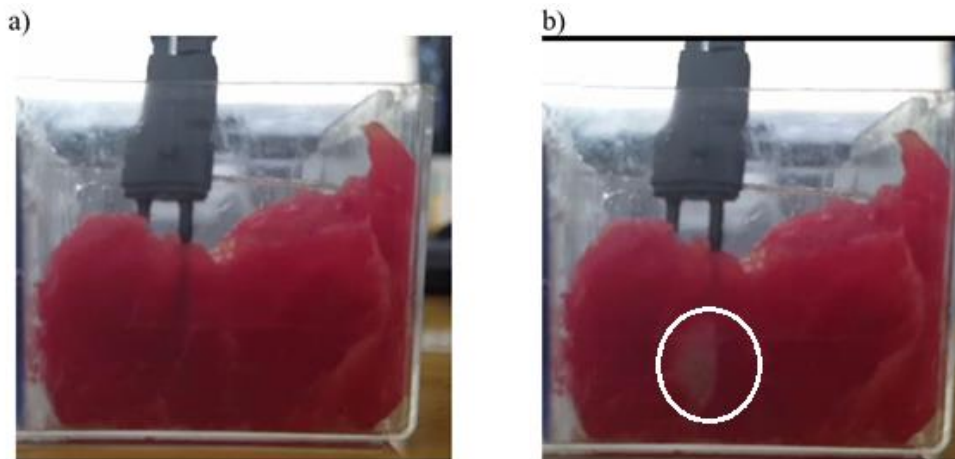

Figure 4- 27 Coagulation experiment with real time impedance monitoring on meat inside a transparent cavity so that the changes to be observable   a) meat with inserted bipolar applicator before applying RF energy b) coagulation process was done automatically by coagulation algorithm and feedback ($Z_{coag} = Z_{min} + 100\ \Omega$), white region as coagulated tissue is less than prior experiment.

5. Discussion

Nowadays volumetric tissue reduction in upper airways with RF therapy as a successful approach and routine minimal invasive method requires being considered and improved its drawbacks. Currently, the existent systems offer either temperature control by a direct thermocouple or impedance change on the target tissue, which thermocouple usage leads higher manufacturing cost for the disposable applicator in one hand and no control on other boundary conditions like sparkling due to the high voltage drop between tissue and applicator on the other hand. Moreover, all these systems utilize frequency in the range of a couple of hundred kilohertz, whilst researches have shown that higher frequencies in the range of megahertz represent less painful recovery for the patients. But such systems do not have feedback from the tissue to control the ablation process and physician had to coagulate by estimation or experience. Therefore, overtreatment, scar, and perforation could happen and jeopardize the patient.

A reliable solution would be a combination of advantages of both approaches to benefit not only from direct feedback of the ablating tissue, but also from less painful recovery due to the higher frequency. Hence, a reliable method which samples the bio-impedance at this frequency and controls the ablation process ensure a successful process. In fact, a closed loop control system can regulate the system by multi-factors and reduce the risk of unwanted temperature or scar and relief the physician not to exceed boundary conditions.

This thesis started with the design of radiofrequency generator in the range of 4MHz which was a superior frequency to pass the current both intra- and extracellular space, which means a lower tissue impedance and consequently lower current density passing through the tissue. Likewise, in RF design a very precise and flexible switching power supply, facilitate a precise control on the output power. This power supply provides system with a closed loop control system for a constant power over a wide range of the load.

Although the basic approach was based on the impedance calculation by current and voltage sensing directly on the tissue, in this thesis only voltage is sensed and another indirect controlling parameter corresponds to the calibrated load used to elicit the transfer function of the system. The advantage of these approaches is that current sampling circuit and consequently fault of current measuring is eliminated and a definite parameter (PSSV) is substituted. In addition, this method corrects the nonlinear current behavior and capacitive leak current.

A precise impedance detection system facilitates the system to regulate the power which is given to the tissue over the wide range of variable tissue. Since the system power is a function of impedance and does not behave independently of the tissue properties over coagulation or ablation process.

Moreover, a precise power control which is the function of the impedance was utilized to define a thermal distribution or concentration to have a very secure and intelligent coagulation corresponds to the biological properties of the tissue. This approach prevents blind or out of control coagulation and provides minimum side effect over recovery period. In addition, this conservative method provides repetitive therapy so that a satisfactory result is achieved.

Also, transfer function of the system was elicited mathematically with a scientific approach and calibrated with an external calibrated load. Final results in a qualitative point of view were completely obvious in size of the coagulated region when the impedance of tissue was changed just 100 Ω above prior setting.

As a matter of fact, closed loop control system guarantees an automatically coagulation based on the preset range of intentional necrosis grade. This process ensures the physician not to exceed mandate temperature in one hand and a very successful coagulation with a predefined size and no risk of perforation in mucus layer on the other hand.

Although this approach has above-mentioned advantages, it is still an invasive method and inserting applicator inside the tissue under the mucous layer is not pleasant for the patient. In addition, applying an electrical energy to the body requires a really sustainable and safe system to avoid electric shock for both patient and physician, which increases the manufacturing costs and complexity.

For the next step in the future, energy profile and thermal distribution profiles can be simulated by thermodynamic properties of the tissue with software like COMSOL and control the procedure more precise and efficient. Moreover, a control system can develop to set therapeutic parameters automatically based on the patient specification, which needs more clinical outcomes.
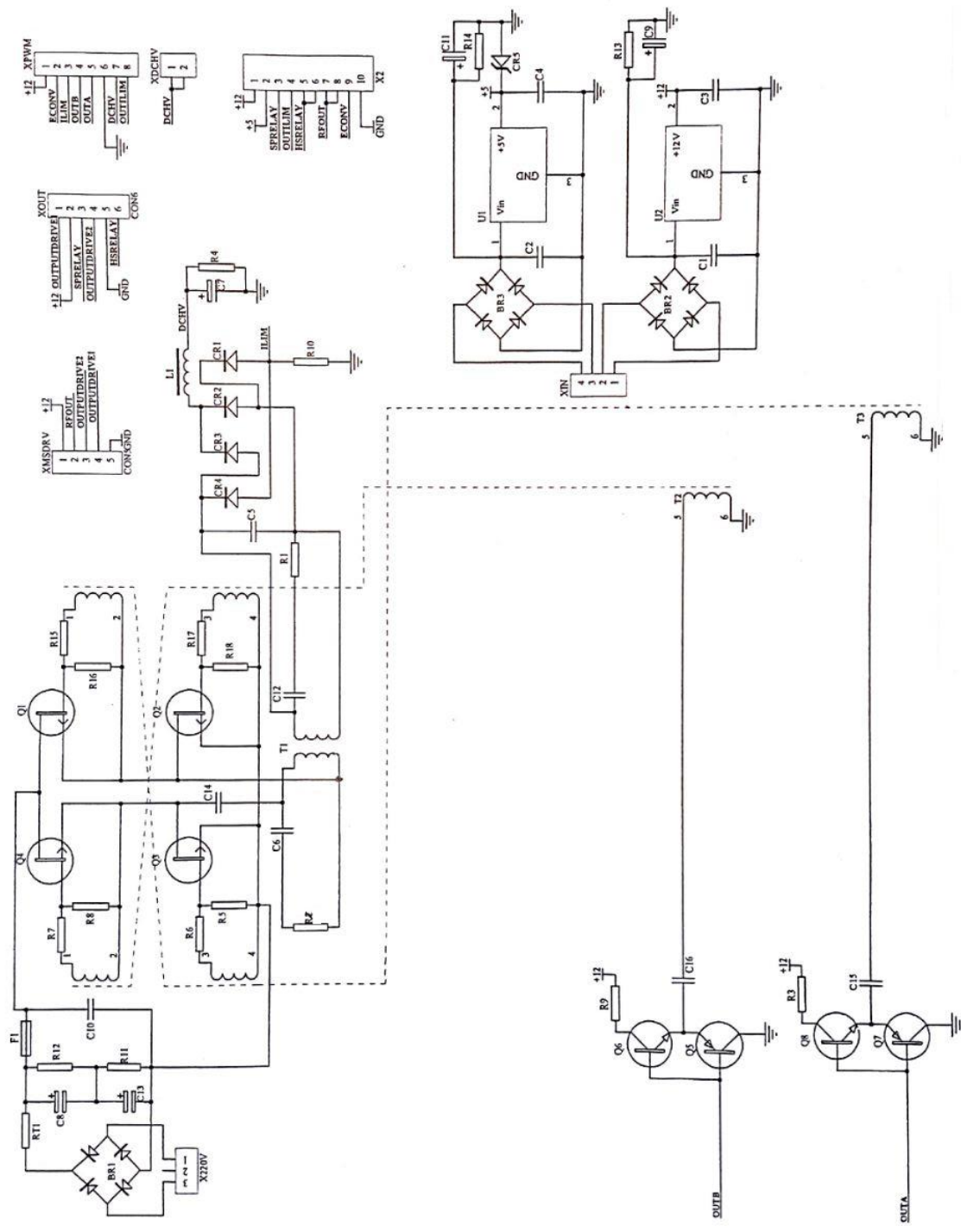
6.Appendix A

FigureA-1 System block diagram
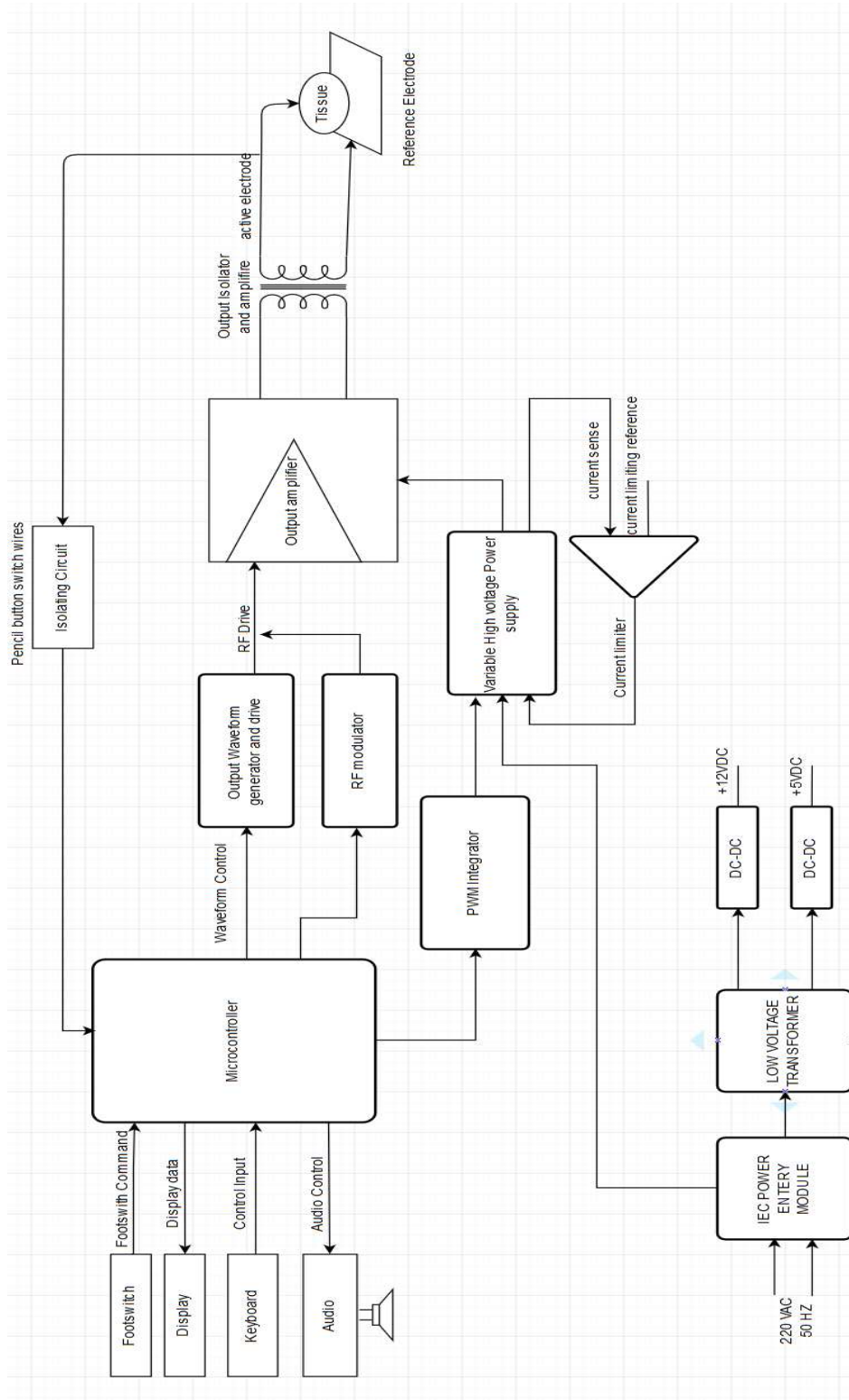
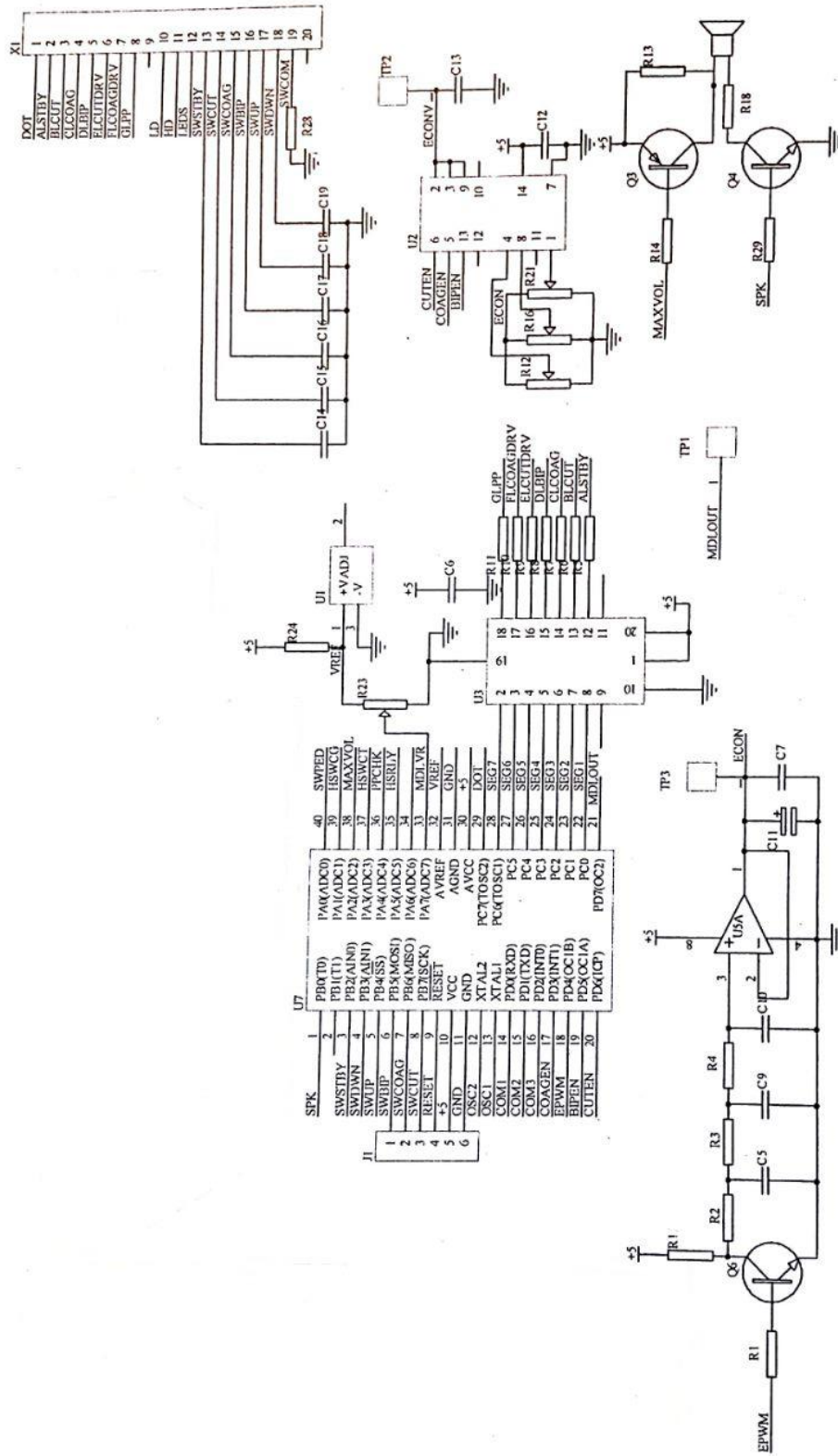**FigureA-2 control unit for variable power supply**
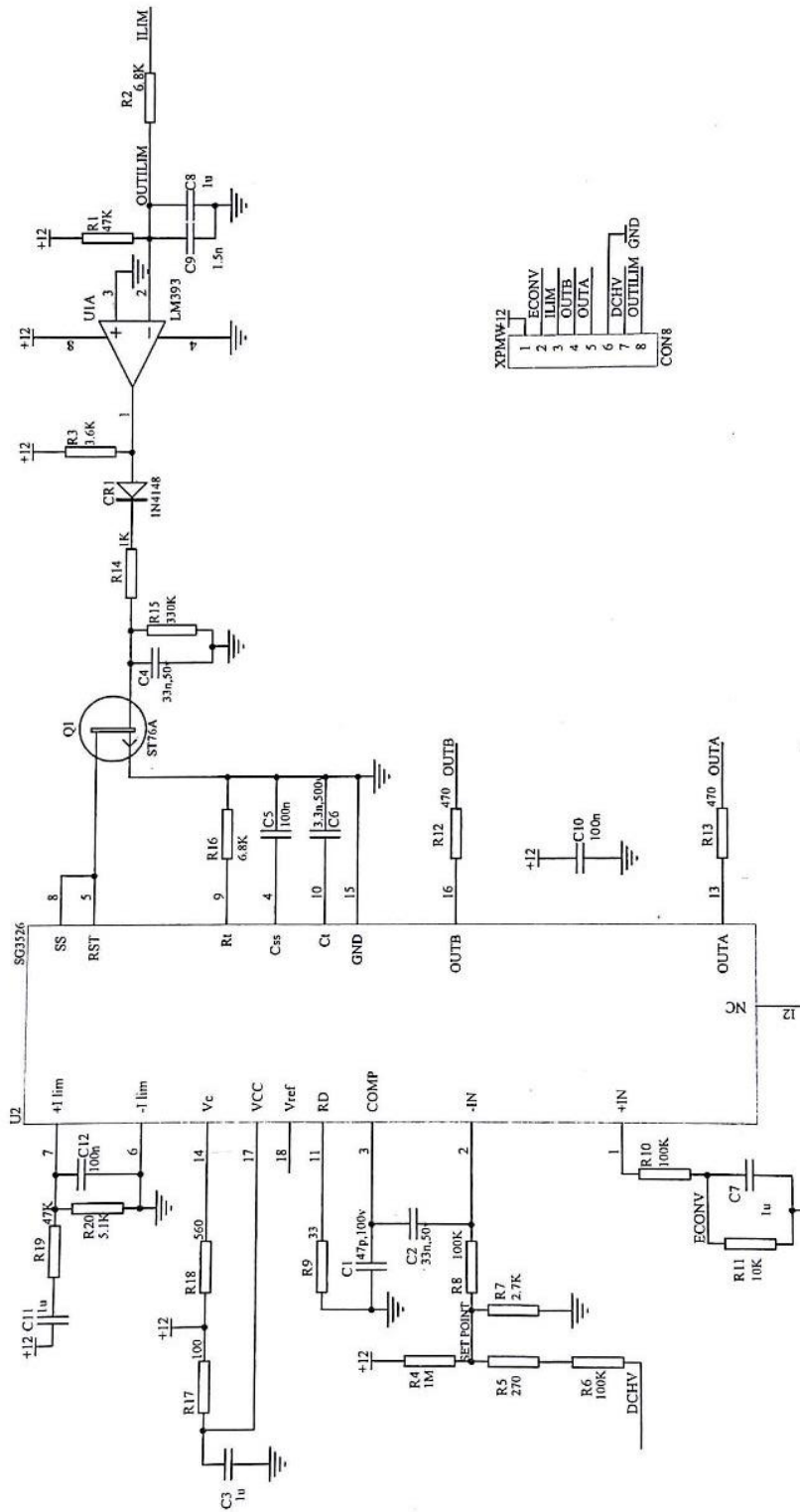
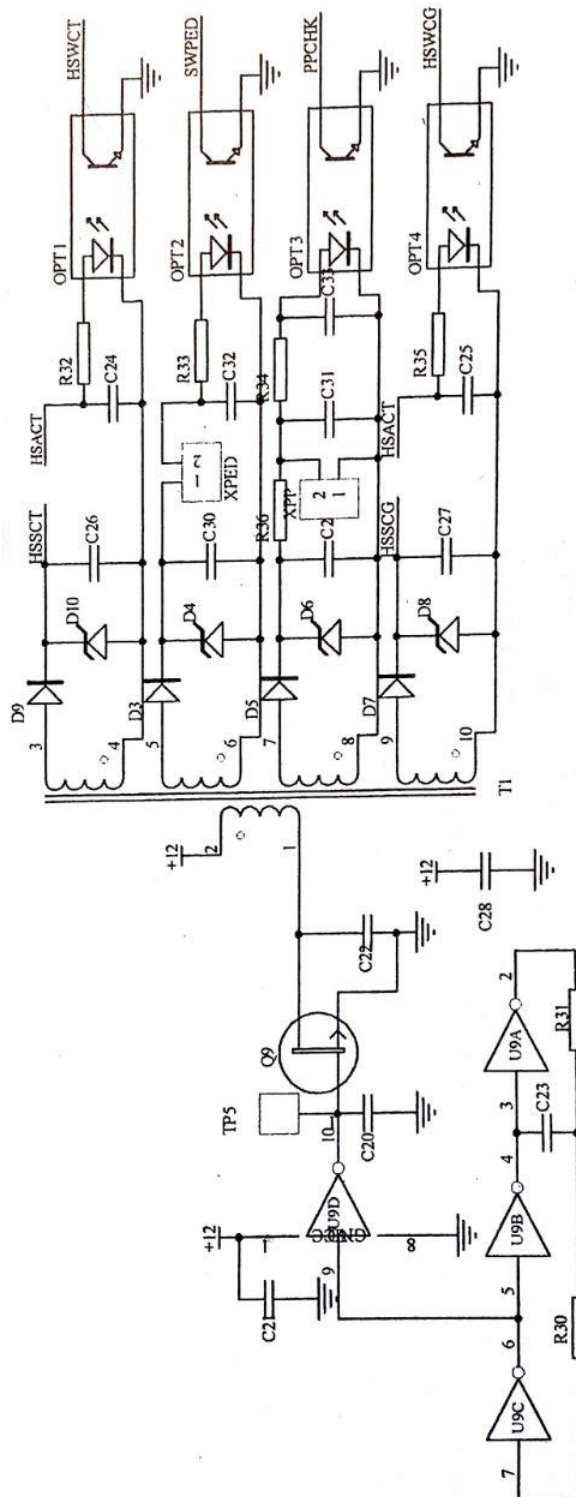**FigureA-3 switching high voltage DC-DC convertor**

Figure A-4 Control unit

FigureA-5 Isolation

FigureA-6 keyboard and display
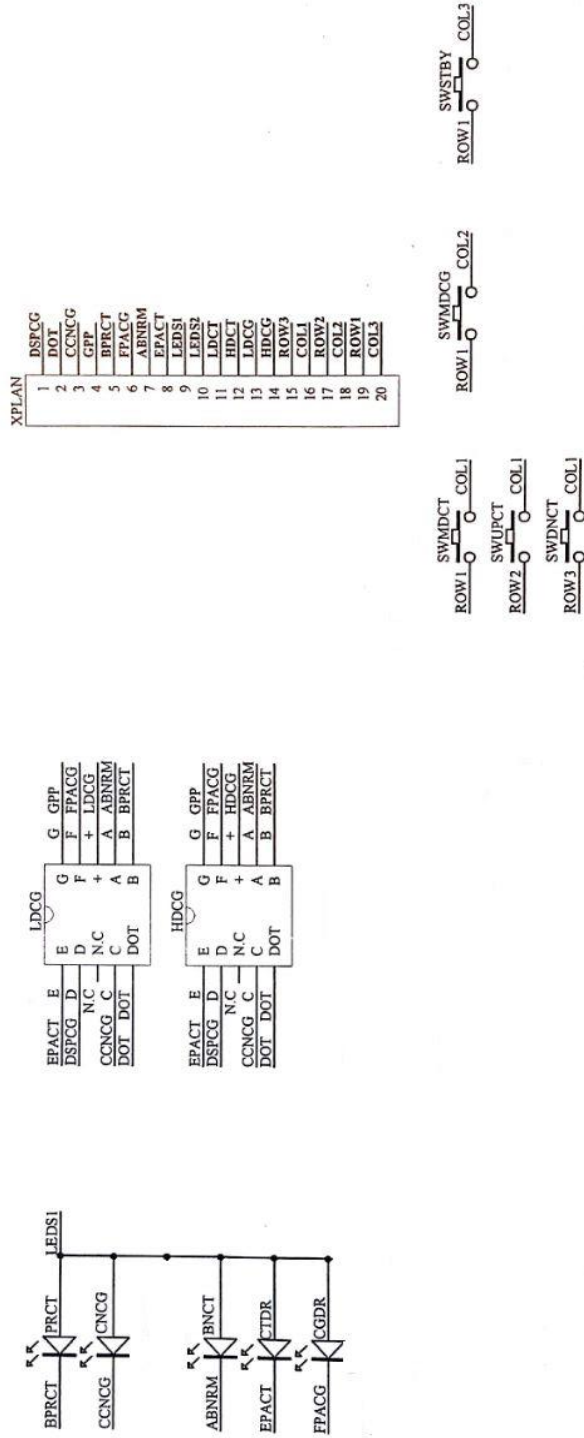
FigureA-7 Evaluation board of STM32F103VET6-1 hardware
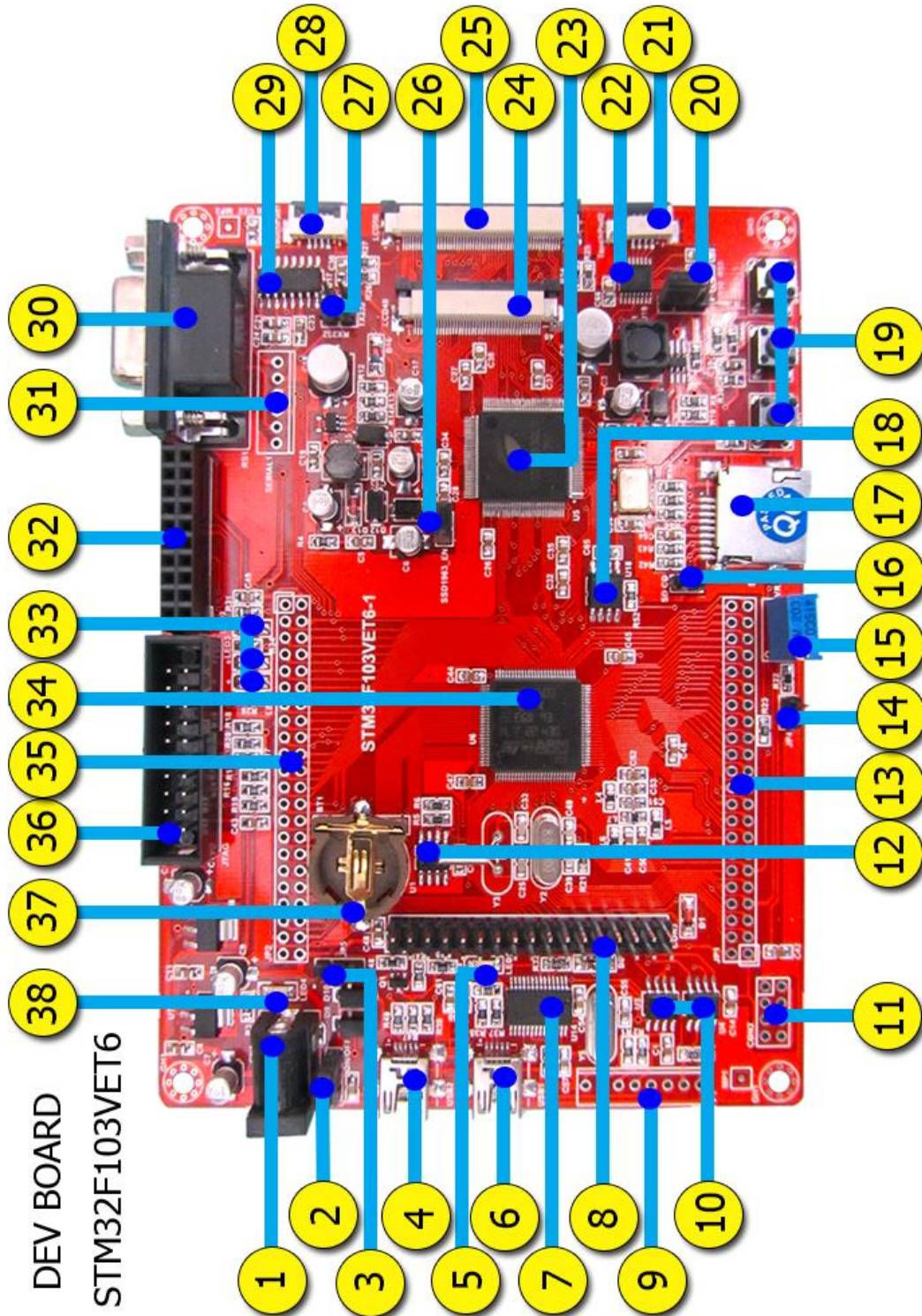
The evaluation board labels and description:

Label and description

1. Power Jack(5.0 DC)

2. JP on/off

3. JP5(POWER MODE USB/POWER)

4. USB2(DEVICE)

5. LED5 (USB 2 POWER)

6. USB1(USB 2 SERIAL TO PL2303TA)

7. PL2303TA

8. CON3(TFT)

9. P1(CAN,RS485 OUTPUT)

10. U3,U4(U3 SP3485 U4 SN65HVD230)

11. CON2(NRF24L01)

12. U1(DS1307)

13. JP1

14. JP4(ADC ENABLE)

15. VR1(POT)

16. SD_CD(SD CARD ENABLE)

17. SD1(SD CARD)

18. AT45161D(U18)

19. USER,RESET,BOOT1 KEY

20. CON4(PWM/3.3 BACK LIGHT ENABLE)

21. TOUCH PAD2

22. XPT2046(U19)

23. SSD1963(U5)

24. LCD40(FOR 3.6,4.3,5.0,...)

25. LCD50(FOR 7.0,9.0,10.1,...)

26. SSD1963_EN

27. RX232/TX232

28. TOUCH PAD1

29. MAX3232(U17)

30. RS1(COM PORT)

31. SERIAL1

32. CON1(CAMERA)

33. LED2,LED3,LED1

34. STM32F103VET6(U6)

35. JP2

36. JTAG

37. BT1

38. LED4(POWER LED)

Bibliography

1. Al-Hussaini, A. and S. Berry, *An evidence-based approach to the management of snoring in adults.* Clin Otolaryngol, 2015. 40(2): p. 79-85.

2. Blumen, M.B., et al., *Comparative study of four radiofrequency generators for the treatment of snoring.* Otolaryngol Head Neck Surg, 2008. 138(3): p. 294-9.

3. *Respiratory tract.* (2017, August 5), Retrieved 15:38, August 10, 2017: In Wikipedia The Free Encyclopedia.

4. Allen, J.D., *Human Physiology - the Basis of Medicine.* The Ulster Medical Journal, 2008. 77(3): p. 216-216.

5. Kaniusas, E., *Biomedical Signals and Sensors II.* Vol. II. 2015: Springer-Verlag Berlin Heidelberg.

6. Stuck, B.A., et al., *Diagnosis and treatment of snoring in adults–S2k Guideline of the German Society of Otorhinolaryngology, Head and Neck Surgery.* Sleep and Breathing, 2015. 19(1): p. 135-148.

7. Deane, S.A., et al., *Comparison of Mandibular Advancement Splint and Tongue Stabilizing Device in Obstructive Sleep Apnea: A Randomized Controlled Trial.* Sleep, 2009. 32(5): p. 648-653.

8. Ramar, K., et al., *Clinical Practice Guideline for the Treatment of Obstructive Sleep Apnea and Snoring with Oral Appliance Therapy: An Update for 2015: An American Academy of Sleep Medicine and American Academy of Dental Sleep Medicine Clinical Practice Guideline.* Journal of Clinical Sleep Medicine : JCSM : Official Publication of the American Academy of Sleep Medicine, 2015. 11(7): p. 773-827.

9. Friedman, M., et al., *Patient selection and efficacy of pillar implant technique for treatment of snoring and obstructive sleep apnea/hypopnea syndrome.* Otolaryngol Head Neck Surg, 2006. 134(2): p. 187-96.

10. Cazan, D., et al., *The effect on snoring of using a pillow to change the head position.* Sleep and Breathing, 2017.

11. Magyar, M.T., *[Beneficial effect of continuous positive airway pressure therapy in obstructive sleep apnea syndrome].* Orv Hetil, 2014. 155(47): p. 1855-9.

12. Lee, C.H., et al., *Obstructive Sleep Apnea and Cardiovascular Events After Percutaneous Coronary Intervention.* Circulation, 2016. 133(21): p. 2008-17.

13. Zhang, X.M., et al., *A novel palatal implant surgery combined with uvulopalatopharyngoplasty and inferior turbinate radiofrequency for the treatment of moderate to severe obstructive sleep apnea: a pilot study.* Eur Arch Otorhinolaryngol, 2015. 272(5): p. 1195-202.

14. Chapple, C.R., M.M. Issa, and H. Woo, *Transurethral needle ablation (TUNA). A critical review of radiofrequency thermal therapy in the management of benign prostatic hyperplasia.* Eur Urol, 1999. 35(2): p. 119-28.

15. Jackman, W.M., et al., *Catheter ablation of accessory atrioventricular pathways (Wolff-Parkinson-White syndrome) by radiofrequency current.* N Engl J Med, 1991. 324(23): p. 1605-11.

16. Sweet, W.H. and J.G. Wepsic, *Controlled thermocoagulation of trigeminal ganglion and rootlets for differential destruction of pain fibers. 1. Trigeminal neuralgia.* J Neurosurg, 1974. 40(2): p. 143-56.

17. Taliaferro, C., *Submucosal Radiosurgical Uvulopalatoplasty for the Treatment of Snoring: Is the Monitoring of Tissue Impedance and Temperature Necessary?* Otolaryngology-Head and Neck Surgery, 2001. 124(1): p. 46-50.

18. Powell, N.B., et al., *Radiofrequency Volumetric Tissue Reduction of the Palate in Subjects With Sleep-Disordered Breathing.* Chest, 1998. 113(5): p. 1163-1174.

19. Li, K.K., et al., *Radiofrequency Volumetric Reduction of the Palate: An Extended Follow-Up Study.* Otolaryngology-Head and Neck Surgery, 2000. 122(3): p. 410-414.

20. Safiruddin, F., et al., *Long-term self-reported treatment effects and experience of radiofrequency-induced thermotherapy of the inferior turbinates performed under local*

anesthesia: a retrospective analysis. European Archives of Oto-Rhino-Laryngology, 2013. 270(6): p. 1849-1853.

21. Troell, R.J., *Radiofrequency techniques in the treatment of sleep-disordered breathing.* Otolaryngologic Clinics of North America. 36(3): p. 473-493.

22. Balsevicius, T., et al., *Efficacy of radiofrequency treatment of the soft palate for patients with mild to moderate obstructive sleep apnea hypopnea syndrome: treatment protocol with nine lesions to the soft palate.* Sleep Breath, 2015. 19(3): p. 1003-9.

23. Kucur, C., et al., *A Rare Complication of Radiofrequency Tonsil Ablation: Horner Syndrome.* Case Rep Otolaryngol, 2015. 2015: p. 570520.

24. Manwaring, D.J.E.a.M.L., *Modeling the interaction of electric current and tissue: Importance of accounting for time varying electric properties.* IEEE Engineering in Medicine and Biology Society, 2007. 229th Annual International Conference of the IEEE Engineering in Medicine and Biology Society, Lyon, 2007, pp. 1117-1120.

25. S.O., K., *Principles of Electrical Engineering Materials and Devices.* 1997: McGraw-Hill; New York, City, NY, USA:.

26. Khalil, S.F., M.S. Mohktar, and F. Ibrahim, *The theory and fundamentals of bioimpedance analysis in clinical status monitoring and diagnosis of diseases.* Sensors (Basel), 2014. 14(6): p. 10895-928.

27. Hainer, B.L., *Fundamentals of electrosurgery.* J Am Board Fam Pract, 1991. 4(6): p. 419-26.

28. Culotta, C.A., *"Arsonval, Arsène D'".* Dictionary of Scientific Biography. Vol. I. 1970: New York: Charles Scribner's Sons.

29. Sebben, J.E., *Electrosurgery principles: cutting current and cutaneous surgery--Part II.* J Dermatol Surg Oncol, 1988. 14(2): p. 147-50.

30. Goldwyn, R.M., *Bovie: the man and the machine.* Ann Plast Surg, 1979. 2(2): p. 135-53.

31. Maness WL, R.F., Clark RE, Cataldo E, Riis D, Haddad AW, *Histological evaluation of electrosurgery with varying frequency and wave form.* 1978: p. 40:304-8.

32. Beriat, G.K., et al., *The comparison of thermal tissue injuries caused by ultrasonic scalpel and electrocautery use in rabbit tongue tissue.* Bosnian Journal of Basic Medical Sciences, 2012. 12(3): p. 151-157.

33. Dargent, D. *Physical Bases of Electrosurgery.* 2005; Available from: http://www.physicianspractice.com/laparoscopy/physical-bases-electrosurgery.

34. Kaniusas, E., *Biomedical Signals and Sensors I.* Vol. I. 2012: Springer.

35. Fish, R.M. and L.A. Geddes, *Conduction of Electrical Current to and Through the Human Body: A Review.* Eplasty, 2009. 9: p. e44.

36. Slivka, A., et al., *Electrosurgical generators.* Gastrointestinal Endoscopy, 2003. 58(5): p. 656-660.

37. Zenker, M., *Argon plasma coagulation.* GMS Krankenhaushygiene Interdisziplinar, 2008. 3(1): p. Doc15.

38. Sadleir, R.J. and T. Tang, *Electrode configurations for detection of intraventricular haemorrhage in the premature neonate.* Physiological measurement, 2009. 30(1): p. 63-79.

39. Pirsig, W. and J.T. Maurer, *Otorhinolaryngology Head and Neck Surgery.* 2017.